MPHIL

Conduction Velocity Selective Recording with Cuff Electrodes in vivo

Seetohul, Vipin

Award date:
2008

Awarding institution:
University of Bath

CONDUCTION VELOCITY SELECTIVE RECORDING WITH CUFF ELECTRODES IN VIVO

By

Vipin Raj Kaushal SEETOHUL

A thesis submitted for the degree of
Master of Philosophy

Department of Electronic & Electrical Engineering

University of Bath

May 2008

ABSTRACT

Conduction Velocity Selective Recording with -
Cuff Electrodes in Vivo -

by Vipin Seetohul.

The objective is to improve the performance of surgically-implanted peripheral nerve recording so that more useful information can be extracted from the neural traffic. The output of such systems consists of the mixed responses to both motor and sensory fibres, and to fibres of all diameters. Professor John Taylor et al. have invented a method for selective recording which allows nerve signals to be classified by conduction velocity (and therefore fibre diameter), in addition to improving the signal-to-noise ratio compared to conventional (tripolar) cuff. The method uses a Multi-electrode Cuff (MEC) and linear signal processing. It is expected to have many applications in neuroprosthetics.

To show that the system does distinguish signals of different function that are carried in fibres of different diameter, it is to be tested by in-vivo experiments in animals. Acute experiments will test the understanding with compound action potentials (CAPs) and then naturally-occurring neural signals after surgical preparation and under several well-defined experimental conditions.

This thesis presents the successful application of conduction velocity-selective ENG recording system to electrically evoked potentials using the frog sciatic nerve. But when it came to testing the recording system on naturally-occurring neural signals from the pig, time constraints and equipment malfunction did not allow for successful recordings. However, after extensive re-designing of the equipment and experiment set-up, a lot has been learnt when it comes to mounting a pig's limb to a test rig and the mechanism behind this tri-segmented limb. The final design of the apparatus will surely be a good continuation for further research in this area.

ACKNOWLEDGEMENTS

The completion of this thesis was brought about by the contribution of many people. First and foremost, I would like to take this opportunity to thank the foundation of my path thus far to my family, who has always stood by me and given me unconditional strength and positivism in support of my attaining this long-held educational ambition.

I would like to express my gratitude to my supervisor, Professor John Taylor, for giving me an opportunity to experience the essence of 'Research'. It has been an enlightening time working under such an experienced and resourceful supervisor like him.

I would also like to dedicate special thanks to Dr. John Hansen for his patience, guidance, advice, assistance and boundless enthusiasm throughout the whole of experiments.

Last but not least, I would like to thank all those from the Department of Electrical & Electronics Department at The University of Bath, colleagues from the Medical Physics Group at University College London, colleagues from SMI (Sensory Motor Interaction) at Aalborg University, Denmark, and finally the EPSRC for making this project possible by providing the financial support.

TABLE OF CONTENTS

LIST OF FIGURES AND TABLES

GLOSSARY OF TERMS

Afferent Fibre. Any of the nerve fibres that convey impulses to a ganglion or to a nerve centre in the brain or spinal cord.

AP. Action Potential: The change in membrane potential occurring in nerve, muscle, or other excitable tissue when excitation occurs.

ATP. Adenosine Triphosphate: An adenosine-derived nucleotide that supplies large amounts of energy to cells for various biochemical processes, including muscle contraction and sugar metabolism, through its hydrolysis to ADP (Adenosine diphosphate; an ester of adenosine that is converted to ATP for the storage of energy).

Axon. The usually long process of a nerve fibre that generally conducts impulses away from the body of the nerve cell.

Axon Hillock. The conical area of origin of the axon from the nerve cell body.

Cell Body. The part of a neuron containing the nucleus but not incorporating the axon and dendrites. Also called soma.

CAP. Compound Action Potential.

CNS. Central Nervous System: The portion of the vertebrate nervous system consisting of the brain and spinal cord. Also called cerebrospinal axis.

Dendrite. Any of the various branched protoplasmic extensions of a nerve cell that conducts impulses from adjacent cells inward toward the cell body. Also called dendritic process, dendron, neurodendrite, neurodendron.

Depolarise. To partially or completely eliminate or counteract the polarization of.

DSP. Digital Signal Processing.

E_k. Equilibrium potential for Potassium.

E_{na}. Equilibrium potential for Sodium.

ECF. Extracellular Fluid

Effector. A nerve ending that carries impulses to a muscle, gland, or organ and activates muscle contraction or glandular secretion.

Efferent fibre. Directed away from a central organ or section.

ENG. Electroneurogram.

EPSP. Excitatory post-synaptic potentials: A local change in the depolarization produced in the postsynaptic neuronal membrane in response to an excitatory impulse; summation of these depolarisations can lead to discharge of an impulse by the neuron.

FES. Functional Electrical Stimulation.

Hyperpolarise. To cause an increase in polarity, as across a cell membrane.

ICF. Intracellular Fluid.

IPSP. Inhibitory postsynaptic potential: A local change in the degree of hyperpolarisation of the postsynaptic membrane of a neuron in response to the arrival of an inhibitory impulse.

MEC. Multi-Electrode Cuff.

Neurotransmitter. Any of the various chemical substances, such as acetylcholine, that transmit nerve impulses across a synapse.

NI DAQ. National Instruments Data Acquisition.

Node of Ranvier. Regularly spaced gaps in the myelin sheath around an axon or nerve fibre. About one micrometer in length, these gaps expose the membrane of the axon to the surrounding liquid.

Organelles. A differentiated structure within a cell, such as a mitochondrion, vacuole, or microsome, that performs a specific function. Also called organoid.

P_k. Permeability coefficient of Potassium.

P_{na}. Permeability coefficient of Sodium.

PNS. Peripheral nervous system, The part of the vertebrate nervous system constituting the nerves outside the central nervous system and including the cranial nerves, the spinal nerves, and the sympathetic and parasympathetic nervous systems

SNR. Signal-to-Noise Ratio.

Soma. The entire body of an organism, exclusive of the germ cells. Also called Cell Body.

Schwann Cell. Any of the cells that cover the nerve fibres in the peripheral nervous system and form the myelin sheath. Also called neurilemma cell.

Synapse. The junction across which a nerve impulse passes from an axon terminal to a neuron, a muscle cell, or a gland cell.

Therians. Theria is a subclass of mammals that give birth to live young without using a shelled egg. This includes both eutherians (placental mammals) and metatherians (marsupials and their ancestors). The subclass includes humans that have an ankle specialised for power and range of motion.

Chapter 1

INTRODUCTION

1.1 Situation

Spinal cord injuries can cause permanent loss of sensation and voluntary motor function. This can be due to either stroke or accidents for example. Spinal cord injuries are devastating and the effects irreversible, leaving parts of the body permanently paralysed. In the absence of spinal cord regeneration, functional electrical stimulation (FES) aims at the full or partial restoration of lost function by stimulation of the intact nerves below the lesion with electrical impulses. Recent research focuses on the stimulation of and recording from peripheral nerves as direct access to the spinal cord is associated with high risks of infection and traumatic surgical procedures. This current research mainly deals with electroneurogram (ENG) *recording*. Several recording techniques to obtain the neural signal (ENG) have been introduced in the past and these are briefly discussed in Chapter 2. The challenge in recording useful signals with any practicable technique lies in the very small amplitude of the ENG. The latter is typically on the order of only a few microvolts, embedded in noise and interference in the milivolt range. Hence, high quality amplification and signal conditioning must take place. This should ideally happen as close as possible to the recording site. This functionality is preferably placed onto the recording nerve cuff, combining the cuff and signal processing, as discussed in the following chapters.

Based on the work by Erlanger and Gasser [1] in 1937 on the generation of APs of different velocities using dispersion, and later by Rushton [2] in 1951, on the relationship between fibre diameter and AP propagation velocity, it is known that neural signals travel at different velocity, depending on the type of information they are transmitting. Investigating velocities and the direction of propagated APs within a peripheral nerve gives an overview of the fibre type (fibre diameter, afferent or efferent fibre) that conducts the APs. From anatomy, it is known that nerves of particular diameters are connected to particular organs. So with Velocity Selective Recording, more information on the source or destination of the ENG signal can be obtained.

The theoretical feasibility of a method to investigate propagation velocity profiles using a multi-contact cuff was discussed by Taylor et al. [3]. It is based on an interlinked arrangement of tripolar (or: double-differential) amplifiers that obtain nine signals from eleven contacts of a nerve cuff electrode.

1.2 Objectives

The general objectives of this project are:

1. - To test our model of the nerve/electrodes/processing using Compound Action Potentials (CAPs), propagating in velocity ranges in vitro.

2. - To show that three distinct naturally occurring nerve signals (cutaneous, joint receptors and tendon stretch receptors) in one nerve can be separated in vivo.

3. - To show that the Multi-electrode Cuff (MEC) gives separable signals in long-term use.

This thesis is structured as follows: The next chapter has an in-depth review of the fundamental elements of the nerve anatomy and physiology, explaining the propagation of APs and the concept of conduction velocity. The same section will show the array of cuff electrodes that are commonly in use and most importantly, the use of MEC in this research to show velocity selectivity. Chapter 3 describes the experiments carried out on electrically evoked potentials on the frog sciatic nerve to demonstrate the suitability of the ENG amplifier to cleverly pick up nerve signals. Having obtained successful results, Chapter 4 elaborates on an attempt to study naturally evoked potentials on pig nerves. After some considerable issues with the equipment, Chapter 5 reveals the evolution of the initial design to the final working test-rig. Chapter 6 presents a final set of experiments aimed at investigating the possible causes of noise problems that have been polluting the recordings. The last chapter discusses the findings of the research thus far

Chapter 2

LITERATURE REVIEW

2.1 Nerve Anatomy and Physiology

2.1.1 The Neuron

The Central Nervous System (CNS) consists of the brain and spinal cord. Neurons are the cells in the CNS which are responsible for sending messages. They have three major purposes: firstly to gather and send information from the senses such as touch, smell or sight., then to send appropriate signals to effector cells such as muscles, glands and finally to process all information gathered and provide a memory and cognitive ability thus allowing us to take voluntary action on information received.

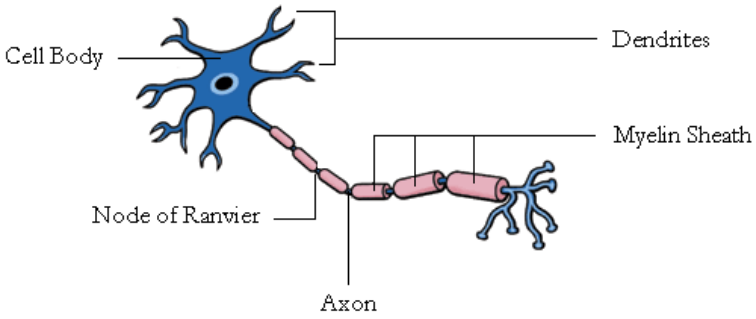

Figure 2-1 – Diagram of a typical neuron -

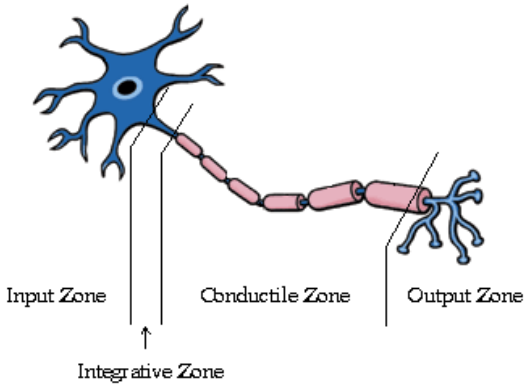

Figure 2-2 – Functional components of the neuron

A standard multipolar neuron in the CNS has four functional parts: an input component, an integrative component, a conductile component, and an output component [4]. Incoming signals to a neuron are received at the dendrites and cell body. Dendrites increase the surface area available for synapses and are specialised to receive a chemically-mediated message. The cell body, containing the nucleus and most of the organelles responsible for maintaining the cell, also receives synapses. The neurotransmitter released at synapses acts upon receptor proteins and the result is a local change in potential (a synaptic potential), which spreads passively

through the dendrites and cell body. Synaptic potentials that depolarise the resting potential are excitatory whereas those that hyperpolarise the soma are inhibitory. The soma membrane also has voltage-gated ion channels necessary for AP production. Along with the dendrites, the soma is specialised for reception of neurotransmitter and generation of synaptic potentials. It can also generate APs just like the axon.

The axon hillock is the junction point of the cell body and axon. It acts as a summation point for the excitatory post-synaptic potentials (EPSPs) and inhibitory post-synaptic potentials (IPSPs) that have been generated in the dendrites and cell body. If the EPSPs are large enough, APs will then be generated at the axon hillock. It has the lowest threshold for AP production because of the high density of voltage-gated channels for Na^+ and K^+. Therefore, this is the trigger zone where APs are first generated.

Neuroglial cells are associated with the axons of neurones. In the CNS these are the oligodendrocytes whereas in the peripheral nervous system (PNS) these are the Schwann cells. Both of these types of cell can associate with axons in two different ways. This will produce either a myelinated or a non-myelinated neurone.

In the first case the Schwann cell (or oligodendrocyte) wraps its cell membrane around the axon a number of times. This forms a segmented sheath around the axon known as the myelin sheath. Myelin is a lipid (fatty) substance which is pale in colour and it is this colour which leads to the terms white matter and grey matter within the nervous system. The white matter contains myelinated axons predominantly whereas the grey matter contains mainly neurone cell bodies which are non-myelinated.

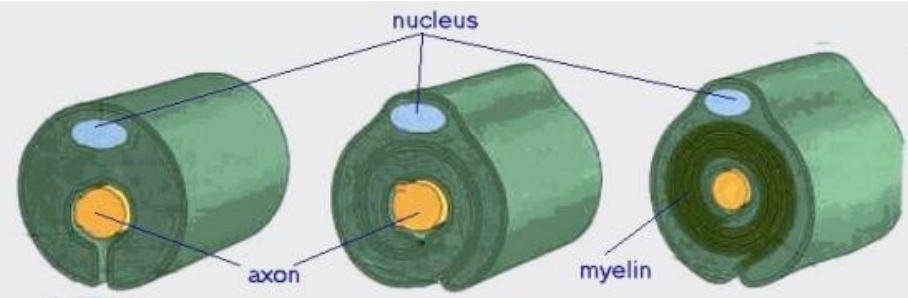

Figure 2-3 – The various stages in the myelinisation of an axon by a Schwann cell.

The main functions of myelin are to increase the electrical capacitance of neurones and also to insulate against any leakage of the bio-electrical nerve impulse. The higher the capacitance and the better the insulation the faster the nerve impulse will travel along the neurone. The main difference between the Schwann cell and the oligodendrocyte is that the former will myelinate only one neurone whereas the latter may associate with a number of axons.

The gaps between the segments of the myelin sheath represent the junction between adjacent neuroglial cells. They are approximately 1mm. apart along the length of the axon. These tiny gaps are known as the nodes of Ranvier.

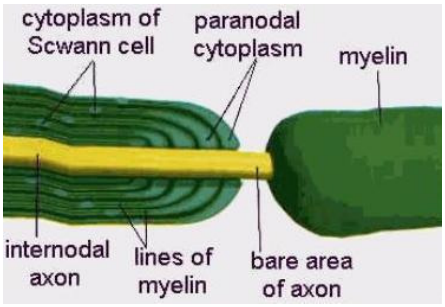

Figure 2-4 – Diagram of node of Ranvier

These nodes play an important role in the physiology of the neurone. At these points there are gated sodium ion channels of which there are none in the myelinated areas of the axon. How this affects nerve transmission is discussed later.

In the second type of relationship between the neuroglial cells and the neurones the axon is still enveloped in the Schwann cell (or oligodendrocyte) but it does not continue to wrap itself around to complete the process of myelinisation [5]. Therefore, myelinated neurones will transmit nerve impulses more quickly than non-myelinated neurones.

It is important that there is a range of speeds at which nerve impulses are transmitted as what determines the body's response depends upon the number of impulses being sent and their speed of transmission. Neurones can be classified by either structural or functional terms.

The transmission of nerve impulses around the body depends on two properties which are unique to neurons: Excitability and Conductivity. Excitability refers to the fact that nerve cells are able to respond to a stimulus. This stimulus may be internal or external. Muscle fibres are also able to demonstrate excitability giving them the ability to contract if stimulated. Conductivity refers to the property that neurones alone have of transferring their excitability along their length and then on to other neurons or even muscle tissue. It is these two properties together which allow neurons to deliver appropriate messages to appropriate parts of the body as and when required.

2.1.2 The flow of electrical current along nerves

The axon can be imagined as a series of little imaginary compartments or units. For each unit, current has a choice: it can either leak away across the membrane, or it can carry on to the next unit. If a voltage is applied at one end, the further we go down the axon the more current has leaked away, thus decreasing the voltage across the membrane exponentially. The behaviour

depends both on how good its insulation is (resistance of the axon membrane) and also on how much resistance is offered to currents flowing longitudinally through the axoplasm. The transverse, insulating, resistance of the membrane for one unit can be called R_M, and the longitudinal resistance of the axoplasm per unit R_L. If we assume that the external medium offers only a negligible resistance to current, then all the outer ends of the individual R_M can be treated as if they were short-circuited together, producing the ladder-like network of resistors shown in Fig. 2-5 [6] that is called the equivalent circuit of the nerve fibre.

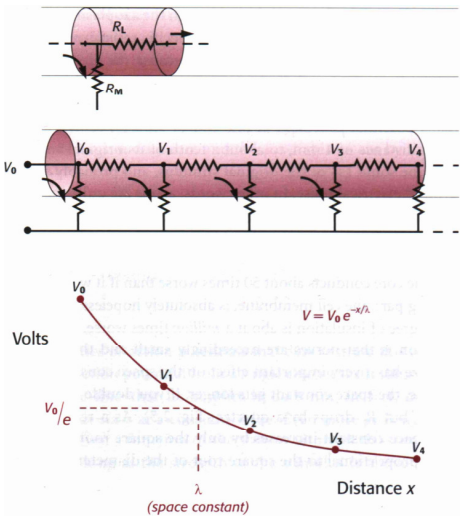

Figure 2-5 – *Above*: Ladder-like equivalent of longitudinal resistance transverse or membrane resistance of axon. *Below*: Expotential decay of Voltage measured at different distances along the axon because of leakage through membrane.

Thus, V is given by $V_0 e^{-x/\lambda}$, where e is the constant whose value is about 2.718, and λ is a parameter called the space constant that describes how quickly the voltage declines as a function of the distance x. It turns out that λ is actually equal to $\sqrt{R_M / R_L}$.

Axons are quite incapable of acting as reliable passive conductors of electricity over distances of more than a centimetre or two at most. There are two reasons for this: (1) Materials that nerve fibres have to be made of are not ideal. (2) Nerves are remarkably small and the layer of insulation is extremely thin. Size has a very important effect on the space constant: the space constant is proportional to the square root of the diameter. But there is a limit to how much nerves can be improved in this way.

For most nerves, passive conduction is not a practical possibility. In nerve fibres that have to conduct over long distances there are channels in the membrane, called voltage-gated channels that open in response to small changes in voltage across the membrane. When they open, they trigger off a very large voltage burst, with a fixed size of some 100 mV in amplitude but only 2-3 ms in duration, and this is what is meant by the AP or spike.

2.1.3 Action Potentials

2.1.3.1 Regeneration

If an AP is recorded from a single electrical stimulus at different points along a nerve fibre, it is found that its amplitude does not decrease at all as a function of distance, but stays at a constant value. The size of this AP is not even a function of the size or nature of the stimulus that initiated it in the first place. As long as the strength of the stimulus is above a certain threshold value (below which no AP is seen at all), neither the amplitude nor the shape or speed of the AP is in any way influenced by the nature of the original stimulus, a property known as the all-or-nothing law.

In the mechanism of AP propagation, the original stimulus to the fibre causes local currents to flow passively through the membrane, causing a spread of potential as in Fig. 2-6 [6]. This voltage is sensed by neighbouring regions of the fibre and triggers a mechanism in the membrane that generates a larger voltage (thus introducing an amplification of the original signal), which in turn sets up local currents that cause a potential change still further down the axon and so on, until the potential change has been transmitted from the point of stimulation to the end of the axon (Fig. 2-6). This whole cyclical process is known as the local circuit mechanism of AP propagation.

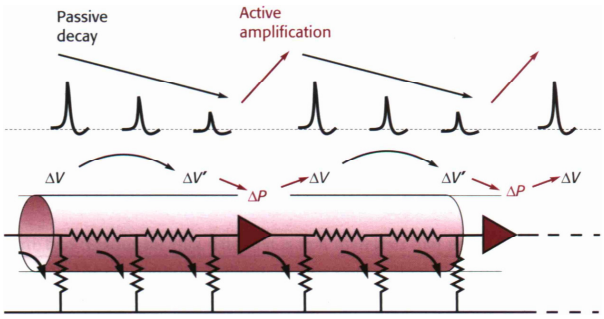

Figure 2-6 – The components of AP propagation.

Each cycle consists of three distinct stages: The mechanism by which (1) a potential at one point results in a passive flow of current and thus in depolarisation of regions further down the axon; (2) this depolarisation triggers off some change in the membrane; and (3) this change produces a new depolarisation that is much larger than what originally triggered it off.

There is a change in the membrane that results in amplification of the voltage that triggers it. This change consists of a change in permeability of the membrane to certain ions.

2.1.3.2 Ionic Concentrations

The interior of axons is composed of the intracellular fluid (ICF) whereas extracellular fluid (ECF) provides the ionic environment in which the axons reside. The most important feature between ICF and ECF is that ICF has a higher concentration of potassium than sodium, whereas ECF is the opposite. The difference in concentration is maintained in two ways: (1) By overall homeostatic mechanisms involving the kidney and the regulation of intake, which determine the composition of the ECF; and (2) By mechanisms within cell membranes that determine the ICF. The most important of the membrane processes is sodium-potassium ATP-ase – the sodium pump (Fig. 2-7 [6]). There is an exchange of sodium ions on the inside with potassium ions on the outside (three sodium ions for two potassium ions). Such pumps consume energy as the ions are moved against their concentration gradient - hence the ATP-ase activity.

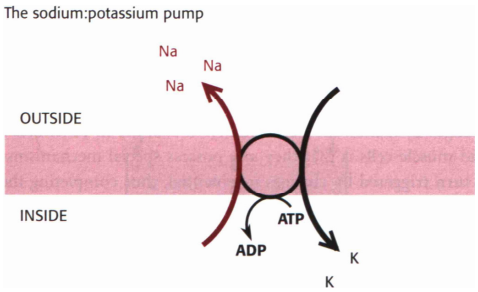

Figure 2-7 – The 3:2 sodium:potassium pump, using adenosine triphosphate (ATP) to transport sodium out of the cell and potassium in, against their respective concentration gradients.

This pump creates a store of potential energy such that (1) It can be harnessed very much more quickly than any conventional chemical store; and (2) It is specifically available at the membrane of the cell. Many cells use this energy for transporting other substances through coupled transport. Potassium is not used in this way – the axon membrane is considered to be slightly permeable to potassium in its resting state, through one or more kinds of potassium leakage channels.

Fig. 2-8 [6] shows how it is possible to have a channel that is specifically permeable to potassium and not to sodium, an ion which is also singly positively charged and has a smaller hydrated size. Charges associated with the channel proteins attract positive ions, while carboxyl oxygens substitute for the water to which the ion is normally wedded: unhydrated sodium, being bigger than unhydrated potassium, is then excluded.

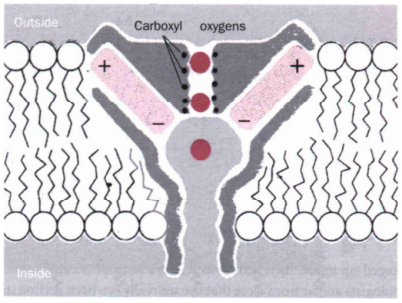

Figure 2-8 – Postulated molecular structure of one class of potassium channel.

This is the ionic backdrop against which the axonal membrane operates. Much of its operation is common to all cells. They all share physical mechanisms that convert any changes in membrane permeability to changes in potential. What is unique about nerve and muscle cells is that they also possess special mechanisms by which such changes are in turn triggered by changes in potential, thus completing the cycle of three links by which the AP is propagated over the membrane surface (see Fig. 2-6).

2.1.3.3 The dependence of potential on ionic permeabilities

Considering a system of two compartments, *A* and *B*, where initially *A* contains a strong solution of potassium chloride, and *B* a weak one; and suppose that the membrane separating them, initially impermeable, suddenly becomes permeable to potassium ions. There will be a tendency for potassium ions to diffuse through the membrane down the concentration gradient between *A* and *B*. Because the ions carry a positive charge, compartment *B* will become more positive with respect to *A* as they migrate in this way, setting up an electrical gradient that will tend to oppose the entry of further ions from *A*. Eventually, there will come a point at which the concentration gradient from *A* to *B* will be exactly equal and opposite to the electrical gradient from *B* to *A*, and the system will be in equilibrium, as there will be no net flow of ions across the membrane.

The resultant electrical potential between *A* and *B* is called the equilibrium potential for potassium, E_K. To work out how big this potential will be, the energy involved in moving one potassium ion from *A* to *B* is considered. The work done in moving it against the electrical gradient will be given by its charge, *e*, multiplied by the potential difference, E_K. Because the system is in equilibrium, this work must be exactly equal to the energy gained in moving down the concentration gradient as such:

$$kT \ln \frac{[K]_A}{[K]_B}$$

where *T* is the absolute temperature and *k* is Boltzmann's constant. So, we can write:

$$eE_k = kT \ln \frac{[K]_A}{[K]_B}$$

or -

$$E_k = \frac{kT}{e} \ln \frac{[K]_A}{[K]_B} = \frac{RT}{F} \ln \frac{[K]_A}{[K]_B} \approx 58 \log_{10} \ln \frac{[K]_A}{[K]_B} mV \quad \text{(At } 20^o \text{ C)}$$

(In the alternative form, derived from consideration of a mole rather than a single ion, *R* is the gas constant, and *F* is Faraday's constant, equal to *Ne*.) This relationship (the Nernst equation) is true for any ion in equilibrium across a membrane to which it is freely (and solely) permeable, with the proviso that if the charge on the ion is not +1 (as, for instance, in the case of Cl- or Ca++), we need to include this ionic charge z as well:

$$E_x = \frac{kT}{ze} \ln \frac{[X]_A}{[X]_B}$$

Only a tiny number of ions need to cross the membrane to set up such equilibrium, so that the concentrations of the ions on each side remain effectively unchanged, and the equilibrium potential is set up virtually instantaneously after a sudden permeability change of this kind.

The limitation of the Nernst equation is that it represents a highly idealised and hypothetical state of affairs. Real membranes are in fact, permeable to more than one ion at any given time. Considering a situation where, as before, we have two compartments, with a high concentration of sodium on one side and high concentration of potassium on the other, but this time the membrane being permeable to both ions. The overall potential, *V*, is not just a function of the concentration differences of the ions, but it also depends on just how permeable the membrane is to each of them. So the overall potential must also depend on the permeabilities of the two ions, termed P_K and P_{Na}. These are called permeability coefficients and represent the ease with which the ion can pass through the barrier for a given concentration ratio.

Because of the *P*, the resultant equation for the voltage, *V* - the Goldman constant field equation – differs from the Nernst equation such that it has terms for both ions that are multiplied by their respective *P*. In the limit, if one of the permeabilities is reduced to zero, it turns into the Nernst equation.

$$E = \frac{kT}{e} \ln \frac{P_k[K]_A + P_{Na}[Na]_A}{P_k[K]_B + P_{Na}[Na]_B}$$

E_K and E_{Na} represent extreme values of the range that *V* can take up: it cannot get more positive than E_{Na} or more negative than E_K. These voltages are essentially fixed provided the cells are in good condition, because the concentrations are fixed, the temperature is fixed and the other elements in the Nernst equation (*k*, *e*) are universal physical constants. So the actual

voltage, V, at any moment must lie somewhere between them. The Goldman equation shows that V behaves as if it were under the influence of two forces: P_K pulls it towards E_K, and P_{Na} pulls it towards E_{Na}. Where it ends up depends on the balance between the two. In other words, changes in permeability cause changes in potential.

2.1.3.4 The resting potential

The reason why the resting potential is close to E_K but not actually at it is that, although at rest the permeability for potassium is much higher than for sodium, sodium permeability is not, in fact, zero: the ratio of the permeabilities is about 100:1, in frog muscle at least. As a result, the resting potential is pulled a little more positive than would be expected for potassium alone, and the Goldman equation gives a pretty accurate prediction of the resting potential.

In the model it was assumed that chloride ions were unable to diffuse across, so it was justified in omitting them from the constant field equation. But experiments show that real nerve and muscle membranes have significant chloride permeabilities. Nevertheless, two reasons why this ion can, for the moment, be safely neglected; (1) In practice, the Nernst potential for chloride is usually very close to the equilibrium potential of the nerve membrane, so that changes in its permeability have negligible effects on the resting potential. Potassium and chloride are free to move together as KCl until the Nernst potentials for both chloride and potassium are equal: that is, until [K]out/[K]in=[Cl]in/[Cl]out. Because internal [Cl] is so much smaller than [K], a shift of a given quantity of KCI has an enormously greater effect on the chloride ratio than on the potassium ratio (because the external concentrations remain essentially unchanged). Thus chloride adjusts itself to a resting potential that is essentially determined by potassium. (2) During the AP, no significant alterations in chloride permeability occur; this is in sharp contrast to what happens to sodium and potassium. However, in synaptic mechanisms, there are certain occasions on which chloride cannot be neglected at all and, indeed, most inhibitory synapses actually work through changes in chloride permeability.

2.1.3.5 The action potential

If a microelectrode is inserted inside a muscle fibre or squid axon and is stimulated to get an AP, it is found that the potential of the inside relative to the outside suddenly reverses from (in the squid) its resting -50 mV to a peak of some +40 mV, and then rapidly declines back to the resting potential again (Fig. 2-9 [6]). This is the monophasic AP.

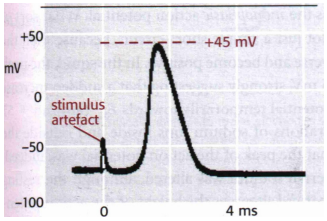

Figure 2-9 – Intracellular recording of AP in squid giant axon. -

The peak of the AP is dependent on E_{Na}. If the concentration of external sodium is altered, although the resting potential does not vary much the height of the AP is altered: the lower the external sodium concentration, the smaller the AP, until eventually it is abolished altogether.

The peak of the AP therefore depends critically on the ratio of $[Na]_{out}$:$[Na]_{in}$, in other words, on the Nernst potential for sodium. So, the natural explanation is that the AP is caused by a brief increase in P_{Na} driving the membrane potential towards E_{Na}.

One idea explaining the increase of P_{Na} at the start of the AP is that the depolarisation of the membrane by local currents from the previous bit of nerve membrane might actually cause the increase in P_{Na}. There would then be positive feedback - depolarisation gives increase in P_{Na}, which in turn causes more.

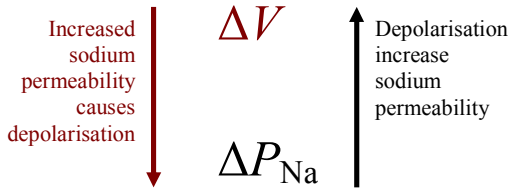

2.1.3.6 Structure of voltage-gated channels

Changes in permeability in response to step depolarisations obey mathematical laws. For instance, the rise of potassium permeability obeys the same kind of dynamics as a fourth-order reaction. In chemistry, an *n*th-order reaction is one in which *n* molecules have to come together for the reaction to occur. If the probability of any one of them arriving is *p*, the probability of the whole reaction occurring is going to be p^n. High-order reactions have a number of characteristics: for instance, they tend to be more temperature dependent than low-order ones, because *p* often proportional to *T*, so any effect of temperature is amplified by the fourth power. They also tend to be slower than comparable reactions of lower order: p^4 is necessarily smaller than p^3 or p^2 or *p*. In fact, by looking at the time course of a reaction after suddenly doing something that increases *p*, we can tell from its shape what order the system is.

Hodgkin and Huxley [7] assumed that the probability, *p*, depended on the voltage at any moment; the potassium channels were normally blocked by four independent particles. When

the membrane is depolarised, there is an increased probability that any particular particle moves out of the way; but to unblock the channel, all four have to move out - hence the fourth order. The recovery is more rapid because it only takes one blocker to flip back for the channel to be blocked once again. The sodium channel can be modelled in a similar way, but with two important differences: (1) It obeys third-order rather than fourth-order dynamics (which is why sodium permeability rises more quickly), (2) Once open it spontaneously closes again, entering the inactivated state.

A model is thus of three blocking particles that move aside when the membrane is depolarised, together with a fourth that does the opposite, moving in to inactivate the channel. A sodium channel is a single protein that does, indeed, consist of exactly four domains, all very similar, composed of six alpha-helixes spanning the membrane. One of the alpha-helixes has a number of positively charged residues and constitutes the voltage-sensitive part of the complex; another part, called the pore loop, makes the channel selective for sodium rather than for other ions. The four domains arrange themselves in the membrane as shown in Fig. 2-10 [6] and when depolarised, they tend to twist in such a way as to open the channel.

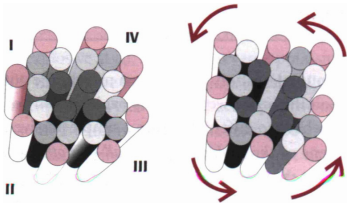

Figure 2-10 – *Left*: Possible structure of a sodium channel. *Right*: Opening of the channel as a result of small rotations of each domain.

2.1.3.7 Summary of electrical propagation of the Action Potential (AP)

A local depolarisation of a section of nerve gives rise, at first, to an increase in P_{Na} that causes the membrane to become still more depolarised as the potential moves towards E_{Na}. Meanwhile, P_K starts to rise and the sodium permeability to fall, causing the potential to start to drop back towards the resting value. This, in turn, tends to shut off both the sodium and potassium channels; but because of the delayed response of potassium permeability, there is a period during which P_K is greater than in the resting state, and the membrane is hyperpolarised; eventually, the resting potential is regained. Meanwhile, the currents generated by this process have spread to neighbouring regions of the fibre, causing them to depolarise and thus initiating, at a distance, the same sequence of changes all over again. In this way the whole pattern of potential and permeability changes is propagated down the fibre (Fig. 2-11 [6]).

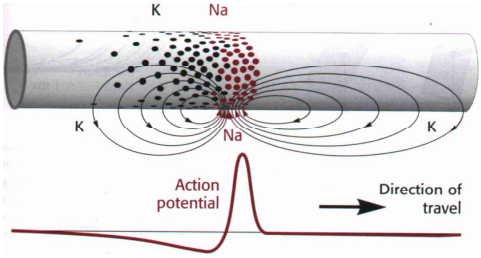

Figure 2.11 – *Above*: 'Snapshot' of a nerve axon with an AP travelling from left to right. The red holes represent the approximate relative density of open sodium channels, the black holes of potassium channels. *Below*: The flow of current and distribution of potential along its length.

2.1.4 Threshold Properties

The fundamental concept that underpins practically everything nerves do is the fact that there are two feedback loops in the nerve membrane, one for sodium and one for potassium. With potassium, a depolarisation causes an increase in P_K, which then tends to oppose the depolarisation by bringing the membrane potential nearer to E_K - a good example of a negative feedback system that tends to stabilise the membrane near its resting potential. The case of sodium is the exact opposite: here, depolarisation again causes an increase in permeability, but this tends to depolarise the membrane still further – there is positive instead of negative feedback.

Considering Sodium – If the membrane is depolarised, sodium permeability rises, and from the Goldman equation, if sodium permeability rises, this will further depolarise the membrane. So we have positive feedback – this is what underlies the membrane's regeneration of APs whose amplitudes have dropped because of the losses caused by passive conduction. But uncontrolled positive feedback can be problematic.

In nerves the positive feedback of the sodium loop is tempered by the negative feedback of the potassium loop. Here, a depolarisation - as with sodium - causes increased potassium permeability, but the difference is that when P_K rises, the nerve becomes less depolarised rather than more depolarised. Potassium has a stabilizing effect. So what matters in nerve is the balance between sodium response and the influence of potassium, whether overall the feedback is positive or negative. However, in the resting state, at the resting potential, the potassium effect is actually stronger than the sodium effect; there is therefore net negative rather than positive feedback, at least for small displacements of potential. But with bigger depolarisations, there comes a point at which the response to sodium overtakes the response to potassium, so that there is net positive feedback, and this is what sets the fibre off and generates an AP. So the threshold is therefore the point at which the two effects are just balanced. Any factor that favours the potassium mechanism rather than the sodium one will tend to raise the membrane threshold. Two important instances of this occur in the refractory period and in accommodation.

2.1.4.1 Refractory period

If a nerve is stimulated with a pair of shocks while gradually reducing the interval of time between them, there comes a point when the threshold for the second shock begins to rise relative to that for the first. If the stimuli of the intervals is kept decreasing the nerve cannot be activated at all a second time regardless of the size of current used (Fig. 2-12 [6]). This period during which it is impossible to stimulate the nerve for a second time is known as the absolute refractory period. The period during which it can be stimulated, but only by using a larger current than usual, is called the relative refractory period. The latter corresponds quite well with the period just after the peak of the AP during which P_K is still raised relative to its resting level, thus tending to stabilise the membrane potential.

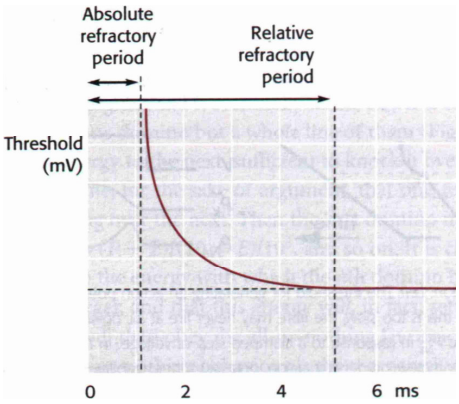

Figure 2-12 – Refractoriness of nerve.

The absolute refractory period is due to a property of the sodium channels. After the peak of the AP has passed, there is a period of recovery during which the sodium mechanism is unresponsive, making the membrane absolutely stable to stimuli of any size. The existence of the refractory period is of considerable functional importance, because this is what prevents the AP from being conducted in both directions at once. Because the local currents flow almost equally both ahead of the AP and behind it, it is essential that the region over which it has just passed should not be reactivated all over again; its refractoriness prevents this happening.

2.1.4.2 Accommodation

Sodium is more responsive than potassium. One consequence of this is that rapid depolarisations are more effective at stimulating the nerve fibre than slow ones, because they get at sodium, as it were, before potassium has time to rise. This is termed accommodation.

This can be explained in terms of the balance between the sodium and potassium mechanisms. There is only a short period during which the sodium mechanism dominates: time is on the side of stability. Considering the stimulation of a nerve with a staircase-like sequence of little ones rather than one large step of depolarisation (Fig. 2-13 [6]); P_K increases cumulatively with each

new step whereas P_{Na} does not, because it is only transient. Furthermore, the transient increase in P_{Na} will steadily decline with increasing depolarisation because of the steadily increasing degree of sodium channel inactivation. Thus, the more gradually a nerve fibre is depolarised, the more the sodium/potassium balance is pushed in favour of potassium, and the further it needs to be depolarised in order to reach the threshold. If it is depolarised slowly enough, there will come a point at which P_{Na} is never great enough relative to P_K for the nerve to fire at all, and the membrane will therefore completely accommodate.

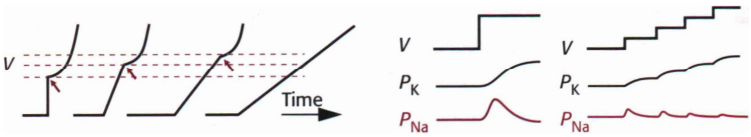

Figure 2-13 – Accommodation. Left: Threshold for generating an AP (arrows). Right: The changes in P_K and P_{Na} in response to a clamped step of voltage.

2.1.4.3 The all-or-nothing law

When recording APs, it is noticed that their size is not affected by the size of the stimulus that causes them. This is the true for of any system that relies on propagation through regeneration via positive feedback. Any system with positive feedback will tend to behave in a manner approximating to all-or-nothing behaviour. In nerves, the all-or-nothing law is not strictly obeyed if one records close to the point of stimulation - within a space constant or two - because the stimulus energy then contributes in part to what is recorded. But as the AP is propagated further away from its origin, this contribution becomes increasingly negligible, and it eventually settles down to its standard form. Thus, the basic cause of all-or-nothing behaviour is the regenerative process that produces APs. A common misconception is that it is caused by the all-or-nothingness of the individual channels.

This law is of fundamental significance in the nervous system, and has functional implications. It clearly imposes very severe limitations on the kinds of messages that nerves can convey, prohibiting direct transmission of graded quantitative information (of the kind conveyed, for example, by the varying concentration of a hormone in the blood), the only messages permitted being of the binary 'yes/no' variety. In the case of nerve axons, the length over which they are required to conduct is greater than the space constant that many thousands of such stages of amplification would be required; each Node of Ranvier is, in effect, a booster of this kind.

All amplifiers, however good their quality, suffer from two defects: they introduce noise and they create distortion. Noise includes both the hiss that arises inevitably in any electrical system - including neurons - from the random movements of the electrons or ions in its conductors, and also disturbances picked up from external sources of interference. The noise generated by each

amplifier will be amplified all the way down the line and added to that of the others, making the final output very much noisier than if there were only one amplifier. Distortion arises through inaccuracies in the linearity of the amplification. This, too, becomes exaggerated if a number of amplifiers are connected in series. Thus, accurate transmission of quantitative information becomes almost impossible: the system almost automatically becomes all-or-nothing in character, because signals either vanish or become saturatingly huge.

The only kind of system that is capable of transmitting messages reliably over distances that are much bigger than the space constant is precisely what has been found in the nerve axon itself: a series of regenerative amplifiers (the voltage-sensitive sodium channels) exhibiting a threshold that prevents the fibre from producing spurious signals in response to its own noise. There is no advantage in such a system for conduction over shorter distances, and in practice it is found that short neurons (as, for example, the bipolar cells of the retina) never use APs, but rely on the much simpler and more informative method of passively propagated electronic potentials.

2.1.5 Conduction velocity

The sequence of events by which one active region of nerve can trigger off a similar pattern of activity in another one at a distance from it by means of local currents has been discussed. Conduction velocity is a matter of how far and how quickly these currents spread, and of how long it takes for them to be regenerated.

The space constant, λ, is a measure of how far currents spread; how far we can go before a voltage that has been applied drops to $1/e$ of its original value.

With really bad cables like nerve fibres, passive conduction is very slow indeed - sometimes less than 1 m/s. Passive conduction is so slow because of the electrical property of the membrane called capacitance. Any two conductors separated by a layer of insulation act as a capacitor. The larger the opposed areas of the conductors, and the thinner the insulating layer between them, the larger the capacitance (measured in Farads) will be. In the case of nerve fibres, the membrane is both a good insulator and extremely thin, and makes an excellent capacitor: it has a capacitance, C_M, of about l $\mu F/cm^2$. The equivalent circuit can be redrawn in the form shown in Fig. 2-14 [6].

In the past, several methods have been described to estimate neural AP conduction velocity and to discriminate between motor and sensory signals by measuring the delay between two sites. For example, those methods included direct delay measurement [8], arrays of matched filters [9, 10], or correlation techniques [11]. However, in all these signals, only two neural signals are amplified.

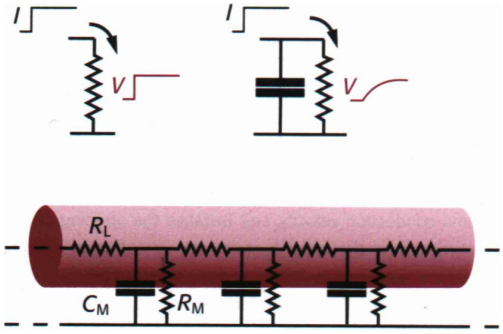

Figure 2-14 – Above: Voltage response of a resistor and of a resistor and capacitor in parallel showing the slow rise of voltage in the second case. Below: Modification of the equivalent circuit to include membrane capacitance, C_M, as well as resistance, R_M.

If a current, *I*, is suddenly passed through a resistor, R_M, on its own, the voltage across it immediately reaches the value $V=IR_M$. But with a capacitor as well, it now takes time for the voltage to reach this value, because part of the current must be used to charge up the capacitor to the new level. On injecting a step of current of this kind, the voltage rises only slowly to its final value of IR_M, with a time course that is exponential and given by $V=IR_M(1 - e^{-t/\tau})$. Here τ is the time constant of the circuit (the time taken for the discrepancy, $I R_M - V$, to fall by a factor *e*), and is equal in this case to $R_M C_M$. For many nerve fibres, this time constant is of the order of a few milliseconds, setting a limit on the rapidity with which the membrane can generate voltages in response to local currents.

A voltage generated at a particular point on the membrane declines exponentially as a function of distance, with a space constant. The space constant and time constant together give a measure of the speed with which an electrical disturbance is propagated passively along the axon. This speed is equal to λ/τ, which has the dimensions of velocity.

The difference between having an active rather than passive conduction: Passive conduction involves just λ and τ; active conduction is actually slower than passive because of the extra time, *T*, needed to regenerate the AP from threshold to full size. The formula for the velocity needs to be modified a bit to take this into account: , $\lambda/(\tau+T)$ is needed instead of λ/τ. *T* is mostly due to the time it takes for the sodium permeability to respond to the change in potential, and normally is very short, so that *T* is small in comparison with τ.

Higher temperatures speed the permeability changes up because they are both high-order reactions, but they affect the fourth-order potassium more than the third-order sodium. As a result, potassium gradually catches up with sodium and the AP actually gets briefer and smaller as the temperature is raised (Fig. 2-15). In some cold-blooded animals, conduction ceases altogether if the temperature exceeds some 37°C.

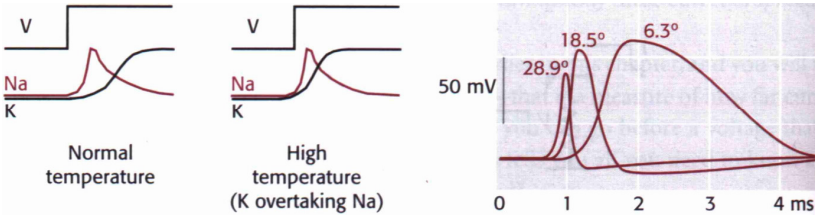

Figure 2-15 – Temperature and conduction velocity – Left: Speed of opening of potassium channels is more affected by temperature than that of sodium channel. Right: APs travel faster at higher temperatures but also get smaller.

The size of the local currents also depends on the ionic concentrations inside and outside the fibre - low external sodium, for instance, reduces the velocity of conduction because it makes the sodium current smaller - and is influenced by local anaesthetics and other pharmacological agents acting on the permeability mechanisms. It is also a function of the density of sodium channels in the membrane. The nodes of Ranvier have a higher density of sodium channels than do ordinary unmyelinated fibres, another factor contributing to the increased conduction velocity of myelinated nerves.

Factors that might influence conduction velocity by acting on λ and τ are:

(1) Diameter, *D*, of the fibre – τ is equal to the product of *C* and R_M, both of which depend on the surface area of the fibre: if *D* increases, the surface area increases in proportion. This makes the capacitance increase, but it makes the resistance decrease and these two effects cancel out so that the time constant does not vary with diameter at all. The space constant varies with the square root of the diameter. So, if the velocity is proportional to λ/τ, and τ is constant, then velocity will also vary with the square root of *D*.

(2) Myelination – Animals rarely have unmyelinated fibres larger than about 1 μm in diameter. Myelination is a far better way of increasing the conduction velocity of large fibres than simply increasing their size. The effect of myelination is to thicken the layer of insulation round the fibre except at the nodes of Ranvier. This has the desirable consequence of increasing R_M and reducing C_M. This increases R_M, but, has the opposite effect on *C*, which gets smaller. Again, the two factors cancel out, so that the time constant is no different. But the extra insulation does increase the space constant, so as a result conduction is greatly speeded up. The myelin forces the external local currents to travel further before they can gain access to the axoplasm through the nodes. Myelinated nerve fibres do not show the square-root relationship for velocity and diameter, but something nearer a linear relation. The reason is to do with optimisation. Realistically, myelin thickness is not constant: there is an optimum thickness for myelin, which varies with the diameter, and the effect of this is to make the curve more or less linear rather than showing a square-root relation. An important consequence of the linear relation for

myelinated fibres as opposed to the square-root one for unmyelinated is that the two curves cross, at about 1 μm diameter. The reason why all fibres are not myelinated is that, although there is a speed advantage in myelinating larger fibres, it is actually better to leave the smaller ones alone, because, for a given overall diameter, the myelin takes up space that impinges on the conducting axoplasm. So there is no point in having myelinated fibres smaller than 1 μm in diameter or unmyelinated ones larger than this.

Because in myelinated fibres the active, voltage-sensitive, sodium and potassium channels are virtually confined to the nodes, the AP moves quickly from one node of Ranvier to the next, but lingers at the node itself while it is being regenerated. This is called salutatory conduction. Myelinated nerves would conduct even faster if there were no nodes at all, but some is needed in order to make up for the loss of current that still occurs despite the thick layers of myelin. In fact, the nodes are separated by the order of a space constant, which provides enough of a safety margin that even if one or even two are nodes poisoned the nerve can still just conduct. The importance of myelination can be seen in multiple sclerosis, a condition in which the myelin gradually degenerates, causing progressive weakness and lack of co-ordination.

2.1.5.1 The compound action potential (CAP)

Considering peripheral nerve, there is typically a mixture of myelinated and unmyelinated fibres all jumbled up together, conducting at a wide range of speeds. As a result of this mixture of speeds, if such a nerve is stimulated at one end and recorded some distance down, a rather complicated electrical response called the CAP (the sum of many different AP all occurring at different times) is obtained. Under these circumstances, the pattern of peaks in the CAP gives a sort of spectrum of the conduction velocities of the fibres in the nerve, though not a very quantitative one, because large peaks may simply be due to large fibres rather than to a large number of fibres of a particular velocity. Often, the fibres appear to fall into groups based on their diameter and therefore their conduction velocity; a common way of classifying fibres is into fast, medium and unmyelinated slow, but with further subdivisions of the 'fast' category.

2.2 Cuff Electrodes

Cuff electrodes are electrodes which are fitted around a nerve fascicle or a sub-set of nerves and do not penetrate the nerve itself. Contemporary cuff electrodes are 1-2 cm long with a maximum diameter of few millimetres. These have been used to record the ENG from peripheral nerves in various experiments [12-20]. A nerve cuff recording electrode consists of an insulating tube typically made of silicone rubber with circumferential metal electrodes placed along the inner cuff walls as shown in the figure below. Here the electrode consists of electrode contacts embedded within a self-curling cuff. In this case it is designed to be compliant so that it

can accommodate to fit accurately around the nerve without the use of sutures to secure it while being well maintained in intimate contact with the nerve. It is self-sizing electrode and can be used to effect selective activation of geometric regions of the nerve enclosed by the cuff. It is manufactured from biocompatible materials such as medical grade silicon rubber and Platinum contacts. Cuff electrodes can also be fabricated using platinum foil electrodes fixed by rubber bands on a Teflon coated mandrel dip-coated with silicone [21]. In contrast to geometry, other experiments have used spiral nerve electrode cuffs for recordings [22].

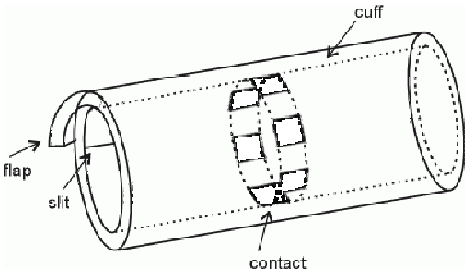

Figure 2-16 – Self-curling cuff electrode.

The recording electrodes usually encircle more than 80% of the perimeter of the cuff and the internal diameter of the cuff must be at least 20% larger than the diameter of the nerve [23] to avoid compression of the nerve bundle and therefore obstruction of the blood supply. Stein [24] has shown that tight cuffs reduce slightly the number of large myelinated fibres. He also observed that there was an increase in the impedance of the electrodes in the first few weeks after implantation but this was attributed to tissue in growth inside the cuff. More details are provided in [25]. It was suggested by Hoffer et al. [23] that the cuff length must at least equal to the wavelength of the neural signal and about ten times greater than the cuff inner diameter. The theory by Winter et al. [26] predicts that there is a maximum in overall amplitude for a particular pitch corresponding to an optimal number of electrodes for a given cuff length.

Geometry of cuff electrodes has been an active area of research – Rahal et al. have discussed the effect of nerve cuff geometry in, firstly, interference reduction [27], and in EMG reduction [28], while Andreasen et al. considered signal strength versus cuff length [29]. There are different ways of arranging electrodes inside the cuff; the monopole was used in early experiments and employs a single electrode located centrally inside the cuff. A second remote electrode is placed at a distance as reference. This monopolar arrangement produces large signal amplitudes but the interference rejection is poor. Differential or bipolar recording decreases the electrode sensitivity to external signals. In the bipolar configuration two electrodes are embedded in the cuff and the ENG recorded is the potential difference between these electrodes. The amplitude of the recording depends strongly on the electrode separation, i.e. the enclosed impedance and also on the length of the insulating cuff. An arrangement termed quasi-tripolar arrangement removes the cuff length dependency so that the signal amplitude depends on electrode separation alone [30].

The ENG is recorded between two shorted outer electrodes and a centre electrode halfway between the outer electrodes as a reference. This arrangement yields the practical advantage of interference cancellation. The true-tripolar arrangement implements additional trimming capability. In this configuration, three amplifiers are used. The two first-rank amplifiers record differentially between the outer electrodes and the centre electrode as the reference. A third amplifier sums the output signals of the first-rank amplifiers. The screened true-tripole is an extension to the true-tripole with two or more additional end electrodes. Shorting the end-electrodes reduces the potential difference between the cuff-ends, thus also reducing the field inside the cuff. The principle is the same as the quasi-tripole, but the end electrodes can be optimised to give maximum field reduction. The effectiveness mainly depends on the area of the end electrodes and SNR improvements varying between 18% and 73% were found in studies using a rabbit model [31]. Pflaum et al. [32] compare two modes, namely 'quasi-tripolar' and 'true tripolar' configurations. Schuettler et al. [33] has attempted to further enhance the neural cuff electrode by integrating a multiplexer circuit which was intended to reduce the number of necessary interconnection leads to a stimulator. Cable breakage is one of the main reasons for implant failure and this method greatly reduces this risk.

But all of the methods mentioned so far can unfortunately detect one signal ***only***, resulting in a huge loss of information.

2.3 1-D Analytical Model

The circuit in Fig. 2-17 shows a one-dimensional (1-D) model of a myelinated nerve fibre in a cuff. The intra-cellular resistance per section is denoted by r_a. This is assumed to be uniform in this model. Therefore, R_a, the intra-cellular resistance over the whole cuff can be written as:

$$R_a = nr_a$$

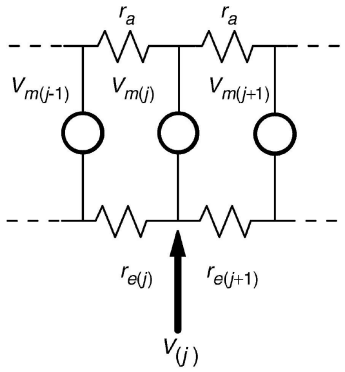

Figure 2-17 – Circuit model of one myelinated nerve fibre in cuff. [2] -

The extra-cellular resistance per section is denoted by r_e and this is not uniform in this model. The extra-cellular resistance over the whole cuff, R_e, is:

$$R_e = \sum_{i=1}^{n} r_{ei}$$

The cuff is assumed to have nodes at the end, and to be an integer number of inter-nodal lengths long. R_a and R_e are divided into n sections by (n+1) electrodes. These external end nodes are both grounded as it is assumed that the resistance outside the cuff is negligible. The voltage generators $V_{m(i)}$, where $0 \le i \le n$, represent the potential differences across the membrane at the Nodes of Ranvier. The potential $V_{(j)}$ at a distance j node from the left hand of the cuff is found using the Thévenin equivalent circuit at a point Q at the right hand. The Thévenin equivalent voltage at Q can be written as follows, assuming that $r_a >> r_{ei}$ for all i. and that R_Q is approximately equal to R_e

$$r_a V_j = \sum_{i-1}^{j} r_{ei}\left(V_{mi} - V_{mi-1}\right) \tag{1}$$

When re-connected, a current $\frac{V_Q}{R_Q}$ flows out of the network at Q with a fraction $\frac{R_e}{R_e + R_a} \cong \frac{R_e}{R_a}$ flowing through the extra-cellular resistance R_e. The extra-cellular voltage opposite node j is therefore:

$$r_a V_j = \sum_{i=1}^{j} r_{ei}\left(V_{mi} - V_{mi-1}\right) - \sum_{i=1}^{n} r_{ei}\left(V_{mi} - V_{mi-1}\right)\frac{\sum_{i=1}^{j} r_{ei}}{\sum_{i=1}^{n} r_{ei}} \tag{2}$$

This is the case for a monopole electrode mounted in an insulating cuff. So far r_a was assumed to be uniform but not r_e. So in the case that r_e is uniform, the measured monopole voltage, V_{mp} can be expressed as such:

$$V_{mp}\left(t, z_0\right) = \frac{R_e}{R_e + R_a}\left[\left(1 - \frac{z_0}{L}\right)V_m\left(t\right) - V_m\left(t - \frac{z_0}{v}\right) + \left(\frac{z_0}{L}\right)V_m\left(t - \frac{L}{v}\right)\right] \tag{3}$$

Where the cuff length is L, and a single electrode is located at a distance $z = z_0$.from one end, V_m is the TMAP, and v is the conduction velocity. This is the quantitative description of a recorded signal $V_{mp}\left(t, z_0\right)$ due to one axon in a length constriction represented by a narrow cuff. Stein and Pearson [34] first derived this expression for the case of unmyelinated nerve fibres, and later on Marks and Loeb [35] extended it to the myelinated case. Struijk [36] represented it exactly as in Equation (3) and it differs from the Marks and

Loeb formulation in the assumption that the internode is not leaking and that therefore the transmembrane action potential (TMAP) between the nodes has a linear rather than expotential shape.

Equation (3) expresses the effect of the cuff ends on the response and this highlights the importance of the restricted extracellular space. Using three electrodes and a tripole (or double-differential amplifier), the voltage at the amplifier output takes the form $V_{mp1} - 2V_{mp2} + V_{mp3}$. As a result, the cuff end-terms disappear. The tripole output voltage V_{tp} depends only on the instantaneous values of the TMAP opposite the three electrodes, as shown in Equation (4).

$$V_{tp}(t, z_1, z_2, z_3) = \frac{R_e}{R_e + R_a}\left[V_m\left(t - \frac{z_1}{v}\right) - 2V_m\left(t - \frac{z_2}{v}\right) + V_m\left(t - \frac{z_3}{v}\right)\right] \quad (4)$$

Where, z_1, z_2 and z_3 are electrode positions, with respect to one end. This equation shows that, as long as the electrodes are equally spaced, a tripolar signal can be recorded whose form is independent of the tripole position within the cuff and which is insensitive to EMG interference [3, 28, 36]. This means that if additional electrodes are introduced into the cuff, more than one tripolar signal can be recorded.

2.4 Multi-Electrode Cuff

The general layout of a Multi-Electrode Cuff (MEC)-based VSR system is shown in Fig. 2-18. In such an electrode arrangement, the MEC consists of N tripolar signals, N+1 first-rank differential amplifiers, and N+2 electrodes. This set-up makes use of the fact mentioned previously, that a true-tripole recording is independent of the tripole position within the cuff, resulting in more than one ENG signal that can be generated from the same AP. The delay between successive MEC outputs is inversely proportional to the ENG propagation velocity. Artificial delays are placed in cascade with the MEC tripole outputs so as to cancel the naturally occurring delays. When the outputs are subsequently added, the sum will be a maximum for one particular velocity, enabling the ENG velocity to be found [3]. This property enables velocity-selective recording and improved SNR. A complication in this process is that the amplitude of the ENG signals recorded using the nerve cuff method are very small, on the order of a few microvolts, with most of the signal power lying in a bandwidth between about 300 Hz and 5 kHz. Therefore this system, like all nerve cuff-based ENG recording systems, relies critically on the availability of low-noise, high-gain amplifiers [37-39].

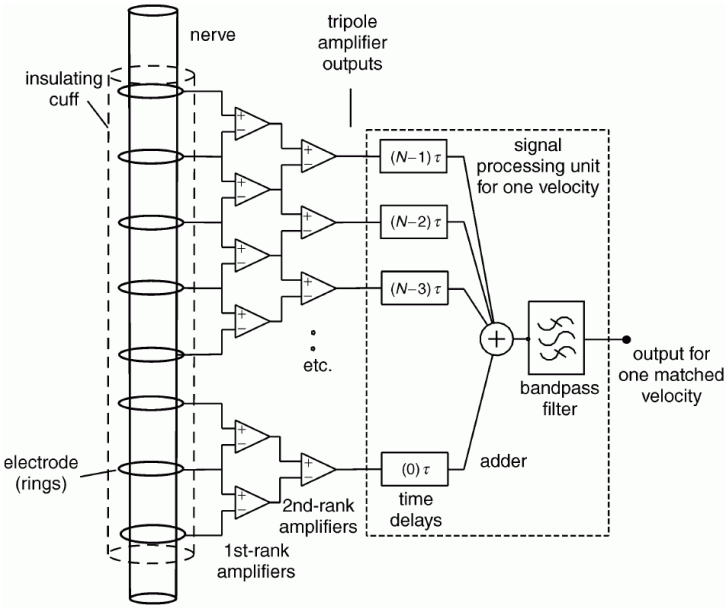

Figure 2-18 – Multi-electrode cuff (MEC), array of tripole amplifiers and signal processing unit for selecting one velocity. [2]

The paper by Taylor et al. [3] provides an in-depth explanation of a MEC which provides several tripolar signals that are then subjected to a signal processing operation. By contrast, Jezernik et al. [40] used more complicated signal processing of the signal from a tripolar cuff that involved autocorrelation and an artificial neural network.

2.5 Velocity Selectivity

From a typical distribution of fibre diameters in the human sural nerve, there is an approximately proportional relation between fibre diameter and propagation velocity, with a conversion factor of the order of 5m/s per μm [41]. Therefore, even within a single nerve a wide distribution of velocities can be encountered. If naturally-occurring nerve signals are to be used for the detection of signals that are not dominant in the nerve traffic, it will be essential to discriminate between traffic with different propagation velocities and direction.

It has been proposed that the MEC can be used for the purpose of discriminating between traffic with different propagation velocities and directions in the arrangement shown in Fig. 2-18 [3, 42], similar to a technique used by Merletti et al. [43, 44]. However, Merletti used the array for surface EMG recording. This poses a different set of requirements and challenges compared to this application. The MEC with equally spaced electrodes allows obtaining recordings of the same nerve signal, delayed in time. Consider the following expression:

$$T = d/v$$

Where '*T*' is the time delay, '*d*' is the electrode distance relating to electrode pitch and '*v*' is the finite propagation velocity of the AP.

In a cuff length L with equidistant electrodes, the electrode pitch d is described by

$$d = L/n$$

where n is the number of electrodes. The time delay is visible in the recorded data for several overlapping true-tripole recording channels.

A method for the measurement of propagation velocity is to sum the outputs of the tripole amplifiers after introducing artificial time shifts τ. When τ matches T, the AP peaks add constructively to give the largest signal, since the correlation between the signals on the different channels is maximised. Conversely, when using mismatched delays τ, the correlation decreases and the amplitude remains smaller. The time shift that results in the maximal amplitude corresponds to T and the sign of τ indicates the direction of propagation. Such an arrangement is in effect a velocity-selective filter since τ tunes the arrangement to one matched velocity. Experimental evidence for the suitability of this method is provided by Rieger [45, 46]

2.6 Amplifier System cross-talk testing

The same amplifier system as that used by Rieger [47] has been used throughout this project. Initially, in order to test the resolution and cross-talk of the channels on the ENG recording system, a test box was built. This consisted of 10 oscillator circuits, each producing sine waves at different frequencies ranging from 1000 Hz to 1180 Hz with 20 Hz increments between each channel.

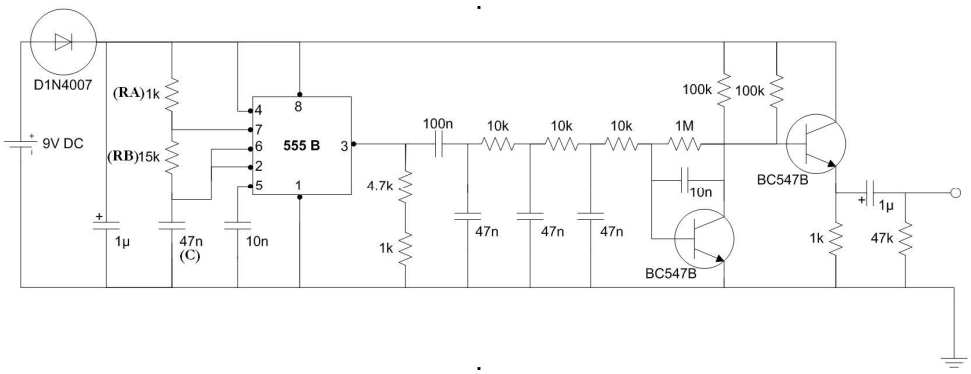

Figure 2-19 – Schematic of one oscillator circuit.

The frequency (F) was set for each oscillator circuit using the following equation: $F = \frac{1.49}{(RA + 2RB) \times C}$, Where RA, RB and C were varied in each case to achieve the required frequency and amplitude. After setting the individual frequencies of the 10 oscillator circuits, they were arranged in an aluminium die-cast box on a PCB board as shown in the following figure.

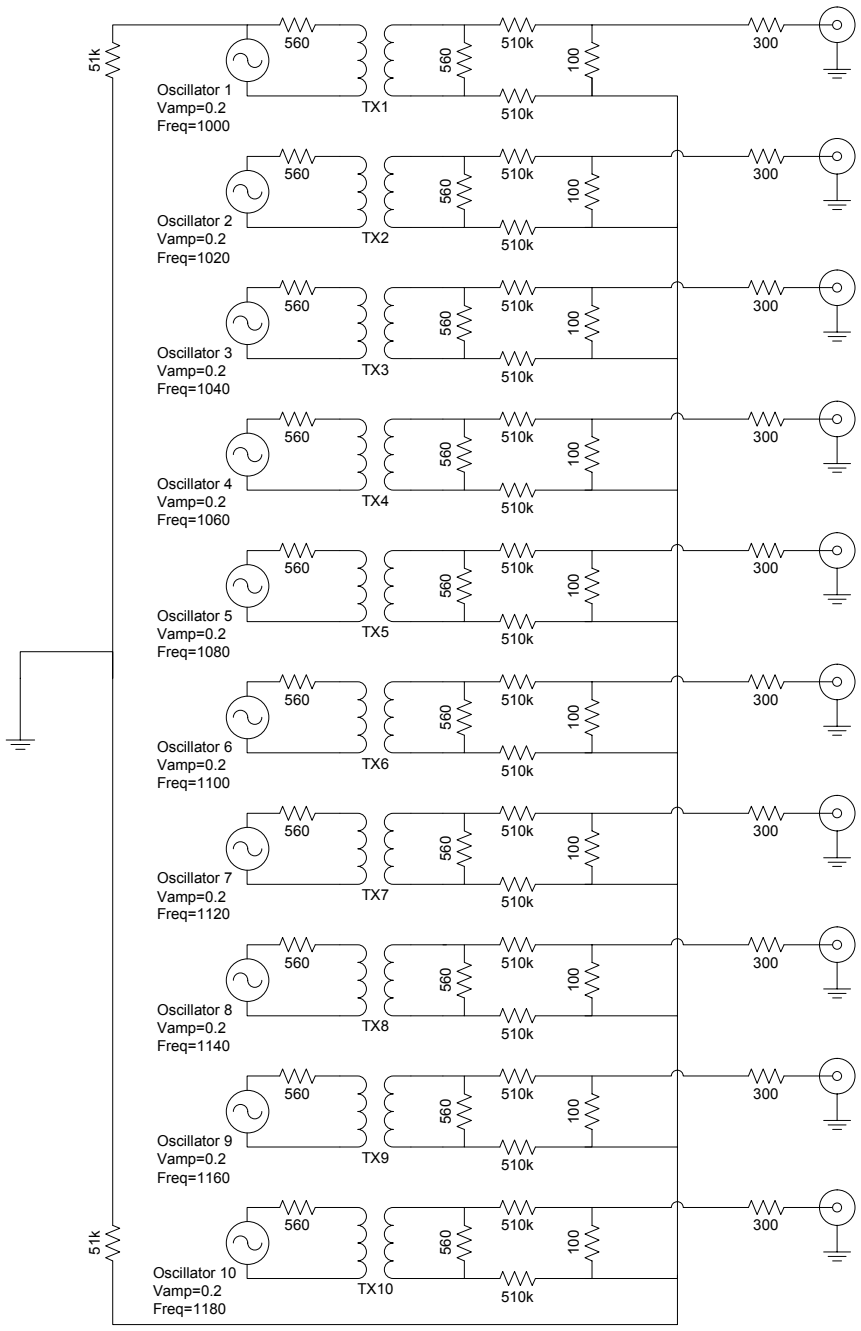

TX → Critchley 1:1 Transformer -
Oscillator → Velleman Oscillator Circuits

Figure 2-20 – Schematic of oscillator circuit test box.

Chapter 3

ELECTRICALLY EVOKED POTENTIALS:

FROG EXPERIMENTS

3.1 Xenopus

Xenopus is a genus of frog. The best-known species belonging to this genus is Xenopus laevis, a common model organism. Xenopus are a clawed, carnivorous genus of African frog. Xenopus are a popular model system for gene and protein expression and knockdown studies. Xenopus laevis is the most commonly used species for developmental biology studies. The African clawed frog (Xenopus laevis, also known as platanna) is a species of South African aquatic frog of the genus Xenopus. It is up to 12 cm long with a flattened head and body but no tongue. Its name derives from its three short claws on each of its hind feet, which it probably uses to stir up mud to hide it from predators.

Figure 3-1 – Xenopus Laevis used in these set of experiments.

3.2 Nerve Stimulation Method

Typically neural stimulation is performed on peripheral nerves by placing a nerve cuff around a nerve trunk. During stimulation APs are initiated at the cathode and propagate in both directions along the nerve trunk. The threshold for activation of the nerve fibres inside the nerve trunk is inversely proportional to the fibre size. This means that the larger nerve fibres have a lower stimulation threshold than the small nerve fibres. This is the opposite of the recruitment characteristics needed for low fatigue stimulation of muscle as the smaller nerve fibres innervate the slow acting low fatigue motor units and the large fibres innervate the fast response fast fatigue motor units in the muscle. Conventional neural stimulation uses rectangular biphasic current pulses typically of constant voltage or current.

3.3 Velocity-Selective Recording

This uses exactly the method described in the previous chapter. An AP travelling along a nerve that is cuffed with N electrical contacts equally spaced along the insulating cuff generates an electrical potential at each of the contacts as a function of time contact position. The resulting electrical pattern that can be recorded from the cuff contacts is specific to the velocity and direction of the AP propagation (Fig. 3-2).

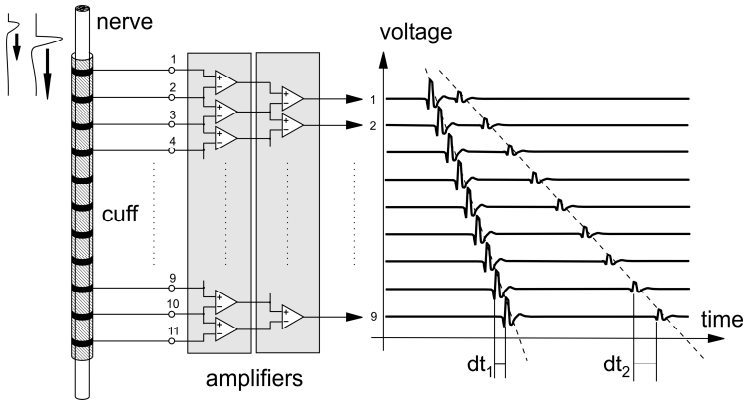

Figure 3-2 – Recording pattern generated by two APs travelling at different velocities along a nerve in an eleven-contact cuff electrode.

After amplification of the signals using a tripolar bank of amplifiers, the recorded signals are shifted in time against each other by (n-1) x dt and summed to a single signal, where n refers the channel number. E.g. channel 1 is not delayed, channel 2 is delayed versus channel 1 by dt, channel 3 is delayed by 2 x dt, etc. In the case that dt matched the electrode pitch l divided by the AP propagation velocity v, the signals of all channels add up constructively. The amplitude of a dt-matched summed signal is up to $N - 2$ times larger than the amplitude after summing with a non-matched time delay (when using a tripolar amplifier configuration).

3.4 Nerve preparation

Four sciatic nerves were obtained from two decapitated adult *Xenopus Laevis* frogs. The nerves were handled by sutures that were tied to the nerve endings. After explanting, the nerves were transferred to the basin of our setup and immersed in amphibian Ringer's solution at room temperature. The nerves had a total length of typically 8 to 9 cm and varied in diameter from 0.5 mm distally to 2 mm close to the spinal cord.

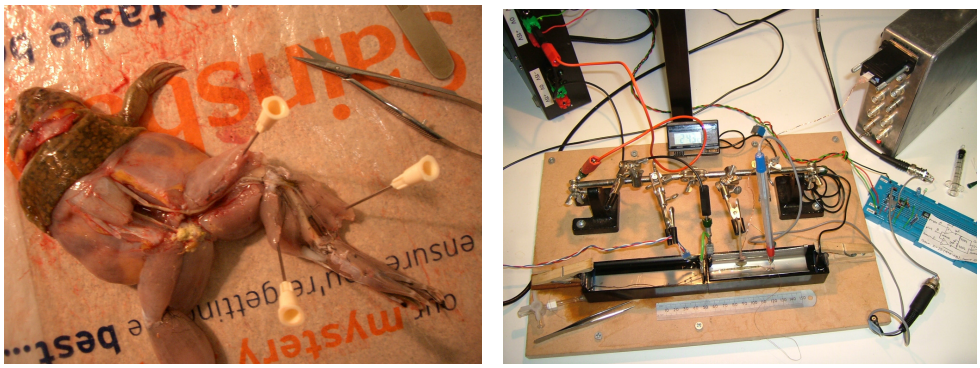

Figure 3-3 – *Left:* Sciatic nerve still on the frog, *Right:* Nerve in basin. -

3.5 Neural Electrodes

The multiple contact cuff electrodes were produced by employing polyimide thin-film technology. These electrodes consist of a 300 nm film of sputtered platinum sandwiched between two 5 µm layers of spin-coated polyimide (Pyralin 2611, HD-Microsystems, Bad Homburg, Germany). A detailed description of the manufacturing process can be found in [48].

The final electrode is 1.5 mm in diameter, 40 mm long and carries eleven 0.5 mm wide, ring-shaped platinum contacts that are equally distributed along the cuff at a pitch of 3.5 mm (Fig. 3-4). The stimulation electrodes were fabricated by Dr. Martin Schuettler, at the facilities of University College London, in the same way as the recording electrodes. They have a diameter of 1.0 mm and carry three ring-shaped platinum contacts (0.2 mm wide) at a longitudinal pitch of 5.0 mm.

A bipolar hook electrode was manufactured from 0.127 mm diameter platinum wire. It was used to record the electro neurogram the same way as Erlanger and Gasser [1] described it and was used to validate the propagation velocity profiles based on the multi-contact cuff recordings.

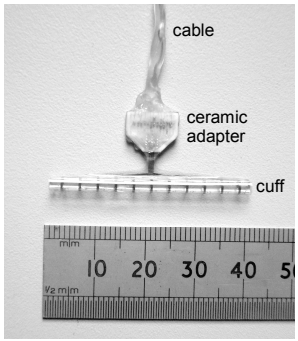

Figure 3-4 – The polyimide thin-film cuff electrode has eleven contacts, visible on this photograph as dark vertical lines. -

3.6 Neural Recording and Data Acquisition

In the initial set of frog experiments, the DAQCard 6062E from National Instruments was used. It is a fast, multifunctional card that has 16 single-ended or 8 differential analogue input channels, 2 analogue output channels, 2 counters and 8 digital lines.

Figure 3-5 – NI-DAQ 6062 E-Series PCMCIA Card.

Specifications: Analogue Input Characteristics

Number of Channels =	16 single-ended, 16 pseudo-differential, or 8 differential. -
Type of ADC =	Successive approximation. -
Resolution =	12 Bits, 1 in 4096. -
Max. Sampling rate =	500 kS/s -

Specifications: Analogue Input Characteristics

Number of Channels =	2 Voltage. -
Resolution =	12 Bits, 1 in 4096. -
Voltage Output range=	± 10 V -
Output Impedance =	0.1 Ω Max. -
Current Drive =	± 5 mA Max. -

The following diagram shows the connector assignments. The pin numbers on the connector on - the left hand side correspond to the pin-connector numbers on the CB-68LPR connector, - shown on the right hand side -

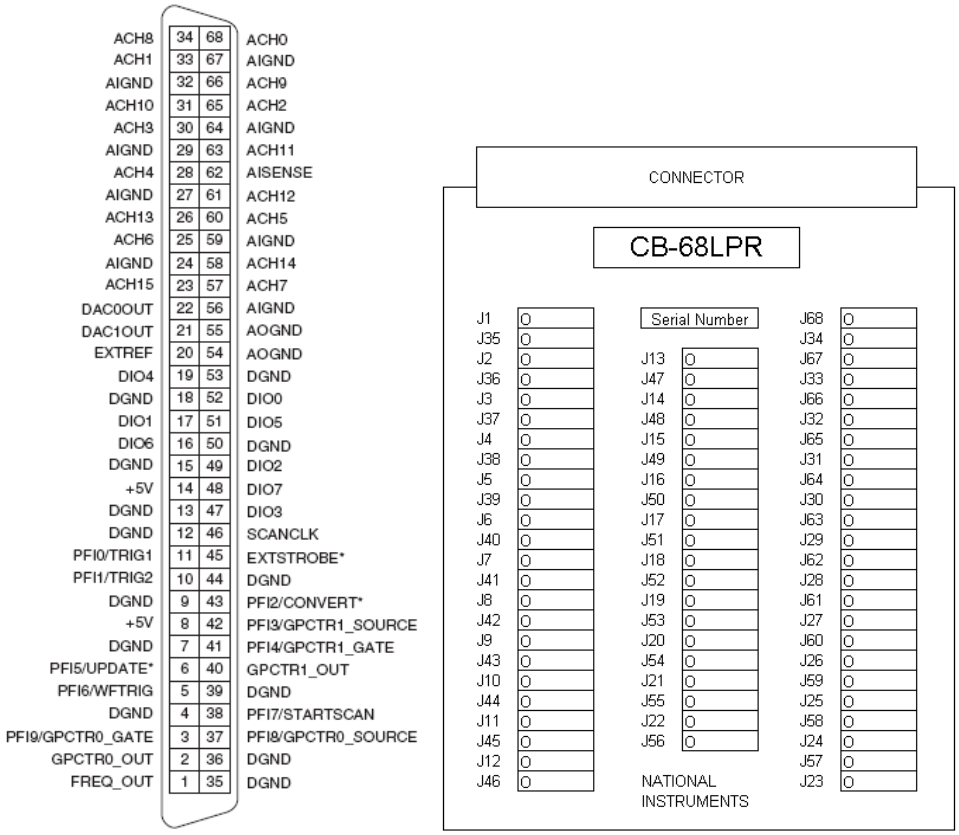

Figure 3-6 – *LHS*: 68-Pin E-Series Connector Assignment, *RHS*: CB-68LPR Connector.

The contacts of the recording cuff were connected directly to the inputs of a custom-built low-noise neural amplifier bank, a developed version of an ASIC described in [19]. This amplifier bank provides ten channels of differential amplifiers with a pass band of 310 Hz to 3.3 kHz, a voltage gain of 10,100, and an input-referred voltage noise density of 3.8 nV/√Hz at 1 kHz. The hook electrode was connected to an instrumentation amplifier with a gain of 500 and a band pass of 17 Hz to 8.8 kHz. The outputs of the amplifiers were fed into a data acquisition system, based on a NI DAQCard-6062E (National Instruments, Austin, TX, USA), that allowed sampling at 40 kHz and a dynamic range of 12 bit for the ten nerve signals, the stimulation signal, and the hook electrode signal.

The setup was controlled by a laptop computer (Dell Inspiron 9200) via a LabView 7.1 user interface (National Instruments). Fig. 3-7 gives a schematic overview of the setup and Fig. 3-8 gives a view of the LabView 7.1 user interface.

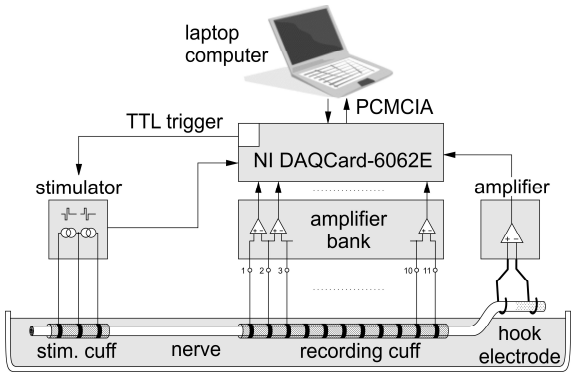

Figure 3-7 – Setup for recording electrically evoked CAPs from frog nerve in Ringer's solution - using an eleven contact recording cuff and a hook electrode (for validation purposes). -

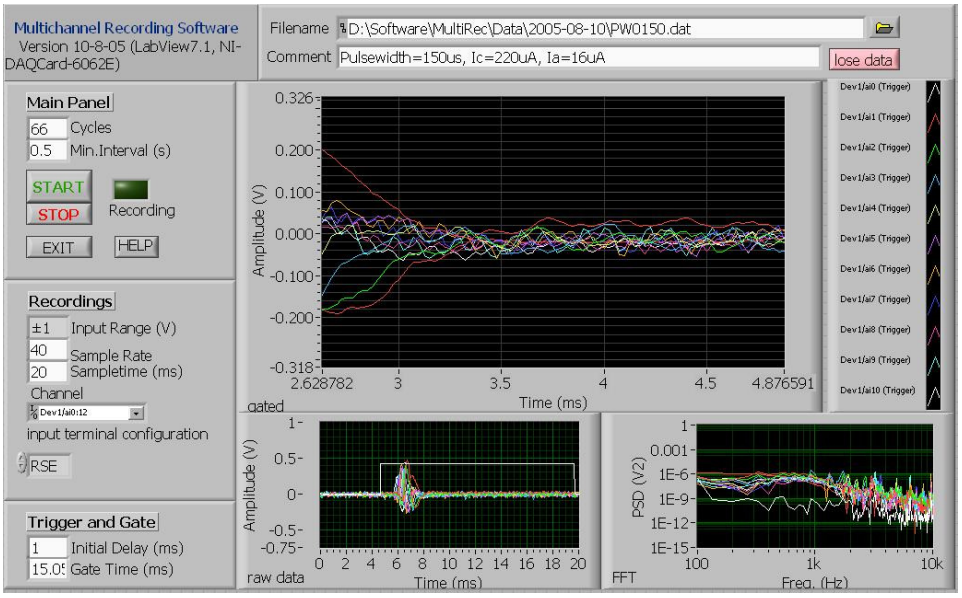

Figure 3-8 – User-interface of the LabView software.

3.7 Neural Stimulation

The stimulation was triggered by the LabView program via the NI DAQCard. A custom made nerve stimulator was used that generates current controlled, charge balanced, rectangular shaped pulses on two latched channels. The stimulating pulse was adjustable in amplitude and pulse width, while the amplitude of the charge recovery phase was set to 20 μA. A set of stimulation parameters was found that just excited a single population of large fibres, resulting in a simple-shaped biphasic CAP recording picked up by the hook electrode. Another set of stimulation parameters was worked out that resulted in a hook electrode neurogram which suggested the presence of at least a second fibre population, slower in propagation than the first one.

3.8 Data Processing

The data for this experiment is located in Appendix A. Data processing was carried out offline using Matlab R12 (The Mathworks Inc., Natick, MA, USA). The Matlab routine calculated nine tripolar signals from the ten outputs of the bipolar amplifiers. Then, the signal of tripole number

2 was delayed in time by *dt* relative to the signal of tripole number 1 and added to it. The signal from tripole number 3 was added to this sum after delaying it by 2x *dt*. Signal number 4 was delayed by 3x *dt* and added, and so on. After summation, the signal was full-wave rectified and its maximum voltage peak was detected. A delay profile was generated by plotting the maximum voltage peak as a function of the delay time *dt*. Appendix A contains the Matlab code.

3.9 Anodal Blocking Theory

As the pulse currents amplitude is increased, APs may be blocked at the anode; this is called 'Anodal Blocking'. Anodal blocking only occurs at currents above the stimulation threshold. Large fibres have a lower blocking threshold than small fibres. Therefore, anodal blocking allows stimulation of small nerve fibres without stimulation of the large fibres ('selective stimulation by fibre size'). The work by Rijkhoff et al. [49] demonstrates this method. However for anodal blocking to be successful the pulses have to be removed slowly to prevent re-excitation of the nerve at the end of the stimulating pulse.

For successful anodal blocking, a nerve cuff must be used which has minimal external current flow. Current flowing outside of the nerve cuff can stimulate the nerve outside of the cuff causing the anodal blocking to fail.

Unlike conventional neural stimulation control of both the pulse amplitude and pulse duration are necessary to obtain successful selective stimulation. Control of the amplitude of the reverse phase of the stimulating pulse is also needed to prevent APs being generated when the pulse is removed.

3.10 Anodal Blocking Set-up

The sciatic nerve of Xenopus Laevis frog was explanted over a length of about 8 cm and kept in amphibian Ringer's solution. A tripolar stimulation cuff "A" was placed at the distal end of the nerve. This cuff as 1.0 mm in diameter, the electrode contacts where arranged at a pitch of 5 mm, were 0.2 mm wide and coated with platinum black (impedance at 1 kHz below 1 kΩ). For AC-block experiments, a second cuff "B" of the same type was wrapped around the nerve with a distance of about 1 cm to the cuff "A". For velocity selective recording, a third cuff "C" was placed at the proximal end of the nerve. This cuff had a diameter of 1.5 mm and carried 11 platinum contacts (pitch: 3.5 mm, width: 0.5 mm). This cuff was connected to custom designed amplifier chip that provided an array of bipolar amplifiers and filters. As described previously in section 3.4, the 10 outputs of this amplifier were similarly monitored by a data acquisition (DAQ) system (DAQCard-6062E, National Instruments), which sampled each channel at 40 kHz with dynamic range of 12 bit. This data was handled by LabView and saved

to disk of the laptop computer. Converting 10 bipolar recording channels to 9 tripolar channels, introduction of time delays dt and summation was carried out off-line by Matlab routine.

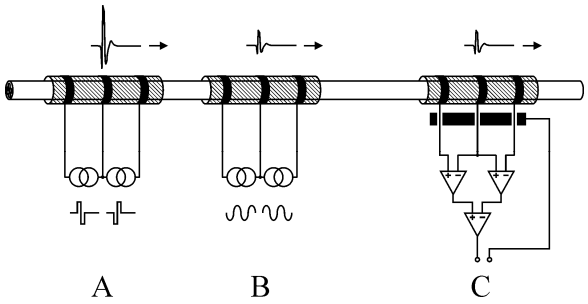

Figure 3-9 – Anodal blocking setup.

3.11 Anodal Blocking Procedure

At first, only cuff "A" and "C" were installed, the stimulation intensity of a charge-balanced, current-controlled pulse was gradually increased while the neural response was monitored by cuff "C" and the DAQ system.

The second experiment involved the third cuff "B", which was used to inhibit propagation of APs excited by cuff "A" travelling towards cuff "C". While cuff "A" stimulates the nerve on super-threshold level, a sinusoidal current (20 kHz) was fed into cuff "B". This current was gradually increased in amplitude while the electrical signals picked up by cuff "C" were monitored.

The third experiment focussed on evaluation of anodal blocking of nerves. Anodal blocking pulses are not purely inhibiting nerves but provide a so-called "blocking window" in which only small fibres are excited while large fibres are electrically blocked. This window is a function of charge. Outside the blocking window either only the large fibres are stimulated or large and small fibres. In this experiment, the intensity (charge) of the anodal blocking pulse was gradually increased and the neural response was monitored.

For all experiments, propagation velocity profiles were generated that show the maximum amplitude of the rectified signal after time-shifting and summation of the 9 tripolar channels over the propagation speed and the related time delay *dt*. The delay domain is also converted to the velocity domain by calculating the velocity $v = p/dt$. The parameter p represents the recording electrode pitch.

3.12 Results and Discussion

3.12.1 Hook Electrode Recordings

The nerve was stimulated at low intensity with a rectangular pulse shape: 1.3 mA x 100 μs = 0.13 μC. This caused the hook electrode (Described in Section 3.5) to detect a CAP that has a pronounced positive phase followed by a much weaker negative phase. Employing larger charges of 1.5 mA x 675 μs = 1.01 μC for stimulation changed the shape of the recorded trace. This resulted in the pronounced positive phase to peak later in time. During its decay, another positive phase appeared (Fig. 3-10). This behaviour was expected and known in electrophysiology as "inverse recruitment": the stimulation threshold of the fast and large diameter fibres is lower than that of the slow and small ones.

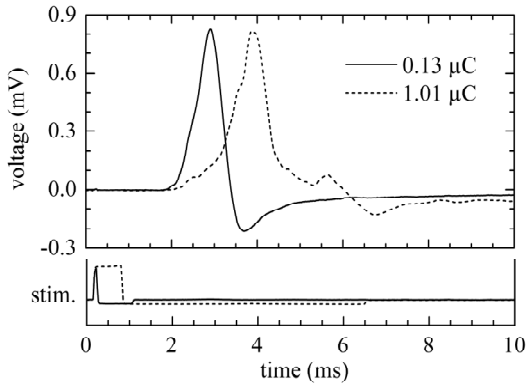

Figure 3-10 – Hook electrode recordings (top) and the stimuli that evoked them (bottom). Solid line: only one fast fibre population was excited. Dotted line: Two positive peaks indicate the activity of two populations.

The distance between the anodal contact of the hook electrode and the cathode of the stimulation cuff was 68 mm. The onset of stimulation took place at 0.15 ms (according to Fig. 3-10), the stimulus duration was set to 0.1 ms, which was just above stimulation thresholds of the large fibres. The positive slope of the CAP started at 2.075 ms, which gives a latency of 2.075 ms – (0.15 ms + 0.1 ms) = 1.825 ms. Therefore, the propagation velocity of this CAP was 68 mm / 1.825 ms = 37.3 m/s.

A larger stimulation pulse width was chosen in order to introduce enough charge for additionally exciting smaller fibres. The onset of the stimulus was at 0.15 ms, the pulse width was now 0.675 ms, and the CAP of the first positive phase of the hook electrode recordings begins at 2.125 ms. Assuming that this first phase was excited by the same charge as in the case described earlier, the calculated velocity is 68 mm / (2.125 ms – 0.15 ms – 0.1 ms) = 36.3 m/s. The onset of the second phase of the recordings was at 5.325 ms. It took all the charge provided by the pulse to excite this fibre population. Therefore the latency is 5.325 ms - (0.15 ms + 0.675 ms) = 4.5 ms. The propagation velocity calculates to 68 mm / 4.5 ms = 15.1 m/s.

3.12.2 Cuff Electrode Recordings

The nerve cuff recordings are smaller in amplitude than the hook electrode signals; interference and noise are more pronounced. Fig. 3-11 and Fig. 3-12 show the amplified bipolar signals after converting them to tripolar signals using Matlab. The y-axis shows the position of the tripole along the cuff. The further distant the tripole, the longer the time the signal needs to appear. Fig 3-12 shows the effect of higher level of stimulation intensity than in Fig 3-11. In this case the dispersion of two different CAPs can be seen.

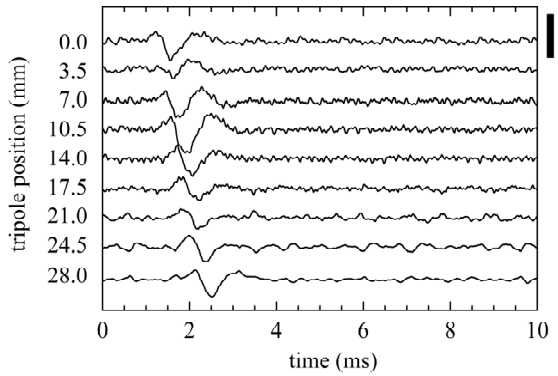

Figure 3-11 – Tripolar recordings of electrically evoked potentials, recorded with the eleven-contact cuff. The stimulation intensity was 0.13 μC. The black bar to the right shows the -amplitude scale: 50 μV. -

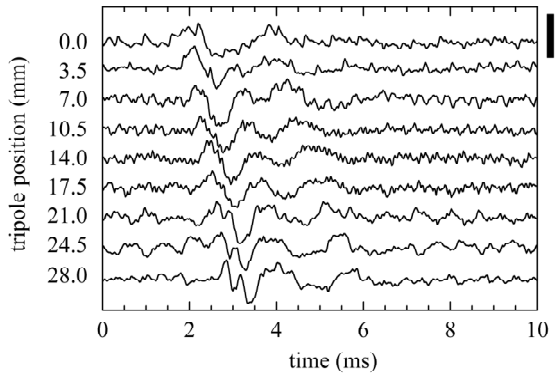

Figure 3-12 – Tripolar recordings of electrically evoked potentials, recorded with the eleven-contact cuff. The stimulation intensity was 1.01 μC. The black bar to the right shows the amplitude scale: 50 μV.

As described earlier, processing the cuff data results in a time delay, with peak amplitude profile for each of the two stimulation intensities (shown in Fig. 3-13). At low stimulation intensities a single distinct peak can be found at a delay of dt = +125 μs. The contact pitch of the cuff electrode is 3.5 mm, therefore the propagation velocity of this fibre population is 3.5 mm / +125 μs = +28 m/s. The plus sign indicates the direction the recorded nerve signals (away from the stimulation electrode towards the recording cuff). At high stimulation charges, we find two

peaks, one at +100 μs that corresponds to a velocity of +35 m/s and smaller one at +250 μs, which relates to a speed of +14 m/s.

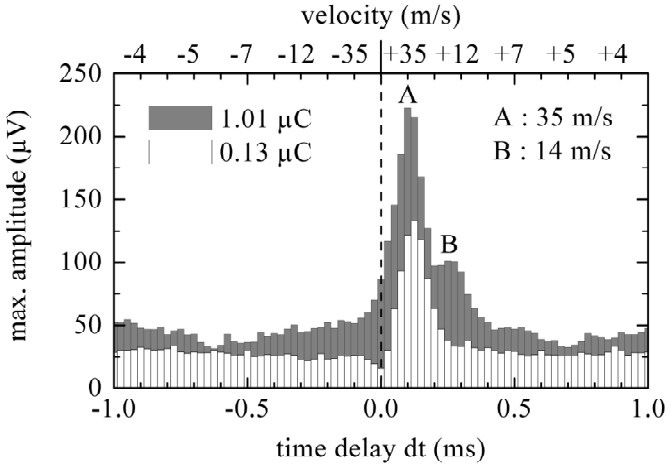

Figure 3-13 – Two delay profiles corresponding to two different stimulation intensities: grey: 1.01 μC, white: 0.13 μC. The bars have a width of 25 μs which is the reciprocal value of the sampling frequency.

3.12.3 Electrode Discussion

Comparing the propagation velocities obtained with the two different methods (cuff and hook), it is clear that the results of both are in the range described in the literature for frog nerve at room temperature: normally up to about 42 m/s [1]. However, the actual values differ, depending on the applied method as shown in Table 3-14.

Stimulus charge	Hook	Cuff
Q_{stim} = 0.13 μC	v_1 = 37.3 m/s	v_1 = 28.0 m/s
Q_{stim} = 1.01 μC	v_1 = 36.3 m/s v_2 = 15.1 m/s	v_1 = 35.0 m/s v_2 = 14.0 m/s

Table 3-14 – Predominant propagation velocities observed with two different methods using a hook and a cuff electrode.

Possible errors are inherent to both methods. For the hook method the exact determination of timing and distance is crucial, but fine measurement of the distance between the hook and the stimulation cathode is difficult and also relating the onset time of a positive slope to the time during a long stimulation pulse when the stimulation threshold reached is a matter of guessing. The main problem with the cuff method is the minimum delay time *dt*, which is the reciprocal value of the sample frequency. Setting the sampling frequency to 40 kHz leads to a coarse resolution of the velocity profile at higher speeds, as shown in Table 3-15. Clearly, the use of a DAQCard with a higher sampling rate would remove this difficulty.

dt (µs)	25	50	75	100	125	150	175
v (m/s)	140	70	47	35	28	23	20
dt (µs)	200	225	250	275	300	325	350
v (m/s)	18	15	14	13	12	11	10

Table 3-15 – The time delay dt is restricted to multiples of the sample interval (here: 25 µs) and therefore the velocity (v) profile has a low resolution at high speeds.

Calculating propagation velocities from a hook electrode recording is not only difficult (the point of fibre excitation during long pulses has to be guessed) but also cannot be transferred to neural prosthetic applications. In those, the nerve traffic is (macroscopically) chaotic and bi-directional.

3.12.4 Anodal Blocking Results

At low stimulation charge of 0.13 µC, only fast fibres (A: 35 m/s) were activated. Increasing the charge to 1.01 µC led to an increased activity of fast fibres but also excited slower fibres (B: 14 m/s), which contribute with a lower amplitude to the velocity profile, shown in Fig. 3-16.

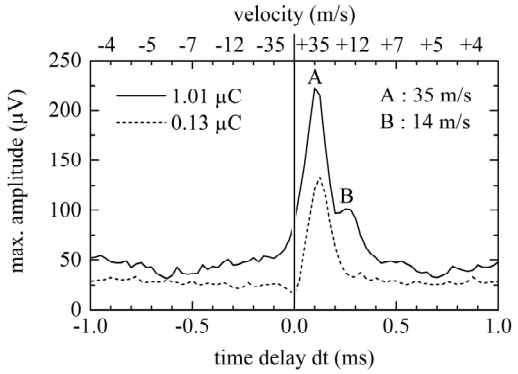

Figure 3-16 – Velocity profile of nerve electrically stimulated with two intensities. At high intensity, two fibre populations (A and B) dominate the profile.

A different nerve gave a similar profile when stimulated at super-threshold level, as described by the dashed line in Fig 3-17. Applying a sinusoidal wave of 10 mA amplitude allows the complete block of the propagation of the CAP. Furthermore, a smaller amplitude (4 mA) inhibits predominantly fast fibres (A: 35 m/s) while the slower fibres (B: 14 m/s) show increased activity compared to the CAP.

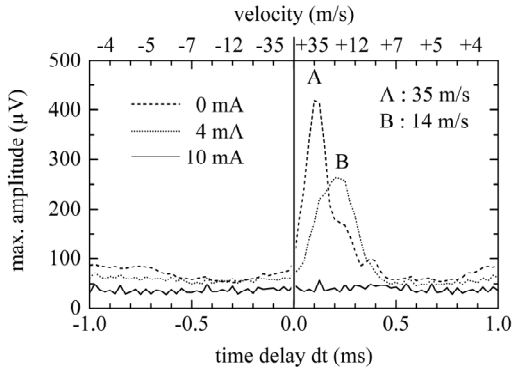

Figure 3-17 – Velocity profile of a nerve which is received anodal blocking pulses of increasing amplitude (charge).

Anodal blocking was carried out on a third nerve applying pulses of 550 µs width that had an exponential decay of a duration of 1 ms. The charge balancing phase was limited to 9 µA. The length of this phase depended on the amplitude of the first phase, which was gradually increased to 620 µA. Figure 3-18 shows that the stimulation amplitude of 140 µA was outside the blocking window, at 430 µA anodal blocking was achieved: The fast fibres (A: 23 m/s) are blocked and slow fibres (B: 11 m/s) are firing. Increasing the current to 620 µA led to inhibition of fast and slow fibres.

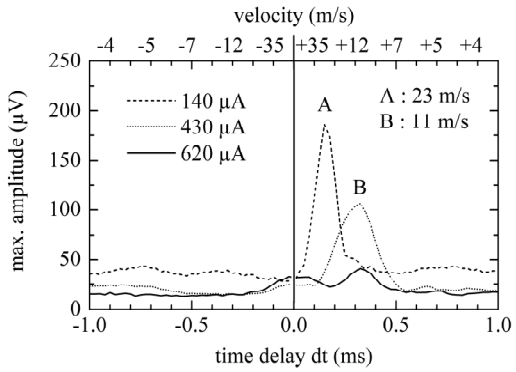

Figure 3-18 – Velocity profile of a nerve which electrically evoked compound AP is gradually blocked using sinusoidal currents amplitude from 1 mA to 10 mA.

3.12.5 Anodal Blocking Discussion

All three anodal blocking experiments show that the method of velocity selective recording based on MEC is capable of providing information on the distribution of fibre activity. Not only the propagation velocity of the fibres was identified, but also the direction of CAP propagation: no increased activity can be found in the negative velocity range in Figs. 3-16, 3-17 and 3-18. However, the method is limited in resolution (delay *dt* domain) by the sampling frequency. At 40 kHz, the smallest *dt* is 25 µs. This causes the profiles to be coarse for high velocities and provides an increasing definition with decreasing velocities.

The obtained velocity profiles match the report of fibre activities given by literature: Gradually increasing an electrical stimulus in intensity, leads to "inverse recruitment", as shown in

Figure 3-16. This stimulus selectively stimulated fast fibres first. AC blocking at low intensities - blocks fast fibres but stimulates slower fibres [50]. Anodal blocking also stimulates fast fibres at low amplitudes, increasing the amplitude caused inhibition of fast fibres while slower fibres were excited [51].

3.12.6 Conclusion

Multi-contact cuff recordings can be interpreted with ease and should work with a bi-directional, neural traffic. This is reflected by the results discussed in section 3.12. Using explanted nerves it has been demonstrated that this method is applicable to in-vitro setups and provides information in the shape of a profile of the conduction velocity of the active fibres as well as their direction of propagation. The anodal blocking experiments show that this method of velocity selective recording based on a MEC is indeed capable of providing such information. This meets one of the objectives of this project, which is to demonstrate real-time velocity-selective classification. These results therefore validate the work thus far.

3.12.7 Next Steps

The next phase of the project takes into consideration naturally evoked potentials by performing acute experiments. The proposed animal model to be used in this scenario is the Medial Nerve of the Danish Landrace pig. This would allow for nerve lengths of about 9cm to work on. It will involve the same procedure as for the frog experiments. The major advantage of experimenting on this type of nerve rather than that of the Xenopus is that it is closer to the nerve characteristics of humans. However, there will be an attempt at having an improvement on smoothness by using a faster data acquisition card that has better spatial resolution, the current one being at 0.025ms.

Chapter 4

NATURALLY EVOKED POTENTIALS:

ACUTE PIG EXPERIMENTS

4.1 Introduction

The object of the acute experiments will be to monitor neural afferent signals generated by natural sensors using multi-electrode cuffs; to show that three distinct naturally occurring nerve signals (cutaneous, joint receptors and tendon stretch receptors) in one nerve can be separated. The work of Haugland et al. [12, 13, 16, 17] encompass the investigation of cutaneous nerve recordings. In the series of experiments, nerve cuff electrodes will be used within the frontal limbs of the pig to demonstrate that the nerves can indeed be triggered at different levels to produce distinct velocities. This would demonstrate real-time velocity-selective classification and recording with multiple-electrode cuff (MEC) electrodes. Eventually it would be ideal to further investigate Chronic measurements – Hansen et al. have shown that signals from cuff electrodes can be used chronically as inputs for neuroprostheses.

In the proposed experiments, the pigs foot will be flexed or extended in order to stretch the forearm muscles and produce 'spindle' and 'Golgi tendon organ' responses. Whether we want to flex or extend will depend on which nerve is recorded from; during these initial experiments, the flexor muscles will be stretched when the median nerve is recorded. However, the apparatus should be 'flexible' enough so as to stretch the extensor muscles and record from the radial nerve as well. For the first set of experiments, the wrist extension motion (which acts to stretch the flexor muscle) will be used. The same routine of recording as done so far will be applied to different scenarios as described by the following 3 category of experiments:

Experiment 1: Trials with only the cutaneous stimulation applied (Cutaneous receptors targeted). There will be NO motion at the wrist;

Experiment 2: Trials with only the wrist rotation (and hence stretch of the wrist muscles – Stretch receptors targeted). A change in angle will cause the muscles to contact, hence causing the nerves to fire. This targets muscle afferents only.

Experiment 3: Trials with both stimuli applied at the same time (Both Cutaneous and Stretch receptors targeted).

At the end of the experiments, it should be possible to look for the superposition of the two response contributions. This can provide information as to the ability of the cuff to separate the

cutaneous afferent activity from the muscle afferent activity. An approach would be to have two arbitrary waveform generators, one for each motor, and a means of synchronizing them. These waveforms will be recorded along with the output data for later evaluation of the nerve responses. The waveforms have to be smooth since the afferent receptors will respond to any 'cogginess' in the waveforms.

4.2 Danish Landrace

Figure 4-1 – A typical Danish Landrace pig.

The species of pig used in our experiments was the Danish Landrace. The latter is a medium to large breed that has a distinct physical appearance. They are white in colour, have a rather fine hair coat, long snouts and heavy drooping ears. They have long bodies, deep smooth sides, and a noticeable lack of excess fat and wrinkles. The following picture, reproduced from [52], depicts the top and side views of the limb nerve anatomy. The portion of nerve we are interested in working on is the medial nerve, highlighted in yellow and labelled as '27' in Fig. 4-2.

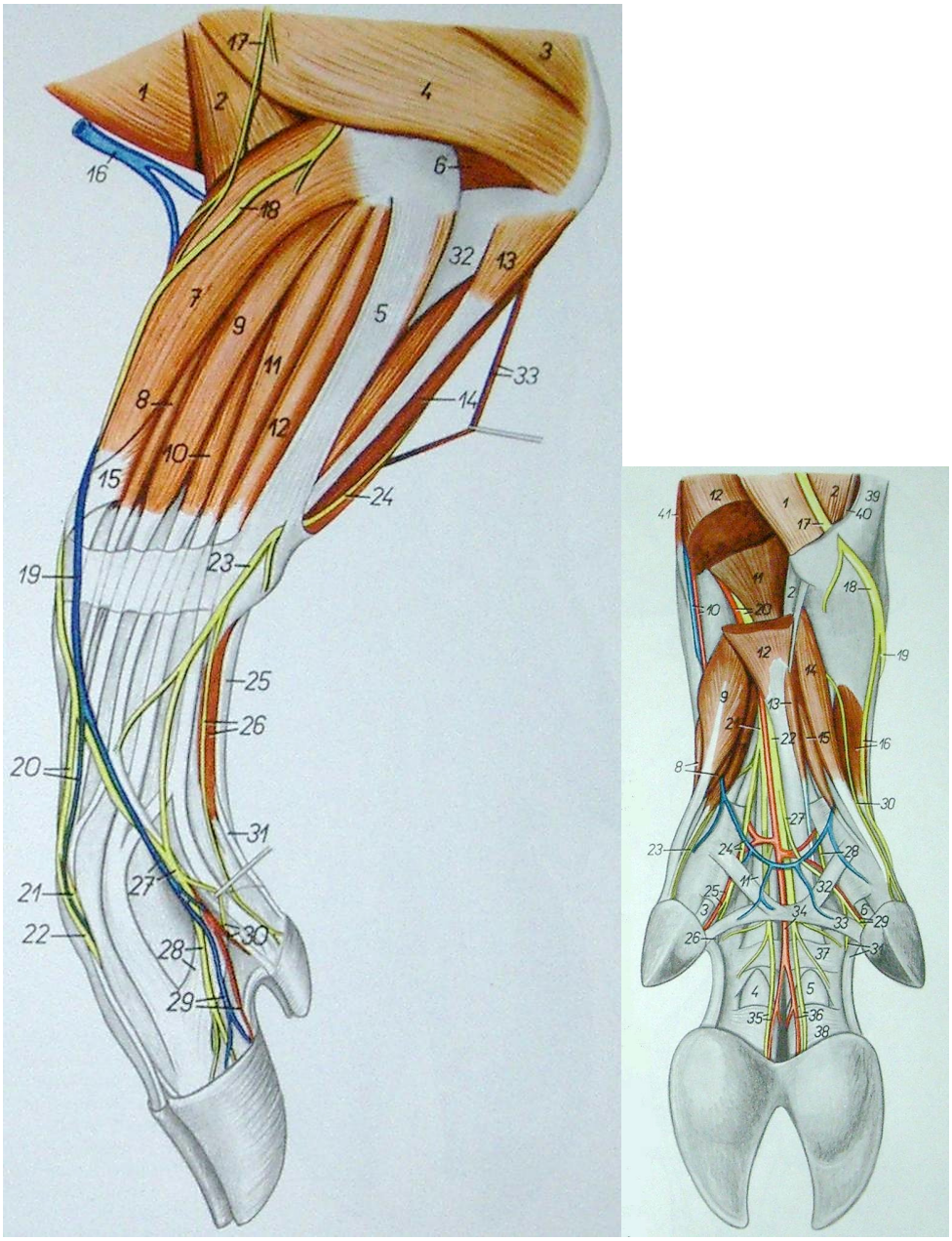

Figure 4-2 – Topographical view of the pig's limb; *LHS*: Lateral view, *RHS*: Anterior view

4.3 Data Acquisition: National Instruments

As mentioned previously, in order to improve on smoothness of the recording quality, a faster data acquisition card that has better spatial resolution has been purchased and the main differences are shown in the following table:

General	DAQCard-6062E	USB-6251
Price	£795	£895
Bus Type	PCMCIA	USB
Product Family	E Series	M Series

Analog Input		
Number of Channels	16 SE/8 DI	16 SE/8 DI
Sample Rate	500 kS/s	1.25 MS/s

Resolution	12 bits	16 bits
Maximum Voltage Range	-10..+10 V	-10..+10 V
Number of Ranges	4	7
On-Board Memory	2048 S	4095 S

Analog Output		
Number of Channels	2	2
Update Rate	0.85 MS/s	2.8 MS/s
Resolution	12 bits	16 bits
Maximum Voltage Range	-10..10 mV	-10..+10 V

Digital I/O		
Number of Channels	8 DIO	24 DIO
Timing	Static	Hardware timed (< 10 MHz)
Maximum Input Range	0..5 V	0..5 V
Maximum Output Range	0..5 V	0..5 V
Programmable Input Filters	No	Yes
Output Current Flow	Sinking, Sourcing	Sinking, Sourcing
Current Drive (Channel/Total)	24 mA/192 mA	25 mA/448 mA
Programmable Power-Up States	No	Yes
Pattern I/O	No	Yes

Counter/Timers		
Number of Counter/Timers	2	2
Resolution	24 bits	32 bits
Maximum Source Frequency	20 MHz	80 MHz
Maximum Range	0..5 V	0..5 V
Timebase Stability	100 ppm	50 ppm
GPS Synchronization	No	No
Pulse Generation	Yes	Yes
Buffered Operations	Yes	Yes
Debouncing/Glitch Removal	No	Yes

Physical Specifications		
Length	8.56 cm	26.67 cm
Width	5.4 cm	17.09 cm
Height	0.5 cm	4.45 cm

Table 4-3 – Difference in DAQ Specifications.

4.4 Motor Variables

The controlled variables of any given motor can be classified as such:

1. Speed Control.

The function of the speed servo amplifier is to keep the prescribed motor speed constant and independent of load changes. To achieve this, the set value (desired speed) is continuously compared with the actual value (actual speed) in the control electronics of the servo amplifier. The controller difference determined in this way is used by the controller to regulate the power stage of the servo amplifier in such a manner that the motor reduces the controller difference. This represents a closed speed regulating circuit.

2. Position control. -

The positioning control ensures a match between the currently measured positions with a target position, by providing the motor with the corresponding correction values, as with a speed controller. The position data are obtained from the digital encoder.

3. Current control

The current control provides the motor with a current proportional to the set value. Accordingly, the motor torque changes proportionally to the set value. The current controller also improves the dynamics of a superior positioning or speed control circuit.

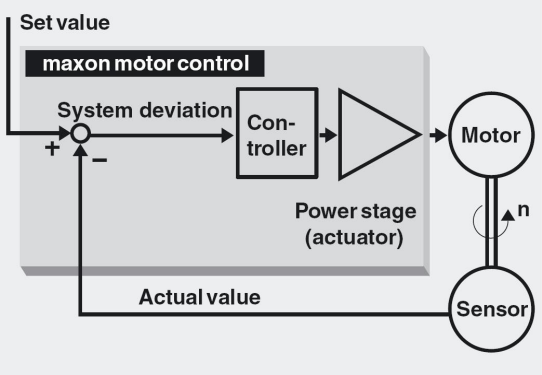

Figure 4-4 – Block Diagram of Maxon Motor Control: Feedback.

The requirements of the motor in our experiments were expected to be such that:

1. - The output shaft must be able to move the pig's ankle. The lever arm for this should be about 10cm up to 15cm to have a safety margin.

2. - 10N of force should be sufficient to rotate the ankle against the passive joint stiffness. Any greater torque capabilities would be welcome if ever the ankle were to be rotated against an active contraction.

3. - The velocity of the rotation should be about 25 degree per second in order to get a reasonable neural discharge from the muscle receptors.

Lower gear ratios for the motor will allow greater torques to be produced. This is more useful than greater rotational speeds considering the possibility of rotating the ankle against some muscle contraction in future experiments. Higher rotational velocities will result in a larger amplitude neural discharge - but if the velocity selective recoding paradigm only works with high velocity joint motions, then the concept will not be useful clinically.

If we design for a torque of 10 N at a lever arm length of up to 15 cm, then this is 10N x 0.15m = 1500 mNm which is needed after the gear train.

Other considerations are the amount of power that the motor would require. We require a controller that needs about 12 to 24 volts and less than about 10 amps because otherwise the motor servo amp will be very bulky and expensive.

4.5 Maxon EC Motor

Maxon EC motors are electronically commutated DC motors. Designed as internal motors, their shafts turn with no detent thanks to an ironless winding. This offers benefits such as high dynamism, low inductance and high efficiency and reliability.

The existing Maxon motor available for the project had for specification 12 Volts and 10 Amps (120 Watts – Maxon EC 40 – Part number 167177 on the Maxon catalogue). A brushless motor is highly appropriate for the nature of our experiments to avoid the possibility of the motor brushes generating electrical noise that would contaminate the nerve recordings.

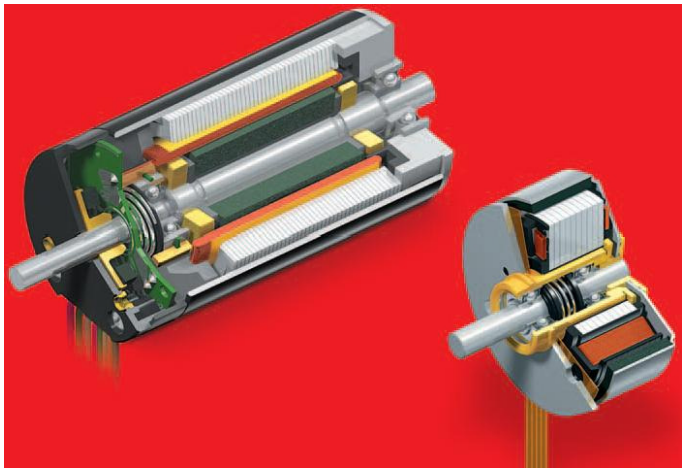

Figure 4-5 – Maxon motor mechanism.

Unfortunately, it was discovered that there was an incompatibility between the existing motor controller and the EC 40 motor and the motor didn't come with a rotary position encoder and a set of gears. Therefore the solution was to buy the appropriate power supply, a gear head, an encoder and controller.

4.5.1 Maxon Planetary Gearhead

Based on the specifications of the Maxon EC 40 motor, the available gearhead that meets our requirements is the Planetary Gearhead GP42C (Part number 203131 on the Maxon catalogue). This has a gear ratio of 230:1.

4.5.2 Maxon HEDL Encoder

The motor is equipped with a digital encoder that provides a certain number of pulses per revolution. The turning direction is detected with the square pulses of channels A and B offset by 90 electric degrees.

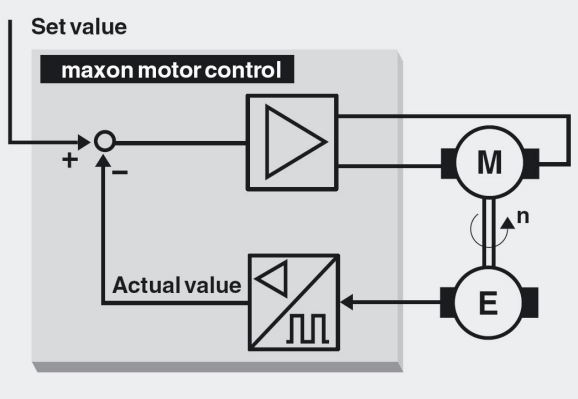

Figure 4-6 – Block Diagram of Maxon Motor Control: Encoders.

Encoders can be generally categorised into optical (photoelectric), magnetic encoders, and mechanical contact types. There are two basic types of encoders: rotary and linear. The technical principles behind them are somehow similar.

Linear and rotary encoders operate on the principle of the photo-electrical scanning of very fine gratings. The so-called scanning unit in an encoder consists of a light source, a condenser lens for collimating the light beam, the scanning reticle with the index gratings, and silicon photovoltaic cells. When the scale is moved relative to the scanning unit, the lines of the scale coincide alternately with the lines or spaces in the index grating. The periodic fluctuation of light intensity is converted by photovoltaic cells into electrical signals. These signals result form the averaging of a large number of lines. The output signals are two sinusoidal signals that are then interpolated or digitized as necessary.

The output signals of incremental rotary encoders are evaluated by an electronic counter in which the measured value is determined by counting 'increments'.

The encoders provide a simple square signal for further processing in the control system. Its impulses can be counted for exact positioning or determining speed. Channels A and B pick up phase shifted signals, which are compared with one another to determine the rotation direction. A 'home' pulse (index channel I) then provides zero crossing and is used as a reference point for precise determination of rotation angle. The line driver produces complementary signals A, B, I which help to eliminate any interference on long signal lines. In addition, this electronic driver installed in the encoder improves signal quality with steeper signal edges.

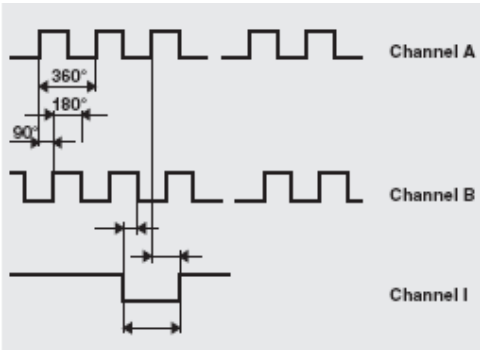

Figure 4-7 – Representation of the output signal of a digital encoder.

Encoders are normally positioned and coupled to the rear of the servomotor or to the screw and opposite to the drive via a backlash-free precision coupling. The spindle or motor shaft is directly connected to the shaft of the rotary encoder. The scanning unit is connected to the encoder shaft by ball bearings, however, without a rigid connection to the housing. Instead, a coupling is located between these components and compensates for alignment errors between both shafts.

An incremental rotary encoder with integral couplings is being used in our set-up, the HEDL 5540 from Maxon (Part number 110516 on the Maxon catalogue). This specific one has 500 counts per turn and 3 channels.

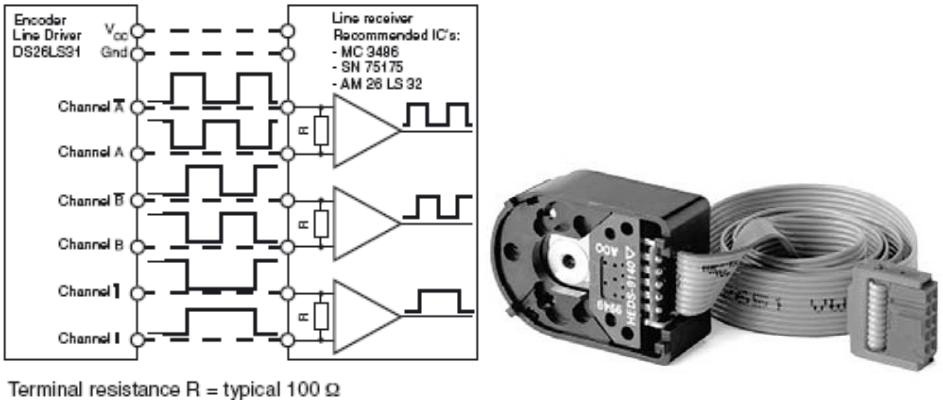

Figure 4-8 – Maxon HEDL Encoder

4.5.3 Maxon EPOS Controller

Maxon motor EPOS 24/5 (Part number 275512 on the Maxon catalogue) is a small-sized, fully digital smart motion controller. The sinusoidal current commutation by space vector control offers to drive brushless EC motors with minimal torque ripple and low noise. The integrated position-, velocity- and current control functionality cleverly suits our positioning application. The EPOS 24/5 is preferably commanded and controlled as a slave node through a serial data bus, the CANopen network. The CAN bus is an efficient data bus, very common in all fields of automation and motion control. The unit is operated through a RS-232 communication port.

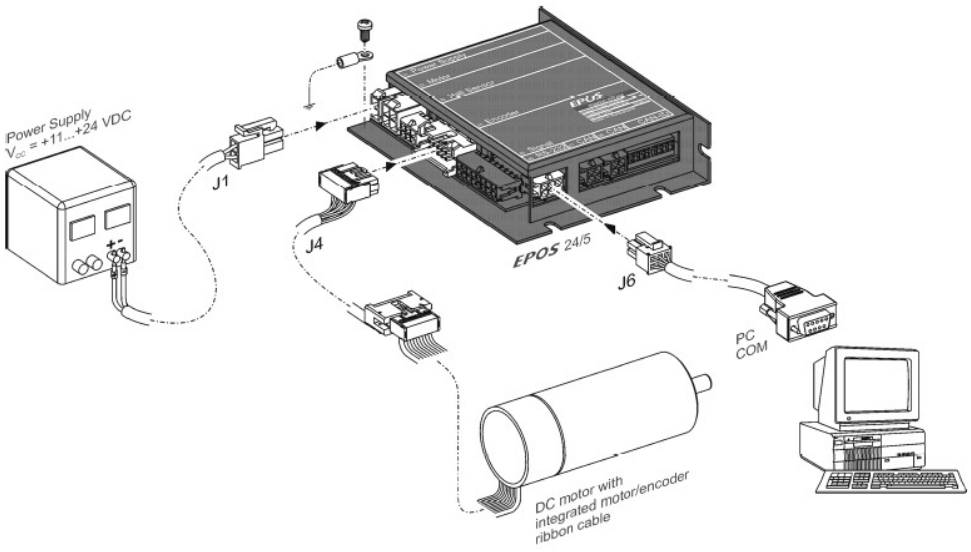

Figure 4-9 – Wiring for maxon DC motor with integrated motor/encoder ribbon cable.

4.5.4 Maxon Software

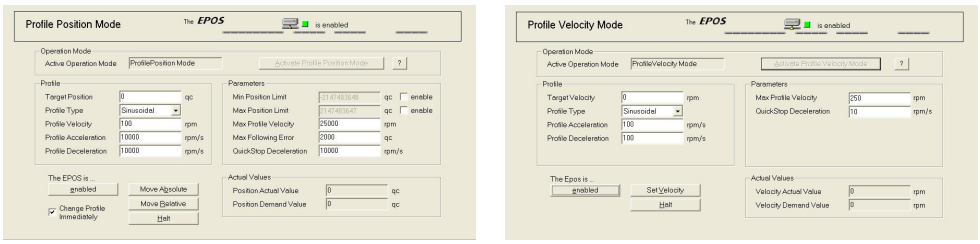

Figure 4-10 – Maxon software views: *LHS*: Position Mode, *RHS*: Velocity Mode

Maxon provides its own software manipulate the controller and DC motor performance. However, we need the motor movement and the solenoid/load-cell setup to be working simultaneously. This instigated the creation of our own software on LabView to have one window controlling all hardware functions.

4.6 Omron Power Supply

The power supply (available to buy from the university workshop) that could safely drive the Maxon EC motor was the Omron S8PS-600-24C. This has a power rating of 600W, output voltage of 24 V and would accommodate an output current of 27 A. This particular model has an interesting overload protection feature; if an excessive current flows for 5 s or more, the output will be turned OFF and simultaneously a protection –ON alarm indicator will be lit.

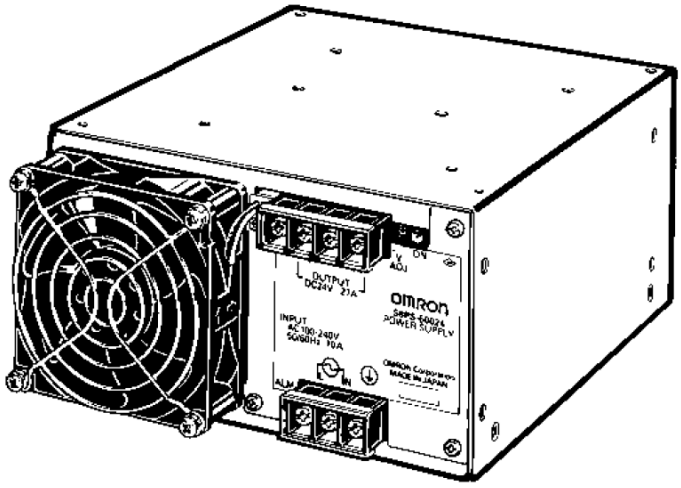

Figure 4-11 – Omron power supply -

4.7 Solenoid & Load-Cell Set-up

The solenoid has just 2 wires. The direction of the current determines the direction of motion and the amplitude of the current determines the excursion. The motor controller can be thought of as a big servo amplifier and a voltage ramp command can be generated by the computer analogue output board. That command will be compared with the position feedback signal to generate the error signal which is what must be ultimately passed to the motor output stage by the controller. The position feedback signal is a voltage provided by a linear potentiometer that will be mechanically coupled to the solenoid motor to measure its excursion.

The load cell is just to provide information about the force that is applied to the toe pad. When using a position ramp, the ramp slope (velocity) can be varied and the peak response of the nerve should be a linear function of the indentation velocity of the toe pad. This will produce a graph for analysis of the recovered nerve activity signal. If the nerve signal doesn't behave in this way then we will then suspect that recorded signal is not PURE cutaneous.

After the plateau of the toe indentation ramp is reached, there will be a certain force being applied to the toe pad. This will result in a tonic (steady state) nerve activity from the cutaneous receptors. This steady state nerve activity level will be a linear function of the force applied. By measuring the force applied graphs can be produced for different excursions and hence different levels of steady state force.

For the solenoid motor, a look up table could be used if the solenoid is not linear. The further the shaft extend (against a spring return) the more current is necessary to get to move out further. So its characteristics can be plotted and an excursion v/s voltage table can be made (The voltage conversion comes from the DC resistance of the solenoid coil). The computer can then look at the instantaneous desired excursion (position on the voltage command ramp) and

determine from the look up table what voltage is needed to get there. That voltage is then fed to the solenoid motor servo amplifier, which determines the correction needed to get there from the present position.

For the solenoid device current must be regulated because that controls the force. Then an error signal is produced by comparing the voltage output of a calibrated load cell to the desired force. This force can be a particular level or it can be a ramp for instance or modulated in any other way. So for force control from the solenoid, a ramp voltage to feed the servo amp is needed (which converts the input voltage to a current).

The load cell is just a 4 legged strain gage bridge. So it has two leads for DC power and two leads to be lead to a bridge amplifier circuit. A voltage controlled source to power the load cell is needed, since the regulation of its excitation is critical to allow calibration. Generally about 2 or 3 volts is called for and the sensitivity of the load cell can be increased by increasing the excitation voltage. But this is limited by any self heating that takes place in the load cell.

The pig's foot will be flexed or extended in order to stretch the forearm muscles and produce 'spindle' and 'Golgi tendon organ' responses. Whether we want to flex or extend will depend on which nerve is recorded from; the plan is to stretch the flexor muscles when the median nerve is recorded. But the apparatus could be 'flexible' so the extensor muscles can be stretched and recordings made from the radial nerve as well. Having two nerve recording cuffs one on the median nerve and one on the radial nerve could allow the joint to be controlled since we would then ideally have a pair of sensors - one to signal flexion and the other to signal extension. For the first study, wrist extension motion alone (which acts to stretch the flexor muscle) is planned. The load cell is in series (mechanically speaking) with the solenoid and the pig toe pad. The sensor sends a signal indicating the compressive force against the toe pad.

The solenoid should be programmed to make ramp and hold force profiles. A range of velocities such as 1 N/s to maybe 25 N/s is needed. This will produce some output from the cutaneous receptors in the toe pad. The transient afferent activity will be a linear relation with the velocity during the ramp portion. The tonic (DC) part of the activity will be much smaller but will be a function of the magnitude of the compression.

Some trials will be run with only the cutaneous stimulation applied; the next batch of trials will consist of only the wrist rotation (and hence stretch of the wrist muscles; and finally, the last set of trials with both stimuli applied at the same time. The simultaneous activity could also include a static level of toe contact with a dynamic rotation of the wrist and vice versa.

Once this is achieved, we need to then look for the superposition of the two response contributions. This can provide information as to the ability of the cuff to separate the cutaneous afferent activity from the muscle afferent activity. The ultimate target is to find a way to synchronize the activity of the solenoid and the rotation motor. Furthermore, the muscle spindles are very sensitive, so any rotation movement at all will cause them to discharge. A mechanical locking of the rotation axis would be a solution. A few holes drilled into the rotation shaft at 30 deg intervals on the shaft and a pin (A tapered pin – To eliminate any play) to push into the hole would be an easy solution.

The load cell is the force sensor in the solenoid servo system. A signal is input for the force profile that we want the toe pad contactor to follow. This will be a sine wave, a ramp or a sigmoid, depending on the sensor polarity we either add or subtract the command signal and the sensor signal to get the error signal that is feed to the amplifier that drives the solenoid (we need to make sure to not make a positive feedback condition). The frequency should be maybe 1 Hz up to 5 Hz. When using a ramp and hold profile the ramp should last between 0.2s to 0.5s then about 2 sec plateau to be able to look at the static discharge from the cutaneous receptors and then relax the skin indentation again with a ramp in 0.2 to 0.5s. But the nerve activity during a sustained indentation of the skin will be very small compared to the activity that will be present during the phasic part of the stimulus.

Extra weight is bad since it limits the bandwidth of the solenoid. When handling the load cell, care should be taken not to subject it to off axis loads, and not to exceed the maximum axial load as well as else it will be destroyed.

4.7.1 Solenoid Details

The solenoid used in our experiments, made by Saia-Burgess, is the STA 26 x 52 Ledex Tubular Push-Solenoid, with a flat surface plunger without anti-rotation flat (Order number STA 195227-126 at Saia-Burgess). The solenoid itself weighs 190.8 g, 33.74 g of which is the plunger alone. This will be an important factor when discussing the design of the rig at a later stage. This specific model is usually intended for on/off operation such as lock/latch operations, and has a holding force of 52.58 N at 20°C. Therefore, appropriate modifications had to be made to suit our purpose. In order to physically fit the solenoid and load-cell together, the end of the shaft of the solenoid core had to be threaded.

Figure 4-12 – Saia-Burgess Solenoid: *LHS*: Solenoid model, *RHS*: Plunger modification. -

Size	Solenoid Type	Package Dimension (mm)		Max Stroke (mm)	Force (N) at Nominal Stroke and Specified Duty Cycle			
		Dia.	Length		100%	50%	25%	10%
STA 26 x 52	Push	26	52	17.8	2.22 – 3.34	4.45 – 8.37	8.90 – 12.9	17.9 – 23.14

Table 4-13 – Solenoid specifications. -

The performance of this solenoid is summarised in the following table and chart: -

Maximum duty cycle		100%	50%	25%	10%
Max ON time when pulsed continuously (Sec)		∞	360	32	8
Max ON time for single pulse (Sec)		∞	470	120	32
Watts (@ 20°C)		10	20	40	100
Ampere turns (@ 20°C)		1166	1649	2332	3688
Resistance	# Turns	VDC (Nom)	VDC (Nom)	VDC (Nom)	VDC (Nom)
8.44	1128	9.2	13.0	18.4	29.0

Table 4-14 – Solenoid performance. -

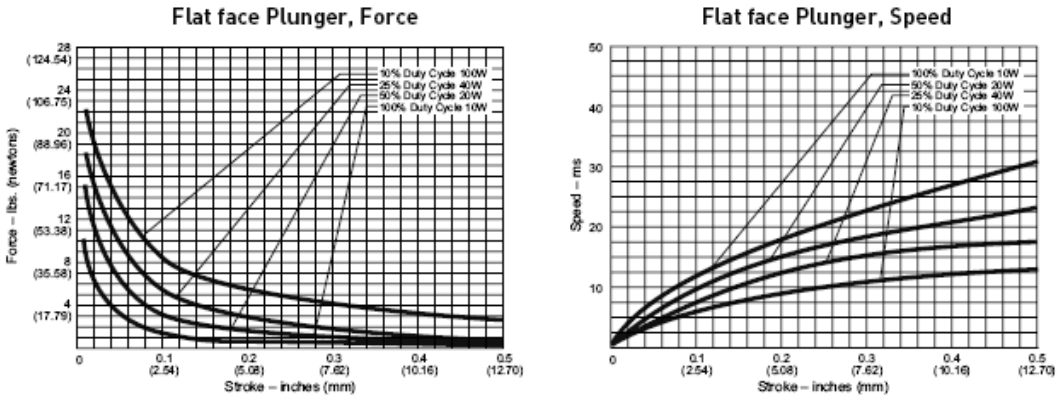

Figure 4-15 – Solenoid performance with flat face plunger. -

However, if there were the possibility of acquiring a new solenoid, one with a 60° plunger would have been more convenient for such a set-up. The main reason being that the latter works away from the fast-rising end of the force-distance characteristic, as shown in the following chart. The distance over which the force is experienced is relatively bigger, giving us a longer stroke.

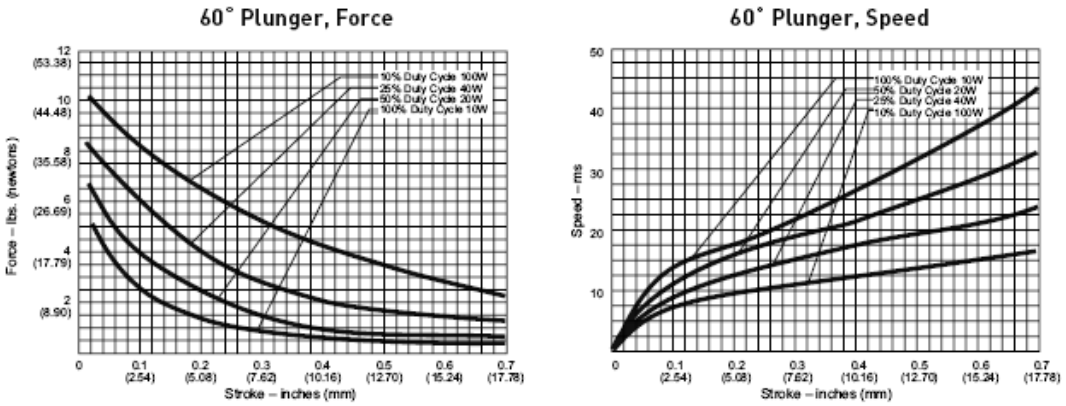

Figure 4-16 – Solenoid performance with 60° plunger.

4.7.2 Load-Cell Details

The Load Cell used was the Honeywell model made by Sensotec Sensors. It has a full scale range of 250 grams, an excitation of 5VDC, an input impedance of 622 Ω, an output impedance of 451 Ω and a calibration factor of 23.8423 mV/V.

4.8 Solenoid & Load-Cell Calibration & Testing

In order to confirm the correctness of the individual characteristics (As provided by the manufacturers) of the load-cell and solenoid when connected together, a series of tests were carried out. This was to ensure that either component would behave as expected even when coupled together.

4.8.1 Experiment 1: Load-Cell Calibration

The first task only involved the load-cell on its own. Using small masses of 20 g, the load-cell was stacked with 20g increments to about 500g. Plotting this graph proved that the load-cell was behaving linearly as expected.

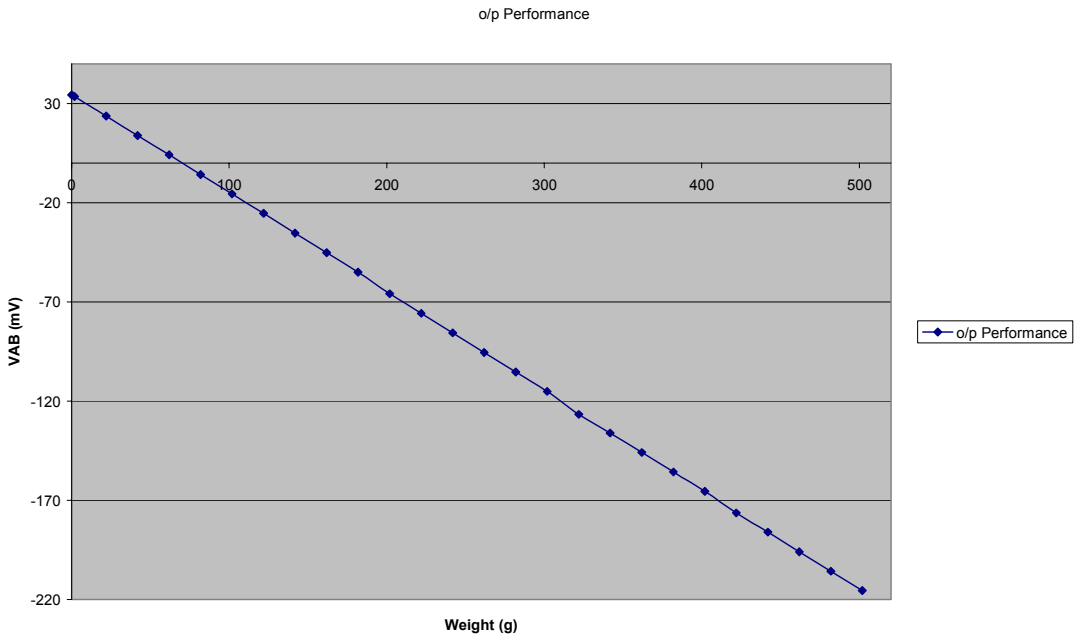

Figure 4-17 – Load calibration.

4.8.2 Experiment 2: Solenoid/Load-Cell against a hard surface

This experiment involved setting up the solenoid and load-cell against a hard surface and varying the voltage on the solenoid while recording the values on the load-cell. The results are shown in Fig. 4-19. In this case, we can see that the solenoid seems to be activated at around 5V and a somehow linear compression of the load-cell to about 7V.

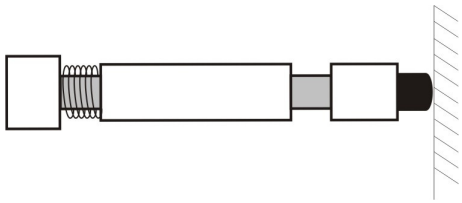

Figure 4-18 – Solenoid and load-cell setup. -

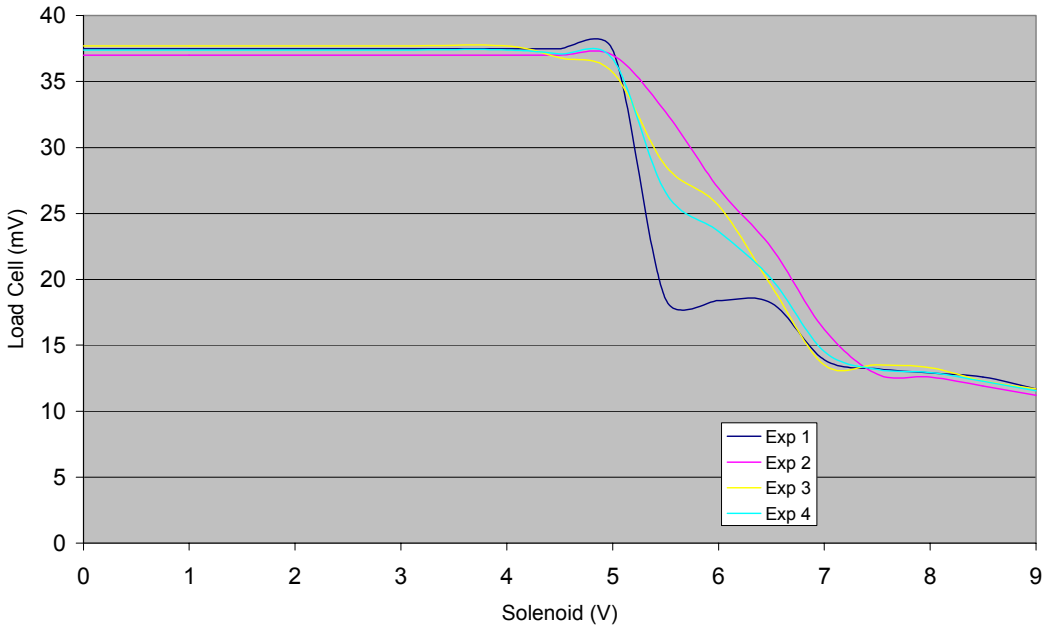

Figure 4-19 – Solenoid/Load-cell performance against a hard surface.

4.8.3 Experiment 3: Solenoid/Load-Cell against a soft surface

Now, to bring the situation closer to what the set-up is intended for, the solenoid/load-cell is set up against a soft surface, a not-so-rigid football in this instance, to mimic the toe pad of the pig's limb.

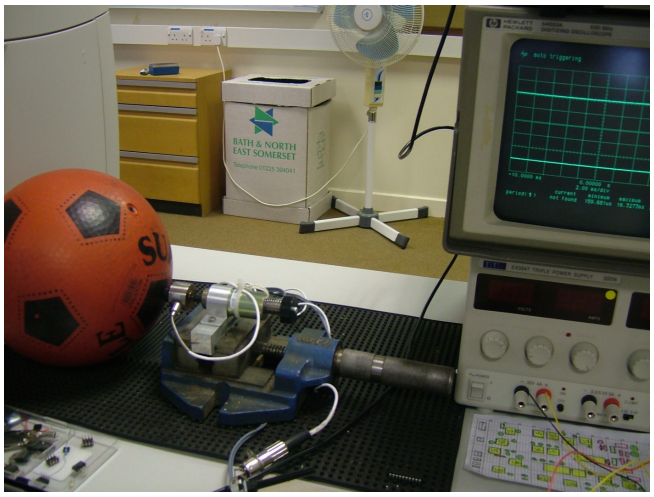

Figure 4-20 – Hard surface and soft surface comparison. -

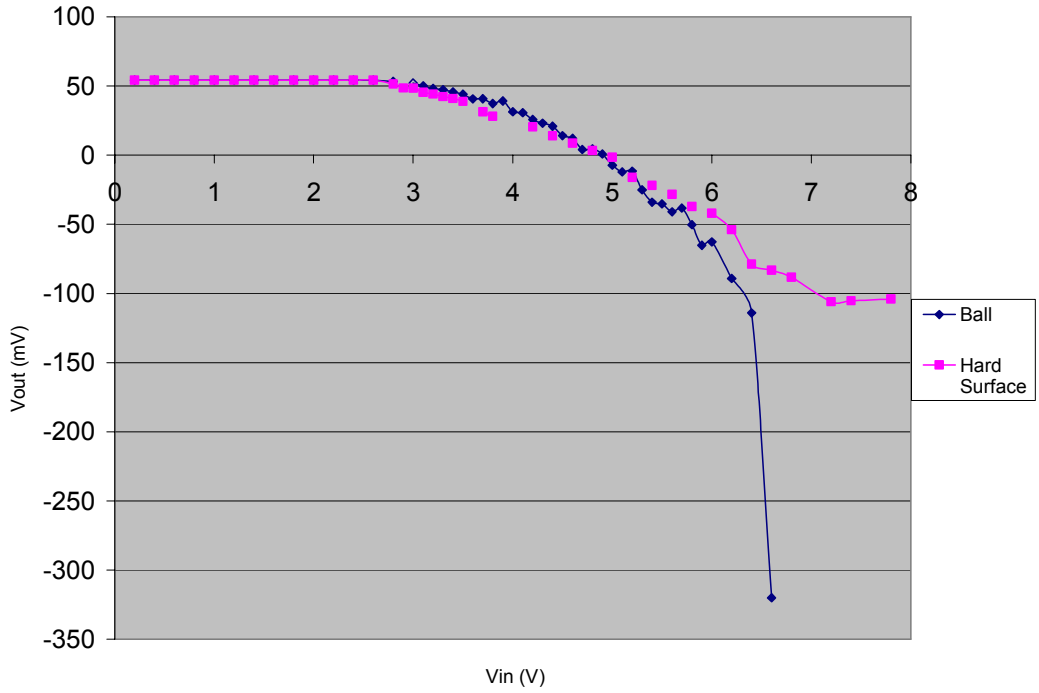

Figure 4-21 – Hard surface and soft surface comparison.

This has been plotted along with the performance of the solenoid/load-cell on a hard surface, so as to highlight any major difference. Considering the somehow linear portion between 3V and 6V, the plot with the hard surface had a gradient of -0.035 compared to -0.050 for that of the ball; Not a big difference. (See Appendix C for more media files)

4.8.4 Experiment 4: Solenoid/Load-Cell against a kitchen scale

In the last set on experiments, there was a similar set-up, the only difference being, instead of the hard surface or football, a kitchen scale was placed vertically against the solenoid/load-cell set-up. This seemed to be a convenient way to read the force generated by the solenoid in grams. Fig. 4-22 demonstrates the relevant outcome. The blue line shows the trend when a pulse wave is applied to the solenoid. Interpolating the two trends causes the lines to meet at the point where the load-cell reads 200g (2N) at an applied force of 0V. This 2N is a pre-load and can be adjusted. A pre-load is necessary to ensure that the loop is always closed for the PID to work properly.

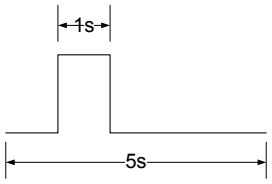

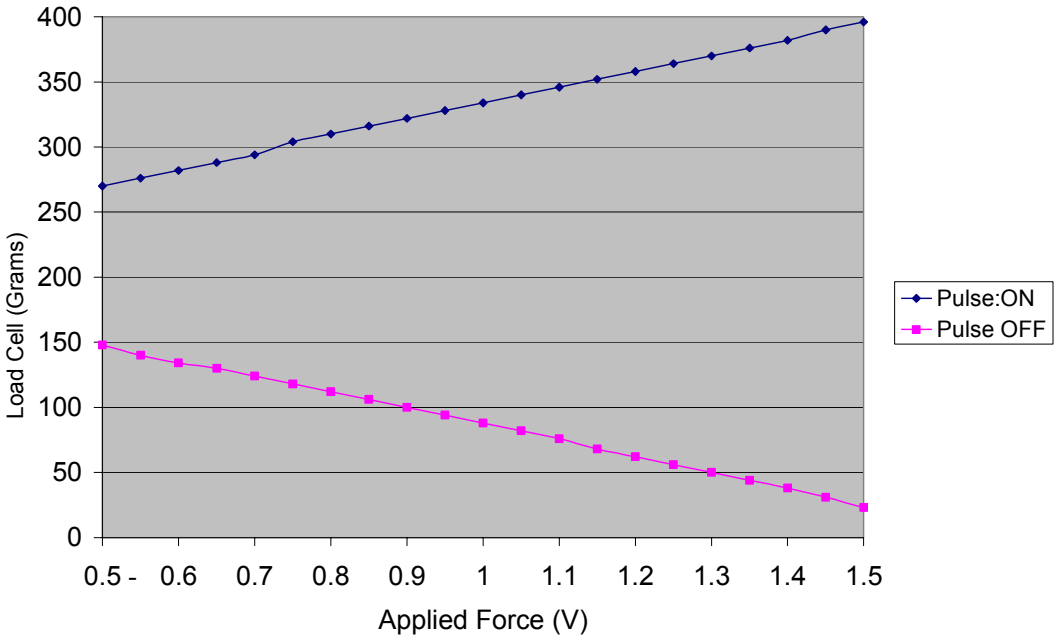

Figure 4-22 – Performance against a kitchen scale in pulsed mode.

4.9 PID Controller

In order to operate the solenoid and load-cell in a closed-loop system, a PID controller had to be designed. A PID controller is a simple three-term controller. The letters P, I and D stand for Proportional, Integral and Derivative respectively. The transfer function of the most basic form of PID controller is as such:

$$C(s) = K_P + \frac{K_I}{s} + K_D s = \frac{K_D s^2 + K_P s + K_I}{s}$$

where K_P = Proportional gain, K_I = Integral gain and K_D = Derivative gain. In terms of a flow diagram, a PID Controller structure can be represented as such:

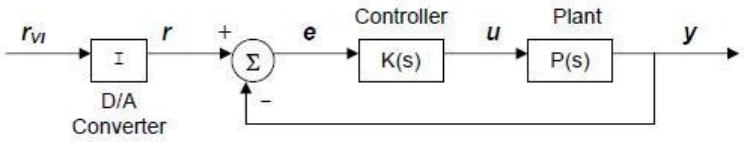

Figure 4-23 – General closed loop system.

The variable *e* denotes the tracking error, which is sent to the PID controller. The control signal *u* from the controller to the plant is equal to the proportional gain (K_P) times the magnitude of the error plus the integral gain (K_I) times the integral of the error plus the derivative gain (K_D) times the derivative of the error.

$$u = K_P e + K_I \int e dt + K_D \frac{de}{dt}$$

In our specific case this theory can be applied as in the following diagram, where the solenoid and load-cell can be considered as the 'plant', and the control circuit as the 'controller'. The whole process can be monitored using an oscilloscope.

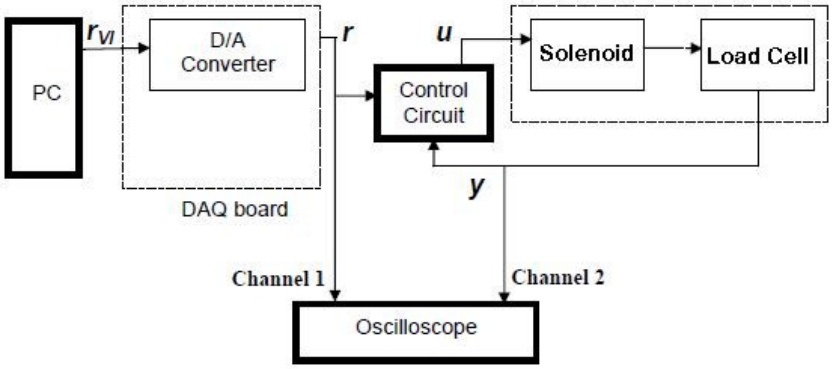

Figure 4-24 – Solenoid/Load-cell closed loop system.

The initial design of the control circuit is shown in the following figure. After considering numerous publications ([53], [54], [55], [56], [57], [58]) this has been adapted from Meyrath [59] so that it is in its most simplistic format.

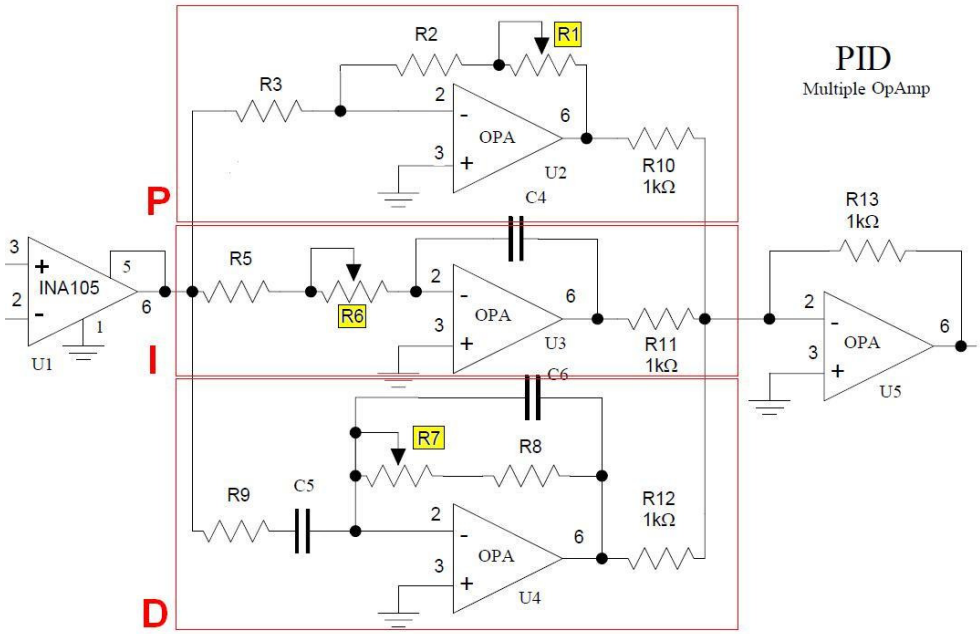

Figure 4-25 – PID Circuit.

Resistors R1, R6, R7 and capacitors C4, C5, C6 are the components that optimise the PID performance as described in Table 4-26. When building the PID circuit board, these specific resistors and capacitors were made accessible so that repetitive handling would not cause too much damage to the whole circuit. The final schematic of the circuit is shown in Fig. 4-27, a higher resolution copy of which is found in Appendix C.

Components	Action
(R1 + R2)/R3	Proportional gain
(R5+R6)xC4	Integration time
(R7+R8)xC5	Differentiation time
C6	Gives high-frequency roll-off
R9	Limits differential gain

Table 4-26 – Summary of PID main component actions. -

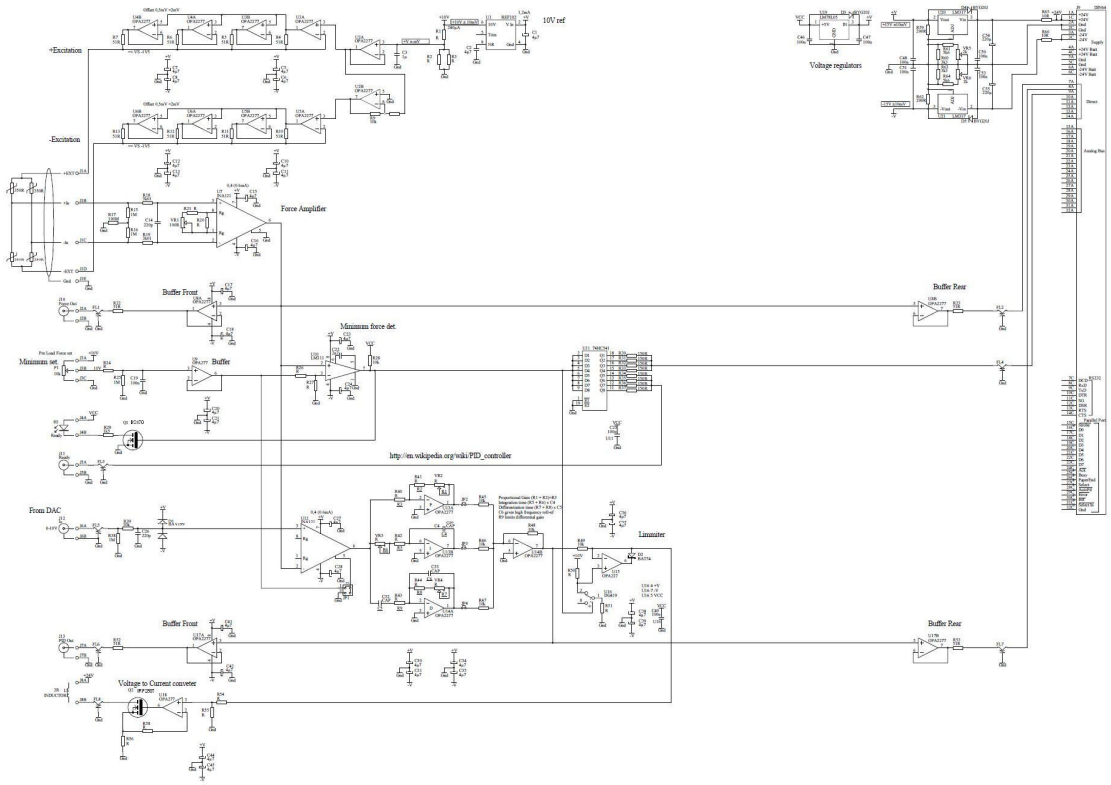

Figure 4-27 – Final PID Schematic.

4.9.1 PID Controller Tuning and Optimisation

When considering tuning of a PID controller according to literature ([60], [61], [62], [58], [55]) there are four major characteristics of the closed-loop step response that need to be considered. They are: (1) Rise Time: the time it takes for the plant output *y* to rise beyond 90% of the desired level for the first time; (2) Overshoot: how much the peak level is higher than the steady state, normalized against the steady state; (3) Settling Time: the time it takes for the system to converge to its steady state; and (4) Steady-state Error: the difference between the steady-state output and the desired output. The effects of increasing each of the controller parameters K_P, K_I and K_D can be summarized as shown in the following table:

Response	Rise Time	Overshoot	Setting Time	S-S Error
K_P	Decrease	Increase	NT	Decrease
K_I	Decrease	Increase	Increase	Eliminate
K_D	NT	Decrease	Decrease	NT

Table 4-28 – Summary of controller parameters. (NT: No definite trend. Minor change)

While designing the PID controller, the following steps were taken: (1) After activating the system, characteristics of the system that needed improving were noted; (2) K_P was used to decrease the rise time. (3) K_I was used to eliminate the steady-state error; (4) K_D was used to reduce the overshoot and settling time.

An interesting method that is commonly used for tuning PID controllers is the Ziegler-Nichols tuning rule [63]: Ziegler and Nichols conducted numerous experiments and proposed rules for determining values of K_P, K_I and K_D based on the transient step response of a plant. They proposed more than one method, but in our case, we limited ourselves to what's known as the first method of Ziegler-Nichols. It applies to plants with neither integrator nor dominant complex-conjugate poles, whose unit-step response resemble an S-shaped curve, with no overshoot. This S-shaped curve is called the reaction curve.

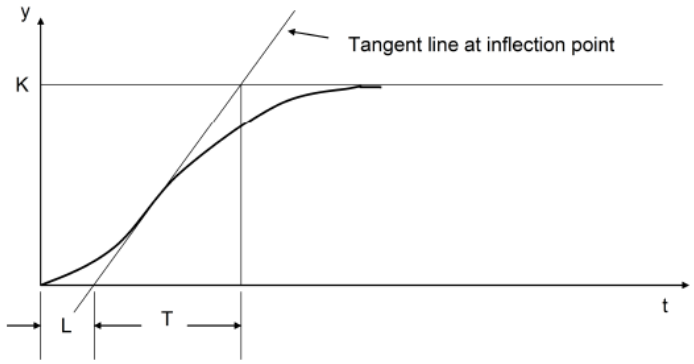

Figure 4-29 – Ziegler-Nichols S-shaped curve.

The S-shaped reaction curve can be characterized by two constants, delay time *L* and time constant *T*, which are determined by drawing a tangent line at the inflection point of the curve and finding the intersections of the tangent line with the time axis and the steady-state level line. Using the parameters *L* and *T*, we can set the values of K_P, K_I and K_D according to the formula shown in the following table:

Controller	K_P	K_I	K_D
P	T/L	0	0
PI	$0.9(T/L)$	$0.27(T/L^2)$	0
PID	$1.2(T/L)$	$0.6(T/L^2)$	$0.6T$

Table 4-30 – Equations to determine KP, KI and KD -

These parameters typically gave a response with an overshoot about 25% and good settling time. We then started fine-tuning the controller using the basic rules that relate each parameter to the response characteristics. Using the previously described method and a lot of trial-and-error, the parameters for the PID controller that showed a sharper response are tabulated below and finally, some screen-shots of the final PID controller.

Parameter	R1	R2	R3	R5	R6	R7	R8	C4	C5	C6
Value	40kΩ	20kΩ	10kΩ	1Ω	100kΩ	100kΩ	1Ω	1nF	1µF	1µF

Table 4-31 – PID parameters -

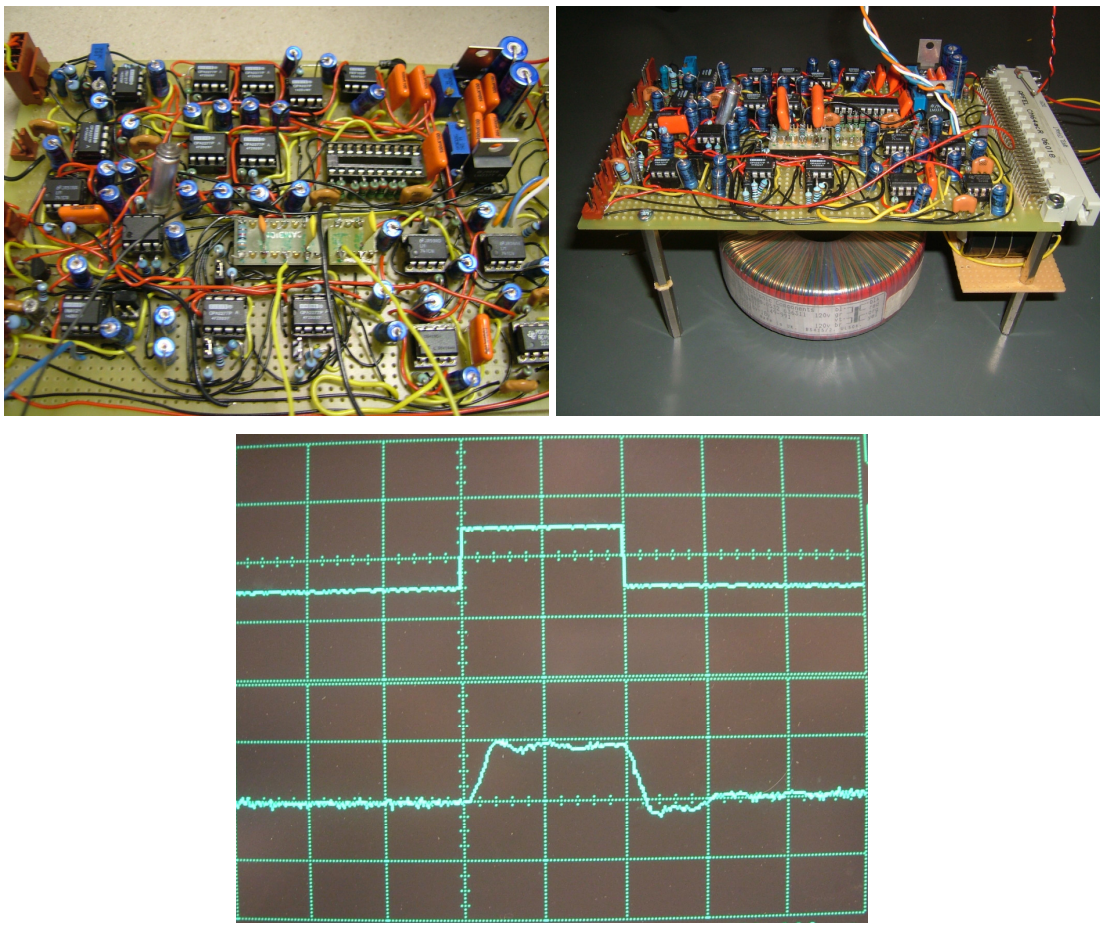

Figure 4-32 – PID screen-shots.

4.10 Test Rig

The test rig for this project was originally designed by Professor Ron Riso, acting consultant. The main idea was to have the pig lying flat on its back, on a base plate, and its frontal end between the vertical posts of the platform. Its left limb would then be held up by an elbow fixation which is supported by a vertical post. The rotation shaft will be confined to the pig left side, and it is the pig LEFT forelimb that will be rotated at the wrist. So the shaft wants to be only as long as needed to position the solenoid apparatus at the left forelimb. The wrist is held in place with a wrist fixation which carries on to: a ball-joint on one side (and further to a wrist

fixation assembly supported by a vertical post), and to a counter-weight structure on the other side. This structure is connected to the rotary motor and also to the solenoid, load-cell and contactor. The limb extremity is secured using a nail fixation method. The following drawing shows how the motor mount tower is coupled to a platform containing the bearing block.

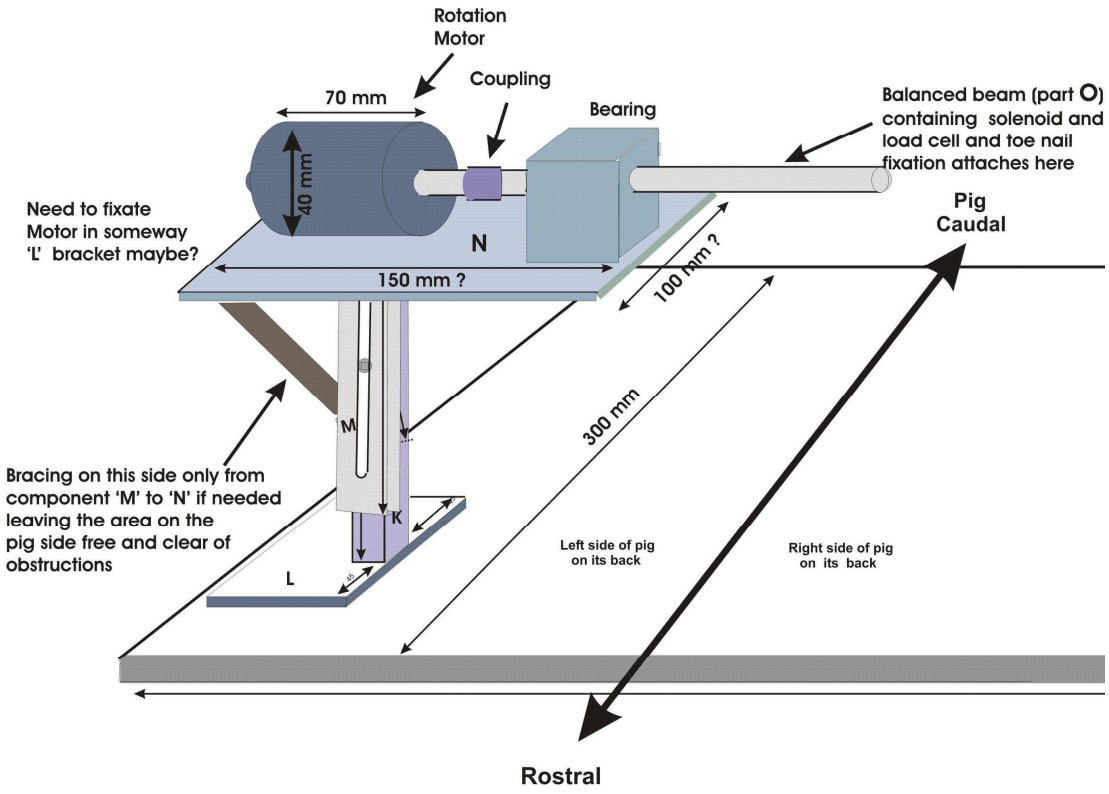

Figure 4-33 – Overview of initial test-rig platform with parts K, L, M and N.

The motor base plate is fixed to the main base plate by using a C-clamp that acts like a 'vise grip' pliers. This is quick and allows the motor tower to be slid around to different locations to get an alignment with the pig. The length of the balanced beam (Part O) is such that it reaches to the left forelimb. It is long enough to extend to about 100mm from the end of the bearing block and it can be adjusted to the correct length (by cutting it) once the size of the pig is known. The end of the shaft will have the solenoid, load-cell and counterweight components attached. This will be quite heavy so the bearing should not be placed too far to the left of the pig.

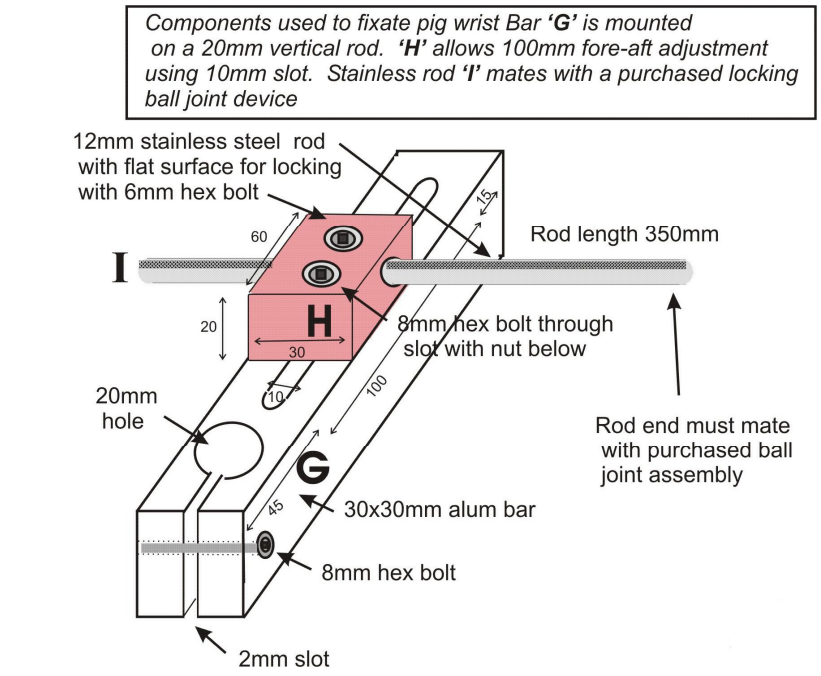

Figure 4-34 – Initial pig wrist fixation bar

In the original structure, the hardware was mounted on both sides of the pig. The elbow and wrist fixation on one side and the rotation motor on the other. With regards to the ball joint, it is intended to attach to the shaft shown in the drawing having parts G, H and I.

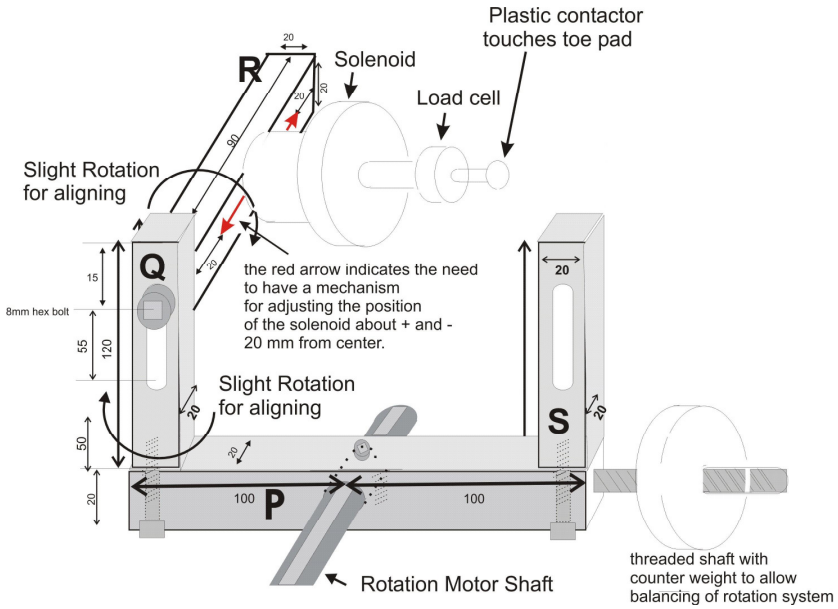

Figure 4-35 – Solenoid/Load-cell support

The following figures show further detailed schematics of the original pieces that make up the test rig. In the top view of the elbow clamp, the left and right bars *A* and *B* are anchored in channels to slide left and right for different width of pig elbows.

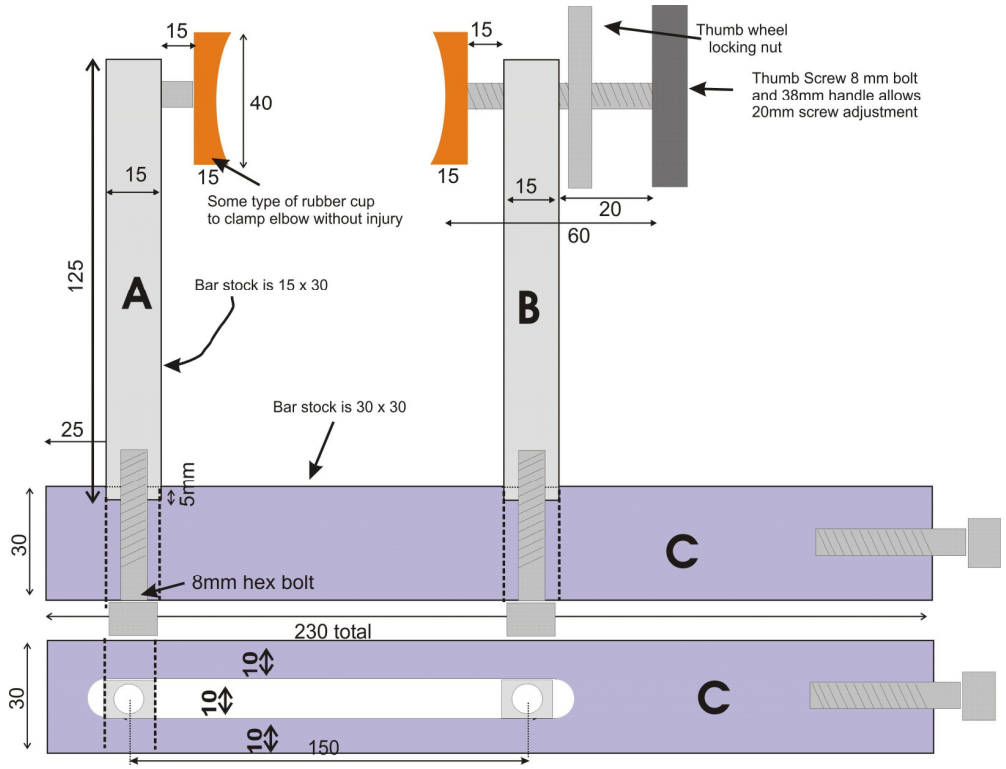

Figure 4-36 – Views of the elbow clamp: Parts A, B, C, and D -

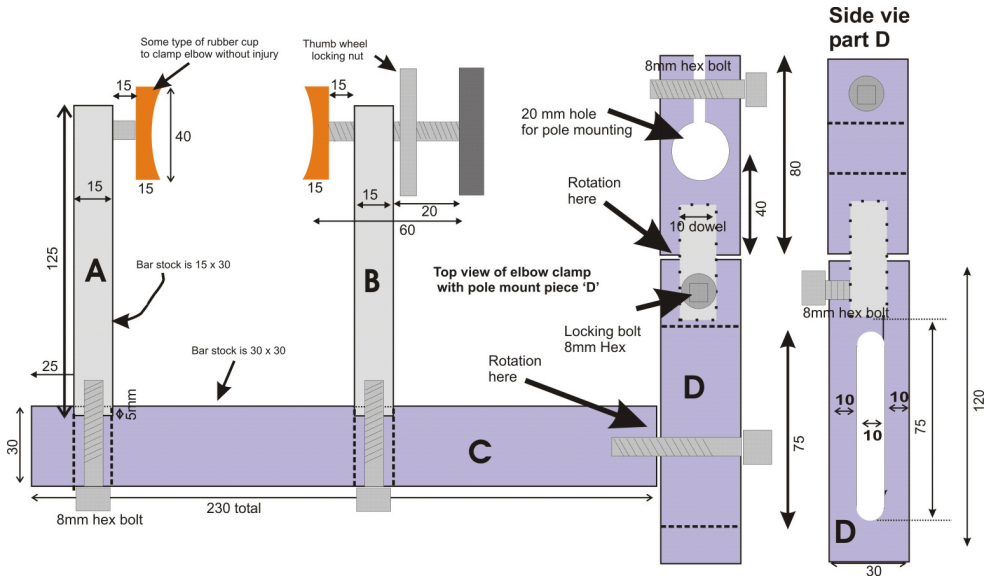

Figure 4-37 – Views of the elbow clamp: Parts A, B, C, and D -

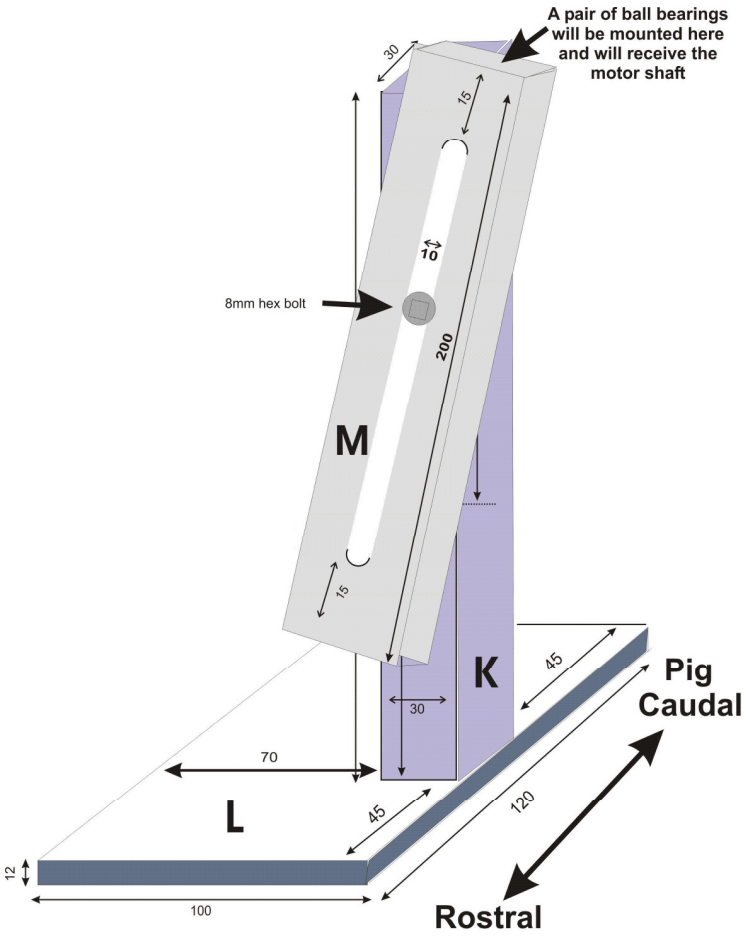

Figure 4-38 – Views of the Motor mount; Parts K, L, M.

Fig. 4-38 shows the side vie of the support for the rotation motor mount, including base *L*, vertical beam *K* and rotational beam *M*. The width and depth of bar *M* is 30 mm by 30mm. A plate will be attached to the top to secure a pair of bearings.

Once the test rig was put together, it was brought in to the animal labs to try on some pig cadavers, just to make sure that the size was adequate to accommodate the animal for the planned experiments. Unfortunately this is where the suitability of the design of this test rig was being questioned. Appendix D1 shows the original design being tried in the hospital.

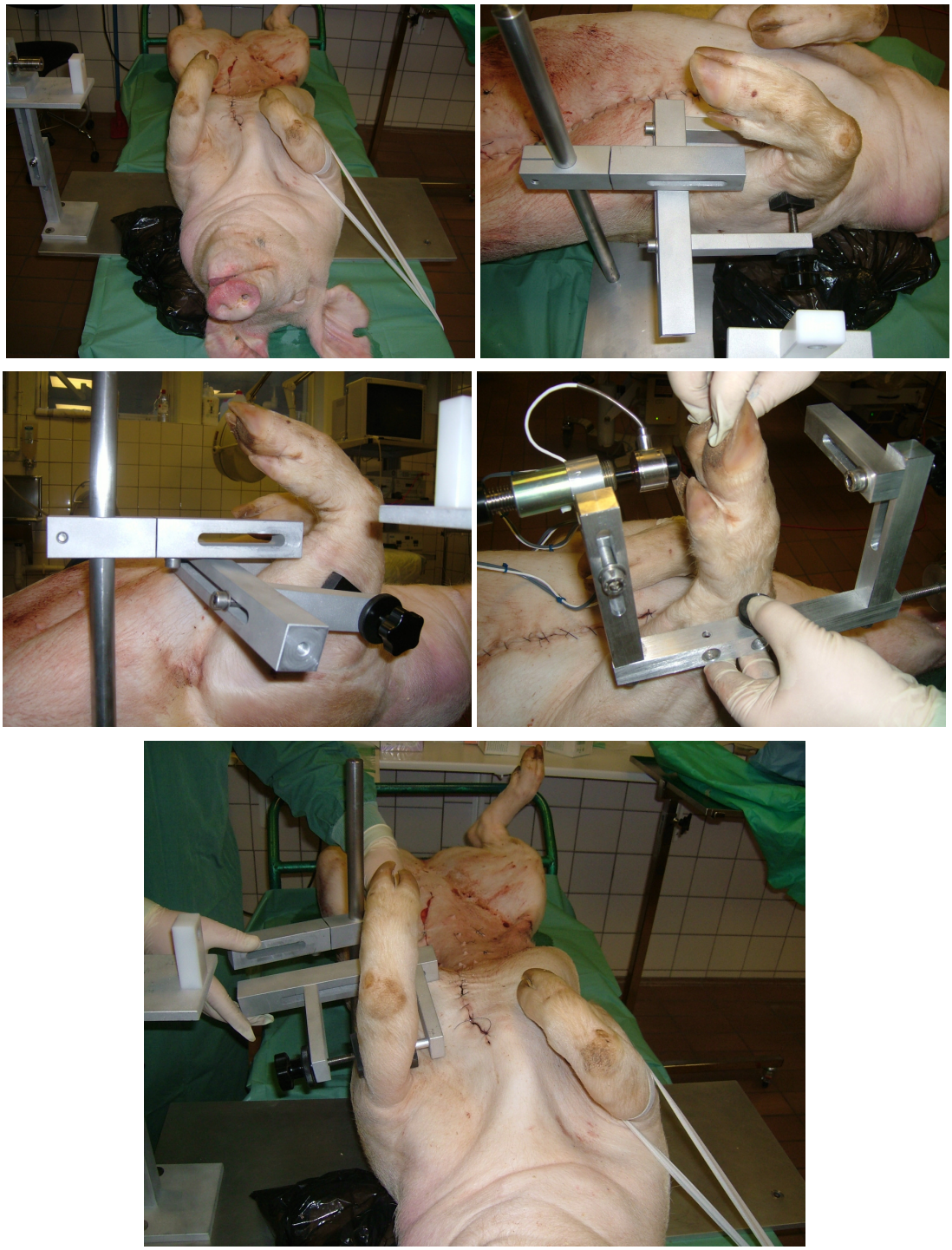

Figure 4-39 – Pictures of the initial pig fitting on the test rig.

4.11 LabView

Since conducting the frog experiments, major modifications had to be made on the LabView software in order to integrate tasks such as manipulating the Maxon motor, controlling the solenoid/load-cell, video capture of the limb movement, online graph analysis, and finally, reviewing graphs of previously saved data files. It should also be worth mentioning that the version of the LabView software was upgraded from version 7.1 in the frog experiments to

version 8.2 in the pig experiments. The following figures show actual screenshots of the 'Velocity Selective Recording Software' (VSR Software), briefly explaining what it does.

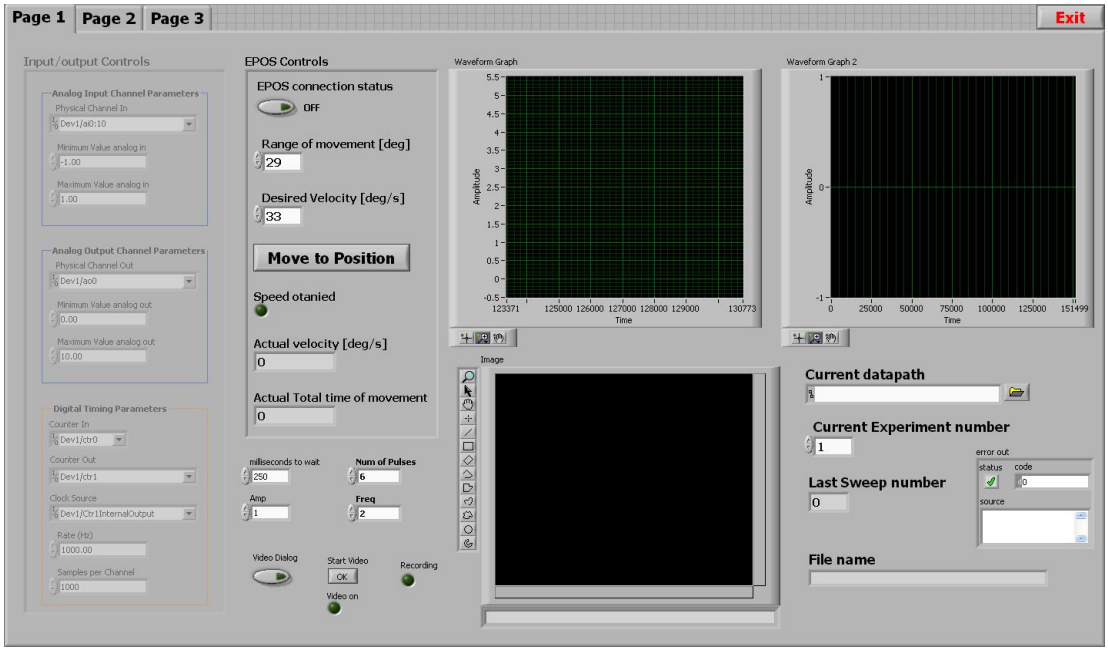

Figure 4-40 – Screenshot of Page 1 of the VSR Software.

The default screen of the VSR software is Page 1. In the first column (Record Input/output controls), the top section 'Analogue input channel parameters' defines the physical channels from the National Instrument USB-DAQ from which data will be acquired. This comes in very handy if ever we want to monitor one or few specific channels. For example, if one of the channels were to be picking up too much noise or maybe even a ring on the cuff electrode were to be damaged for instance. The next section down in that column (Analogue output channel parameters) defines the physical output channel. The last section in this column, 'Digital Timing Parameters', set the acquisition quality of the NI USB-DAQ device. Moving on to the top section of the next column, 'EPOS Controls', this manages the Maxon motor EPOS controller connection and also allows the user to define the values of the motor's range of movement and desired velocity. Once a connection is established, this is indicated by the top indicator which lights green, and the user presses the 'Move to position' button after inputting the desired values. The section just below the 'Move to position' button has been integrated such that it is a feedback system that provides the user with an indication whether the desired speed has been obtained and under what velocity and in what time of movement. Finally, the last part of the section is dedicated to controlling the solenoid. Here, the user has the option of setting the number of pulses desired, its frequency, its amplitude and how long to wait for. It is always better to have more data processing option; based on this, a webcam was integrated in the whole system whereby whenever a motion was made by the motor, the actual limb movement was recorded in '.avi' format. This might be useful in such a scenario where, when a nerve activity

were to be recorded, the user would want to find out at what specific angle of the limb motion it actually happened. Therefore by comparing time-snaps on the recorded graph and that on the movie clip, the exact position of the limb would be known. Moving on to the next column, the top waveform graph displays a real-time recording of the data being captured by all the channels. The lower window displays the view being seen by the USB-webcam. Finally, the top graph of the last column monitors the activity of the solenoid/load-cell and the bottom section sets the data-path of where the user intends to store the recording. It has been designed such that any given experiment may contain several sweeps, one sweep being one recording session. This is also the part of the software that displays any errors at any given time.

Page 2 of the software gives the user the freedom to place cursors on the plots being recorded thus displaying exact values of gaps between peaks of signals for example. The next figure shows a screenshot of that page.

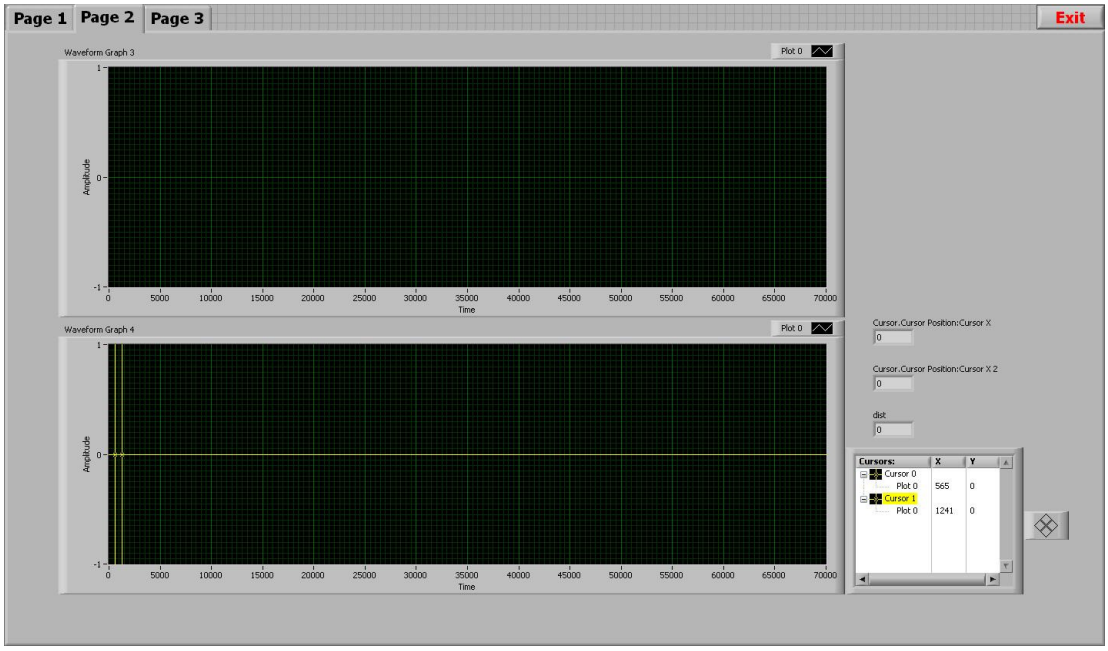

Figure 4-41 – Screenshot of page 2 of the VSR Software.

Finally, the last screenshot in the VSR Software, Page 3, is displayed in the next figure. On this page, the user has the option of reviewing previously recorded signals. In this specific example, the figure displays the performance of the solenoid/load-cell PID system. The user has first to specify the data path where the recorded file is located. The 'Update' button is then pressed. The top-left graph displays the whole recorded session; the top-right graph displays the behaviour of the Maxon motor movement; the bottom-left graph shows the Fast Fourier Transform (FFT) of the acquired signal; and finally, the bottom-right graph shows the performance of the solenoid/load-cell.

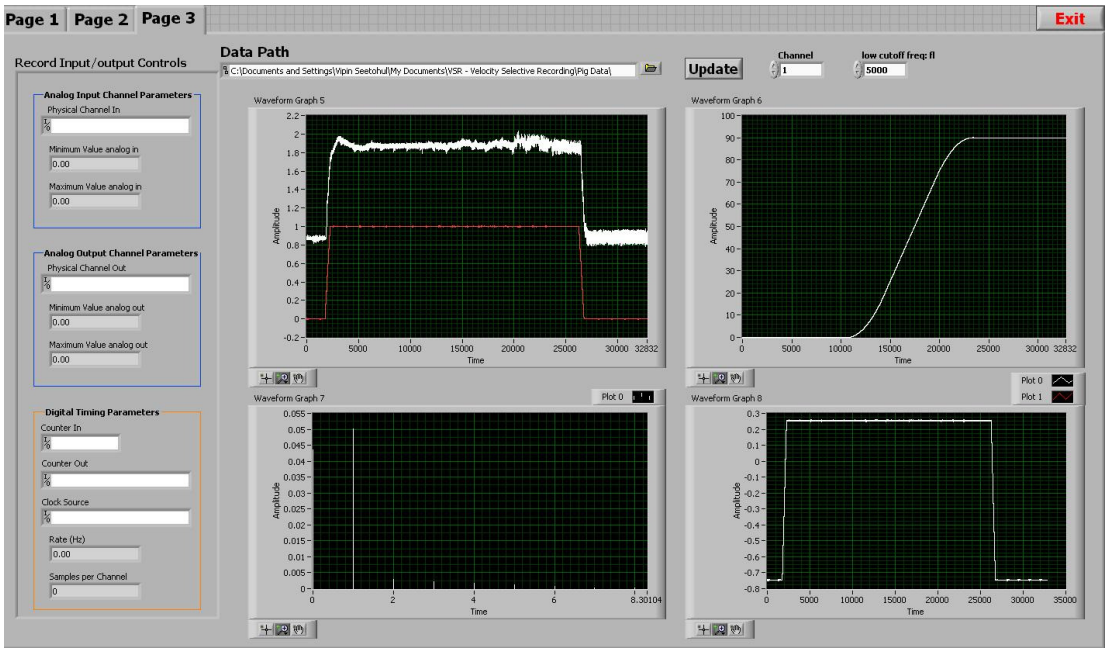

Figure 4-42 – Screenshot of page 3 of the VSR Software. -

4.12 Anaesthesia

In consideration of the ethical issues, the appropriate anaesthetics have to be used to minimise the pig to suffer. The surgery and administering the anaesthetics is performed by a fully qualified surgeon. In experiments of this nature, the standard anaesthesia is Isofluorane, and the typical pig condition should be as such: pH = 7.49, pO2 = 25.0, pCO2 = 5.0. An interesting area for further investigation is the effects of anaesthetics on nerve conduction. A few publications ([64], [65], [66], [67], [68], [69], [70], [71], [72], [73] and [74]) already discuss the topic. Having considered the core aspects of the experiment plan, an experimental protocol can be put together.

4.13 Experiment Protocol

4.13.1 Hypothesis

The object of the acute experiments is to monitor neural afferent signals generated by natural sensors using multi-electrode cuffs; to show that three distinct naturally occurring nerve signals (cutaneous, joint receptors and tendon stretch receptors) in one nerve can be separated. In this series of experiments nerve cuff electrodes will be used within the frontal limbs of the pig to demonstrate that the nerves can indeed be triggered at different levels to produce distinct velocities. This would demonstrate real-time velocity-selective classification and recording with multiple-electrode cuff (MEC) electrodes.

4.13.2 Theory

A large number of fibres (in each peripheral nerve) carry many neural signals with both afferent and efferent traffic. Traditionally, only one signal is available from each cuff and reducing this to only one artificial signal represents a huge loss of information. Various types of neural signal are carried by fibres of different diameter. According to Rushton et. al., it is possible to extract more information from one cuff by fibre diameter-selective recording. This is equivalent to measuring the level of activity in the velocity domain, because of the linear relationship between axon diameter and action potential (AP) velocity. According to Riso et al and Rahal et al, the use of tripoles reduces the sensitivity of the device to contamination from electromyographic (EMG) activity in nearby muscles. Taylor et al use an extension to this method, in which the cuff contains N tripoles. Their outputs are then summed after the insertion of artificial delays to cancel the naturally occurring propagation delays along the cuff. Action Potentials propagating at different velocities (including opposite directions) appear at the electrodes with characteristic time delays. These naturally occurring time delays can be compensated electronically. Delays and summation act as velocity selective filter. There will be a peak at the output corresponding to different velocities.

4.13.3 Surgical Procedure and Preparation

The animal undergoes the following stages:

Stage 1: The pig is pre-anaesthetized with Katelar (Ketaminol vet.®, 10mg/kg i.m. Veterinaria AG, Switzerland) on arrival to the surgical room, and, prior to its delivery to the hospital, Midazolam (Midazolam 0,5mg/kg i.m. Dumex Pharma, Oslo, Norway) is administered as a pre-anaesthetic on the farm. The pre-anaesthetesia is Zoletil, which is a combination of a dissociative anaesthetic agent, tiletamine hypochloride, and a tranquilizer, zolazepam hypochloride. In our case, the Zoletil mix has the following composition: 6.25 Rompun, 1.25 Ketaminol (100 ml / mg) and 2.50 Turbogesic. 1 mL of Zoletil mix is administered per every 10 Kg.

Stage 2: Induction (The administration of anaesthetic agents and the establishment of a depth of anaesthesia adequate for surgery) of the isoflurane is carried out using Katelar (Ketaminol vet.®, 10mg/kg i.m. Veterinaria AG, Switzerland) and Midazolam (Midazolam 0,5mg/kg i.m. Dumex Pharma, Oslo, Norway).

Stage 3: The pig is endotracheally intubated and placed on a thermal mattress.

Stage 4: The animal is mechanically ventilated using the Servo 900 (Siemens Elema-Scönander, Solna, Sweden) and normal blood gas has to be ensured every hour. The ventilator contains Isoflurane (gas 1%). This causes loss of feeling or sensation. Although anaesthesia is used for

loss of tactile sensibility or of any of the other senses, it is applied especially to loss of the sensation of pain, as it is induced to permit performance of surgery. (It is usually used to maintain a state of general anesthesia that has been induced with another drug)

Stage 5: The right carotid artery is cannulated and connected to an external transducer (Baxter, California, USA) for blood pressure measurements. Oesophageal temperature and ECG is monitored by a Cardiomed-CM-4008 (Cardiomed, Oslo, Norway).

Stage 6: The pig is kept hydrated by administration of Lactated Ringer's solution (10ml/kg/hour) through an ear vein. Saline constituents: 1 L contains 5 ml Rentanyl + 5 ml Esmeron (Esmeron is indicated as an adjunct to general anaesthesia to facilitate tracheal intubation during routine and rapid sequence induction, to provide skeletal muscle relaxation, during surgery. Esmeron is also indicated as an adjunct in the intensive care unit (ICU) to facilitate intubation and mechanical ventilation). Infusion is preformed over 3-4 hrs.

Stage 7: A bladder catheter (12 French, Rüsch, Kernen, Germany) has to be inserted to keep the bladder empty.

Stage 8: The Zoletil mix is administered after 4hrs (1 mL/10 Kg)

Stage 9: Finally, at the end of the experiments, it is terminated by an overdose of Pentobarbital iv.[75]

4.13.4 Equipment Used

- Motor platform mounted with a rotary motor (Maxon EC Motor), solenoid (Saia-Burgess) and load-cell.
- Multiple-electrode cuff (MEC).
- Box containing custom designed Amplifier
- National Instruments Data Acquisition card (NI DAQ - USB6251) - Sampling of each channel at 40 kHz with a dynamic range of 16 bit at 1.25MS/s.
- Dell Inspiron 9200 Laptop. (MS Windows XP SP2, Intel Pentium M Processor, 1.70GHz, 1.0GB RAM, ATI Mobility Radeon 9700 Series.)
- Matlab and NI LabView for the processing and display of results

4.13.5 Experimental Set-up: Pig

The pig is placed on the platform such that:

- It has its back flat on the base plate and its frontal end is next to the rotary motor.
- Has its left limb held up by screw fixation to the upper limb. The rotation shaft will be confined to the pig left side, and it is the pig LEFT forelimb that will be rotated at the

wrist. So the shaft wants to be only as long as needed to position the solenoid apparatus at the left forelimb.

- Has its wrist held in place with a wrist fixation which carries on to: a ball-joint on one side (and further to a wrist fixation assembly supported by a vertical post), and to a counter-weight structure on the other side. This structure is connected to the rotary motor and also to the solenoid, load-cell and contactor. The limb extremity is secured using a nail fixation method.

4.13.6 Experimental Set-up: Cuff and Electronics

Once the medial nerve has been located after much care (Any mishandling will cause swelling and this would make it difficult to fit the cuff around), a MEC is placed at the proximal end of the nerve. This cuff carries 11 platinum contacts (pitch: 3.5 mm, width: 0.5 mm). This cuff is connected to custom designed amplifier chip that provides an array of bipolar amplifiers and filters. The 10 outputs of this amplifier are monitored by a data acquisition (DAQ) system (NI DAQ - USB6251), which samples each channel at 40 kHz with dynamic range of 16 bit at 1.25MS/s.

4.13.7 Monitoring and Data Capture

The data from the DAQ is handled by LabView and is saved to the hard-disk of the Dell laptop. The conversion of 10 bipolar recording channels to 9 tripolar channels, introduction of time delays *dt* and summation is carried out off-line by Matlab routine. The format of the VSR software has been designed such that it is very user-friendly and self explanatory. Following the labels will take the user through the required parameters

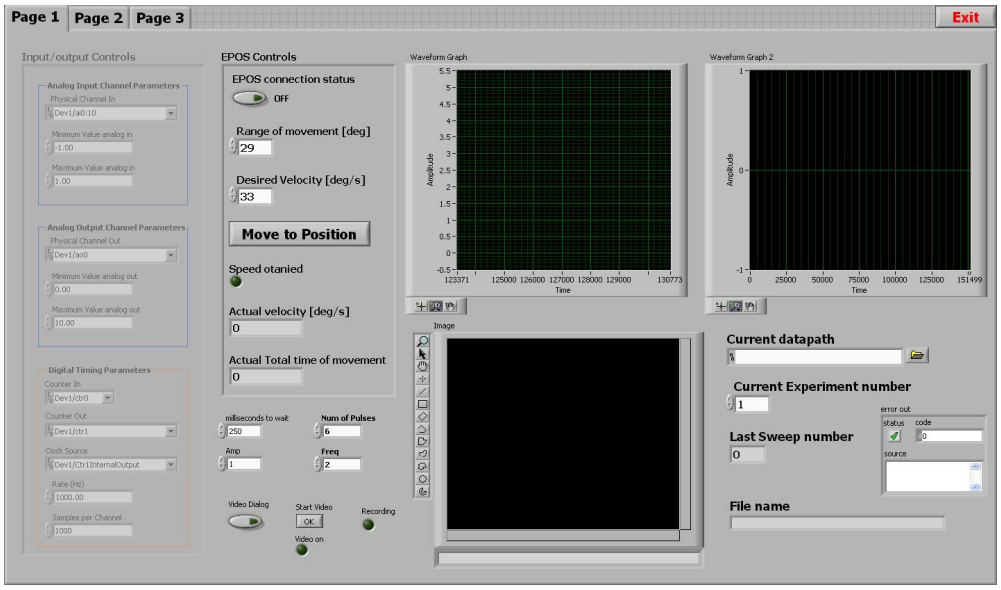

Figure 4-43 – Main window of the VSR Software. -

4.13.8 Experiments

The pigs foot will be flexed and extended in order to stretch the forearm muscles and produce 'spindle' and 'Golgi tendon organ' responses. Whether we want to flex or extend will depend on which nerve is recorded from; during these initial experiments, the flexor muscles will be stretched when the medial nerve is recorded.

For the first set of experiments, the wrist extension motion (which acts to stretch the flexor muscle) will be used. The same routine of recording as mentioned previously will be applied to different scenarios as described by the following 3 category of experiments:

4.13.8.1 Experiment 1

Summary: Trials with only the cutaneous stimulation applied (Cutaneous receptors targeted). There will be NO motion at the wrist; the servo rotation motor will be maintained at fixed position by making an active brake using the motor in position servo mode. The muscle spindles are very sensitive, so any rotation movement or servo-jitter will cause them to discharge:

- Pig rested on platform and under anaesthetics.
- Limb in place and secured.
- Computer and software initialised and ready – All required parameters to be keyed in.
- Cuff electrode 'stand-by', ready to be inserted.
- Medial nerve exposed. (Surgeon's steps to cut open the limb)
- Place multi-electrode cuff and re-seal the wound.
- Press 'Move to position'

Repeat previous step for clockwise and anti-clockwise motion (The software automatically changes rotational direction every time the 'Move to position' is pressed.

4.13.8.2 Experiment 2

Summary: Trials with only the wrist rotation (and hence stretch of the wrist muscles – Stretch receptors targeted). The rotation will be performed at 3 different velocities. A change in angle will cause the muscles to contact, hence causing the nerves to fire. This targets muscle afferents only. Steps:

- Reset software (and make sure limb is in place and secured for wrist rotation only.
- Start recording and Activate motor rotation at velocity 1.
- Stop recording and return limb to initial position.
- Start recording and Activate motor rotation at velocity 2.
- Again, stop recording and return limb to initial position

- Start recording and Activate motor rotation at velocity 3.
- Finally, stop recording and return limb to initial position.

4.13.8.3 Experiment 3

Summary: Trials with both stimuli applied at the same time (Both Cutaneous and Stretch receptors targeted). Same force-time profile as in Experiment 1, motion of the wrist is allowed. The wrist servo makes a controlled-velocity motion while the contactor makes a controlled force. Steps:

- Reset software and make sure limb is in place and secured.
- Make sure software has the correct parameters; (1) Set of parameters A at velocity 1 (2) Set of parameters A at velocity 2, (3) Set of parameters A at velocity 3, (4) Set of parameters B at velocity 1 (5) Set of parameters B at velocity 2, (6) Set of parameters B at velocity 3, (7) Set of parameters C at velocity 1 (8) Set of parameters C at velocity 2, (9) Set of parameters C at velocity 3,
- Start the recording VI and initiate both the motor and the solenoid with condition (1)
- Reset Software and load parameters of condition (2)
- Start the recording VI and initiate both the motor and the solenoid as in condition (2)
- Repeat this sequence until condition (9).
- At the end of the experiments, the cuff electrode is removed and the normal surgical procedures are performed on the pig.

4.13.8.4 Experiment Summary

	Solenoid + Load Cell	Rotary Motor
Experiment 1	ON	OFF
Experiment 2	OFF	ON
Experiment 3	ON	ON

Table 4-44 – Experiment Summary.

4.14 Discussion

Running through the protocol on the first experiments was very insightful as to the outcome of the design of the test rig. To start off with, fixing the limb itself to the motor proved problematic due to the cumbersome sizes of the metal parts. Furthermore, activating the motor with the limb in such conditions clearly showed signs of physical damage to the pig's anatomy (the first experiment consisted of testing the rig with a dead animal – so no harm was caused to any animal). Another aspect of the set-up that was of concern was the amount of noise being picked up in the animal lab. The next steps of the project was definitely to (1) Investigate changes to the test rig so that it is more accommodating to the pig's anatomy (2) Find ways of minimising the effects of noise on the amplifier system.

EXPERIMENTAL SET-UP MODIFICATIONS

5.1 Test Rig – Design 1

In order to tackle the problems encountered by the test rig, a series of modifications had to be made. In the first design, emphasis was placed on enhancing the rotation freedom of the limb and also reducing the amount of metal densities present in the rig.

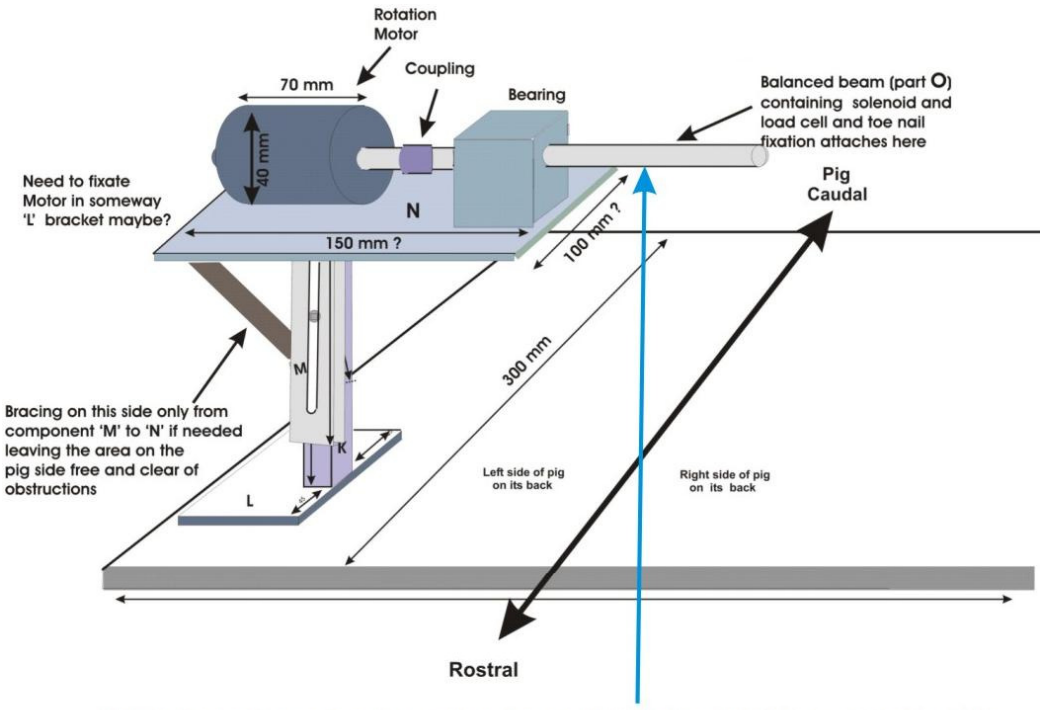

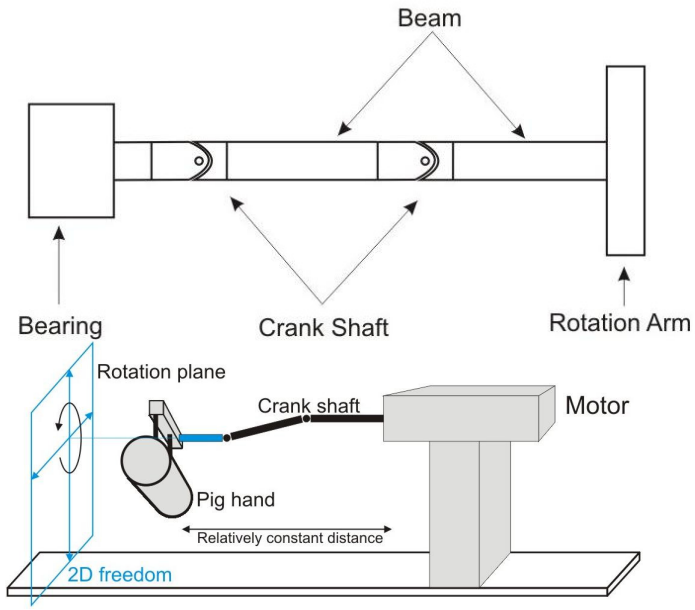

Figure 5-1 – Crank shaft location -

The point of rotation in the wrist varies. Even if the apparatus is positioned such that the shaft lies at a given point of rotation, after an angular movement, this point shifts, causing a displacement of the limb off the platform. The crank shaft was assumed to tackle this problem. One way of reducing the bulkiness of the wrist fixation was to replace the dense aluminium beams by a thinner u-shaped plate. The following figure shows a stick-model of the limb while it is being flexed.

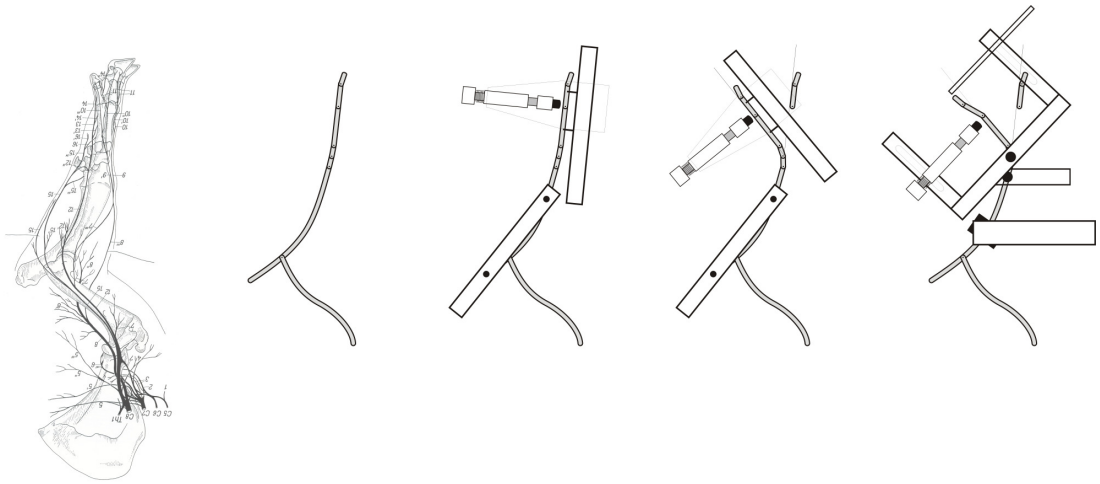

Figure 5-2 – Stick-model of the limb.

One end of the crank shaft is connected to the motor while the other is connected to the end of a rectangular beam. It will be this beam that will support the u-shaped plate that bears the solenoid and load-cell. The figure below shows this set-up in more detail.

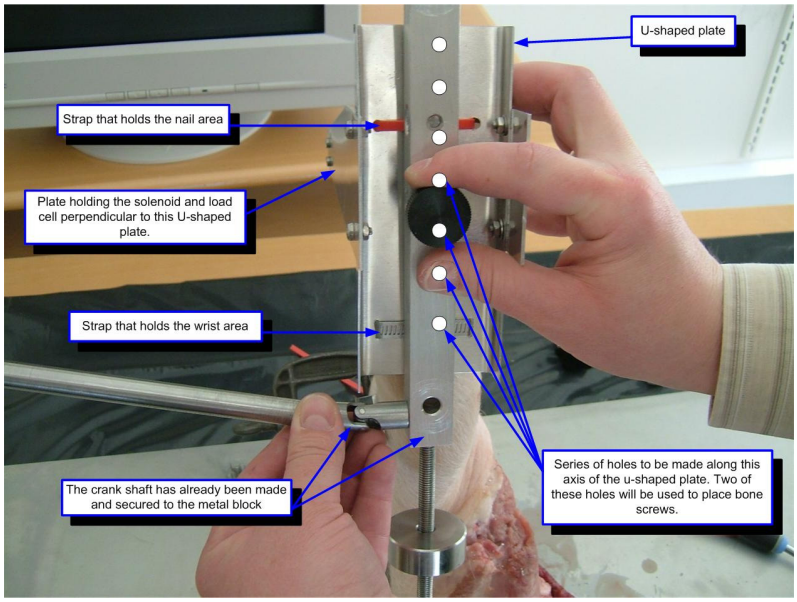

Figure 5-3 – Crank shaft and u-shaped plate connection. -

Moving on to the fixed part of the limb, two thin plates bearing multiple holes are joint to the platform by hinges as shown in the following figures. These allow for variation of pig sizes as well as maintaining a rigid joint. (See Appendix D2)

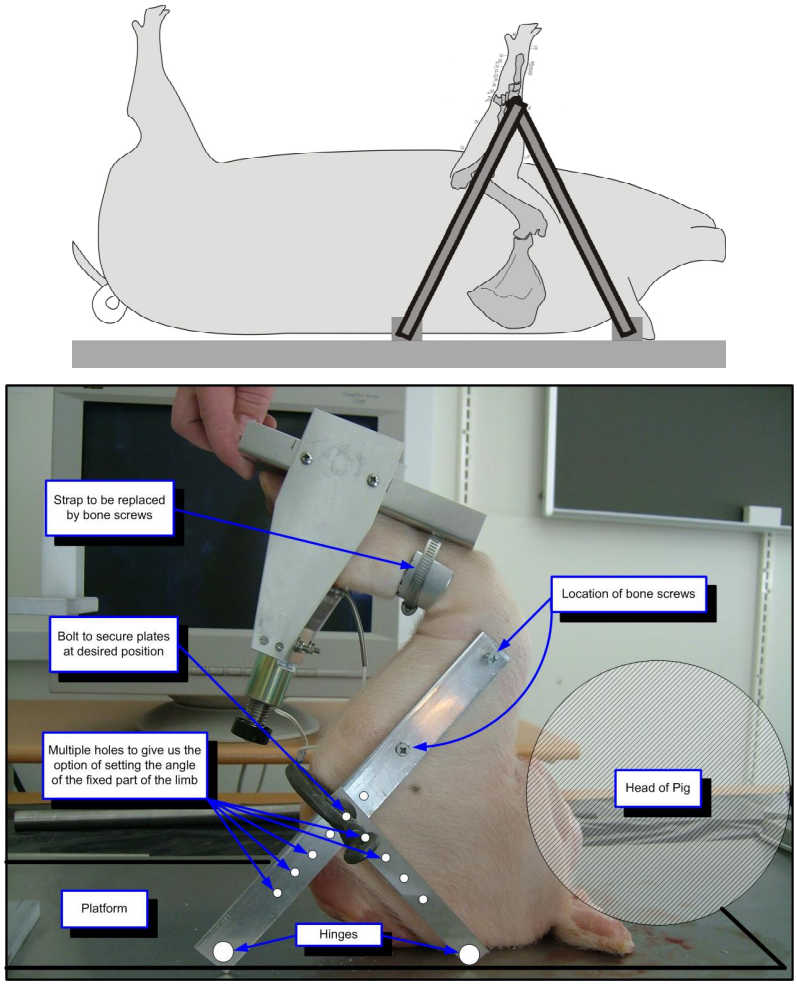

Figure5-4 – Upper limb fixation.

While setting up the limb as in the figure above, it was seen that by putting a metal shoe round the foot and contacting so much skin and hair as, there might be a lot of uncontrolled cutaneous stimulation that would dilute the response from the toe pad stimulation. Also, the added 'plate' shown on the inside of the joint would have to be less noxious, and regardless, its presence is feared to further add to the cutaneous input. However, some good did turn out of this design. It was found that fixing the upper limb to the platform is not a good idea at all. This is where the theory of the tri-segmented limb was read about. Details are to follow in the next section. The other interesting fact was that using bone screws were not too messy after all. As a result, this could well be used to rotate the wrist rather than the metal shoe that seemed to cause a lot of cutaneous stimulation. (Appendix D3 for more media files)

Figure 5-5 – Effect of using a screw on the bone. (Also see Appendix E1)

5.2 Tri-Segmented Limbs

A recent paper in the literature that seems to have given proper consideration to the aspects of the mammalian tri-segmented limbs is that of Fischer and Blickhan [76]. They have reviewed aspects of the tri-segmented limb in locomotion.

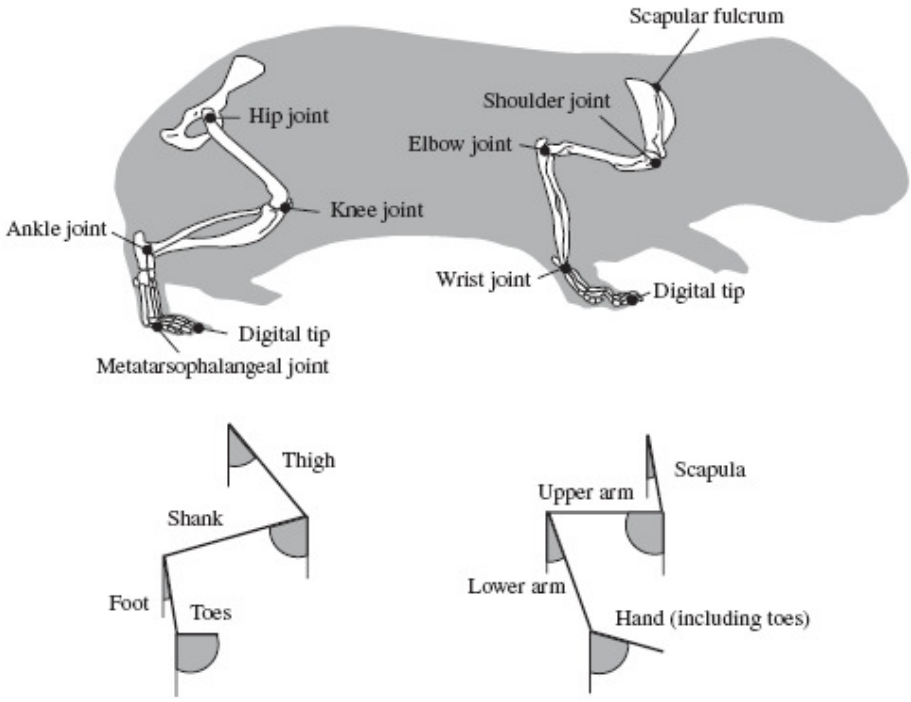

Figure 5-6 – The tri-segmented limb of mammals. Reproduced from [76]

In Therians (See Glossary of terms), the main locomotory action of the forelimb does not strictly take place in a joint. The scapular pivot is dynamically guided by the trunk and shoulder muscles and cannot be located precisely by anatomy. It most probably moves within an instantaneous center of rotation, as for the human scapula. Harmonious motion of the body is achieved by a clear separation of a segment (femur, scapula, lower spine) rotated in the most proximal center (hip joint, scapular pivot, anterior lumbar spine) and more distal

telescoping segments. Measurements done by Fischer et al. of vertical oscillations of the scapular pivot show that the shoulder and elbow joint do their job in modulating external irregularities. Neglecting the wrist joint contributions to progression, the shoulder and elbow joints share the remaining percentage of progression at rates varying between species and to a minor and irregular degree between gaits within species. In an attempt to confirm this theory, we tried some movement with pig's limb. The limb was truncated just above the elbow joint so that a piece of the upper arm was still sticking out. To make its movement more visually noticeable, a piece of plastic rod was stuck in the upper bone as the latter would have been in the first place. The following figure indicates how flexing the wrist causes the upper arm to move by a good 30°-35° angle and Appendix E2 contains all the media file on this experiment.

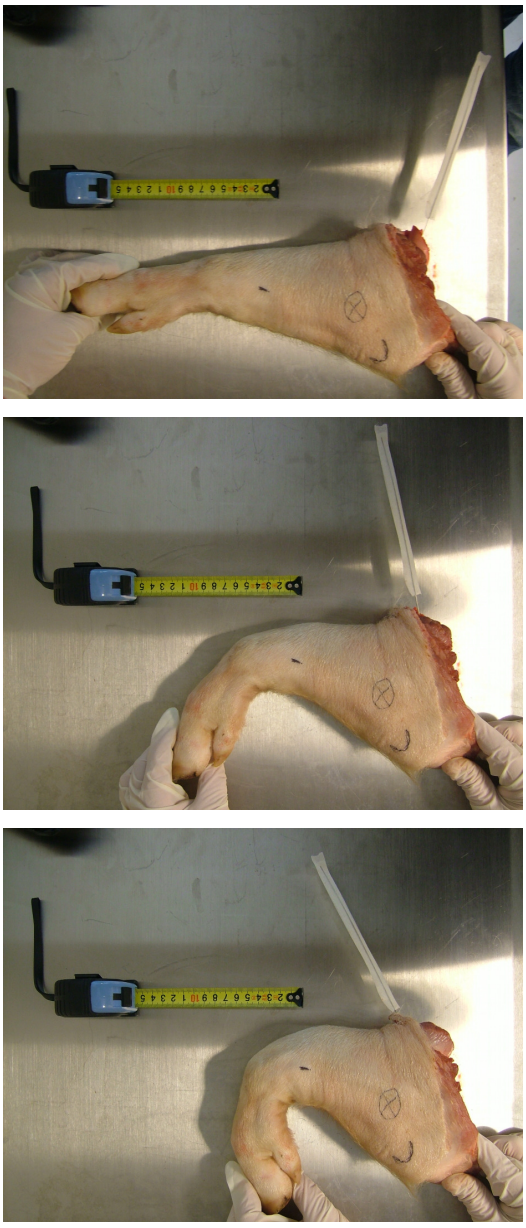

Figure 5-7 – Effect of flexing the wrist on the upper arm. (See Appendix E2) -

This confirms our previous suspicions and when graphically superimposed on a pig lying on its - back, it is seen in the next figure how flexing the wrist might cause the frontal part of the pig to be raised off the table. If the lower limb (in red) is kept fixed and the wrist is flexed, the upper arm (in blue) is also flexed accordingly. This explains the problem previously encountered that was thought to be rigor mortis, in the initial experiments when the original rig was being tested.

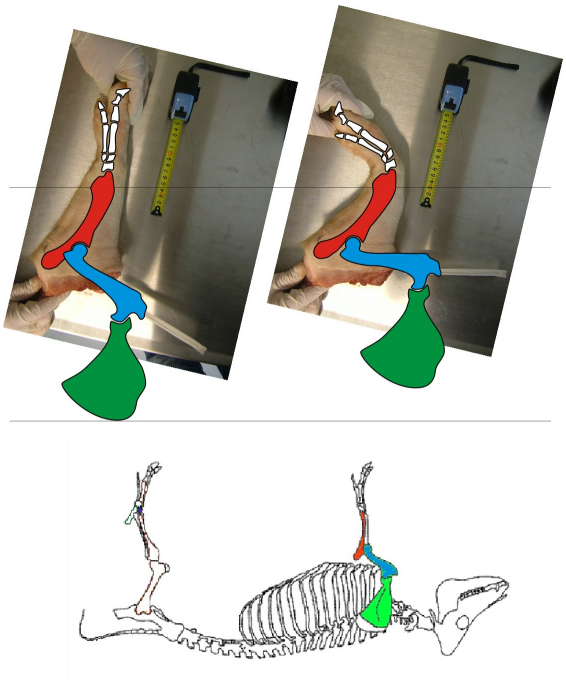

Figure 5-8 – Graphical representation of the effects of wrist flexion.

5.3 Test Rig – Design 2

This design introduced bone screws as an alternative to the nail fixation. Furthermore, in light of the effects of moving a tri-segmented limb, the fixation of the lower limb was abolished. The bone-screw fixation in the lower arm is all that is needed to rotate the foot. In the previous design, placing a thin metal strap against one of the nails (on the toe that will be stimulated) and securing the strap with a small sheet metal type of screw would generate way too much of cutaneous excitation. There would also be some contamination from skin stretch around the joint during the rotation, but that activity cannot be eliminated if the joint is to be moved. The only way to eliminate this activity is to remove the skin; but this is not a good idea since there would be a lot of pain fibres discharging from the injury, and more importantly, the pig would not be studied again.

It was initially thought that the use of the bone screws would have two possible issues (1) It would only serve for an acute experiment, and (2) The limb will have to be opened and the muscles separated so that the screws can be located in the bone without making holes through the muscles and incurring all of the tissue damage and bleeding that that would entail. The

screws would need to be located between the muscles so that the forelimb muscles do not abraid on the screws (and the screw shafts would need to be machined smooth except for the tips to further guard against tissue abrasion). Conversely, when this method was being investigated, it was found that the targeted location for the bone screws did not have any muscle present between the skin and the bone. The skin did not even have to be opened too much; a 50mm incision on the skin at the location of each screw was enough. The screws used were self-tapping therefore requiring no drilling in the bone. The only important aspect was to get the screws in the middle of the inner-bone of the limb. The pig's lower arm is a fusion of two bones. Placing the screws right in-between of the two bones is not a good idea as this is where the bone is more vulnerable. The ideal location is as shown in Fig. 5-14 at the tip of the scalpel.

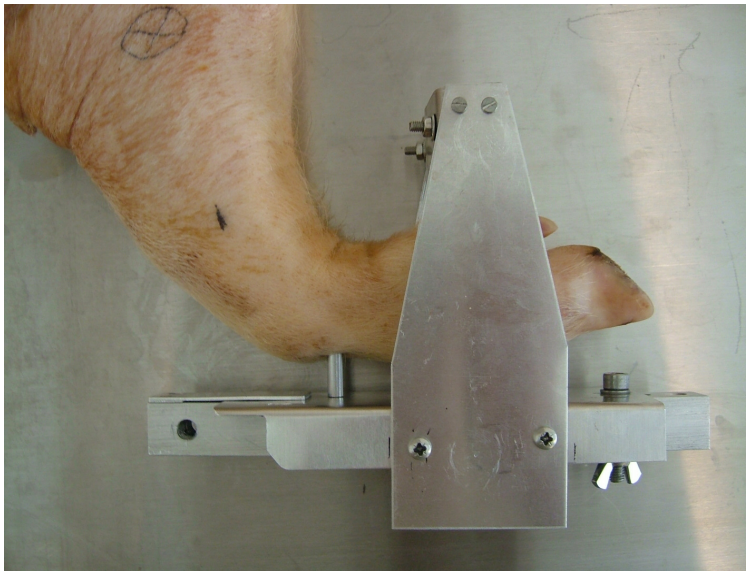

Figure 5-9 – Side View: Bone screw wrist fixation. -

Figure 5-10 – Top View: Bone screw wrist fixation. -

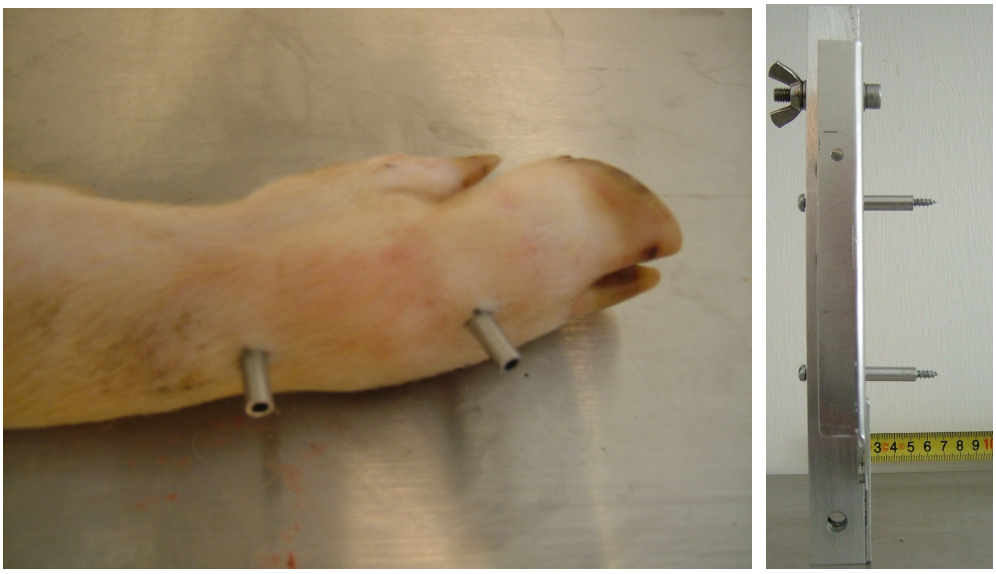

Figure 5-11 – *LHS*: Cylinders used as spacers between the metal block and the bone. *RHS*: - Screw and spacer in place on the metal block. -

The cylindrical spacer fits firmly between the metal block and the bone itself. This way, any motion made by the motor will be as accurate as possible, with the limb moving harmoniously with the metal block. (See Appendix E3)

Figure 5-12 – Location of incisions for placing bone screws and spacers.

As seen above, making an incision in the wrist of the pig is rather clean, with no bleeding. The cuts are as small as possible for it to heal conveniently in any chronic experimentation requiring bone screws.

Figure 5-13 – Effect of bone screws on the bone itself

While investigating the effect or damage, if any, of the bone screw on the bone, it was found that the specific screws available to us were not only accurate, but also had this self-tapping action into the bone. The above picture was taken after a series of experimentation on the limb. The skin was removed for illustrative purposes only. It can be seen that even after several forced limb movement by a powerful motor, removing the screws did not cause any physical damage to the surrounding bone structure.

The next picture has been included to depict the location of the screws with respect to the joint between the wrist and the upper arm. The reason for stripping the skin off this specific limb was to learn a bit more of the structure of the pig's limb. One important factor that had to be taken into consideration was the length of screw to be allowed into the bone; we needed it to be well into the bone for the strongest grip, but also to a minimum so that it doest extrude at the other end. Therefore, to measure the ideal length of screw to penetrate the bone, the skin was stripped off and as the screw was being inserted, the bone was being felt with one's finger to check for any extrusion. Again, thinking ahead for future experiments, we would want to cause as little discomfort to the animal as possible.

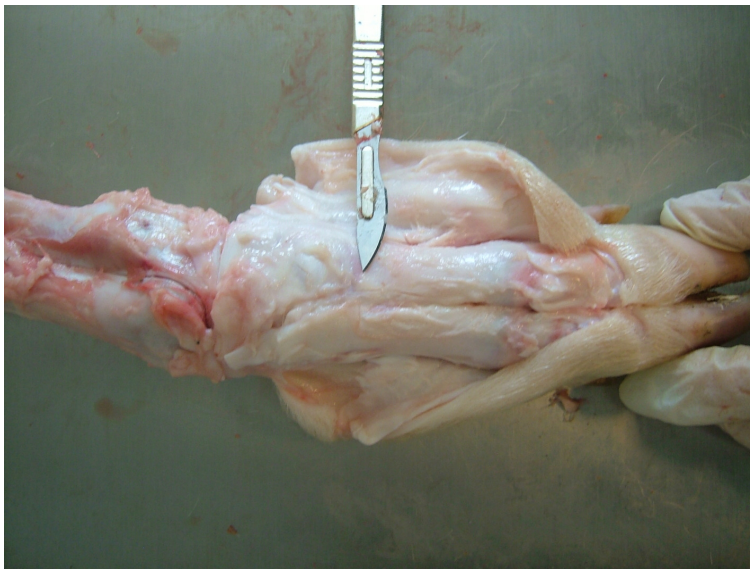

Figure 5-14 – Target location of bone screw.

In the following two pictures, the whole wrist fixation setting is depicted. Again, the strip of skin in this specific case has been removed solely for illustrative purposes.

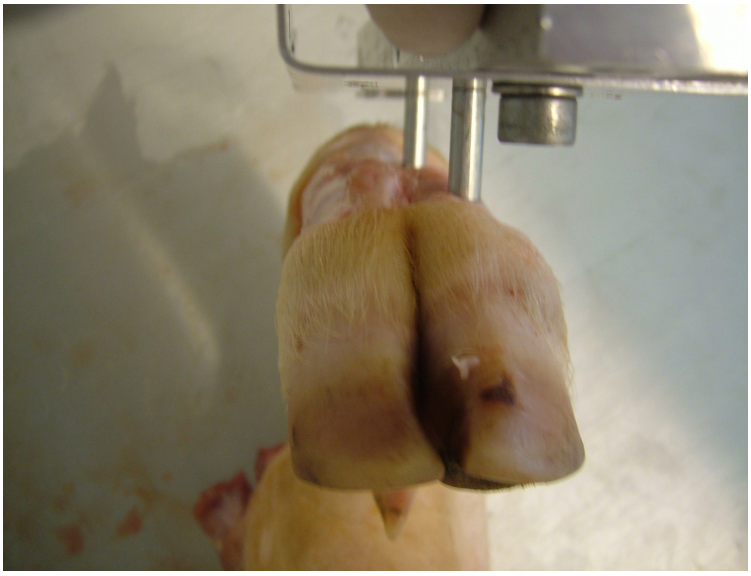

Figure 5-15 – Front View: Bone screw wrist fixation. -

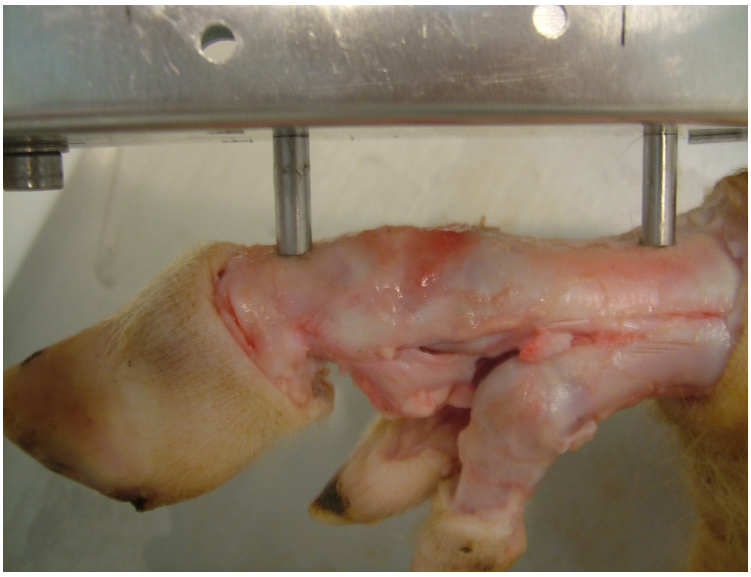

Figure 5-16 – Side View: Bone screw wrist fixation.

After establishing the main point of contact for rotating the limb, we had to figure out how to mount the solenoid and load-cell onto the limb. Replacing the bulky metal blocks with thin, but rigid aluminium was a good step, but this proved to have some further issues with regards to the solenoid positioning.

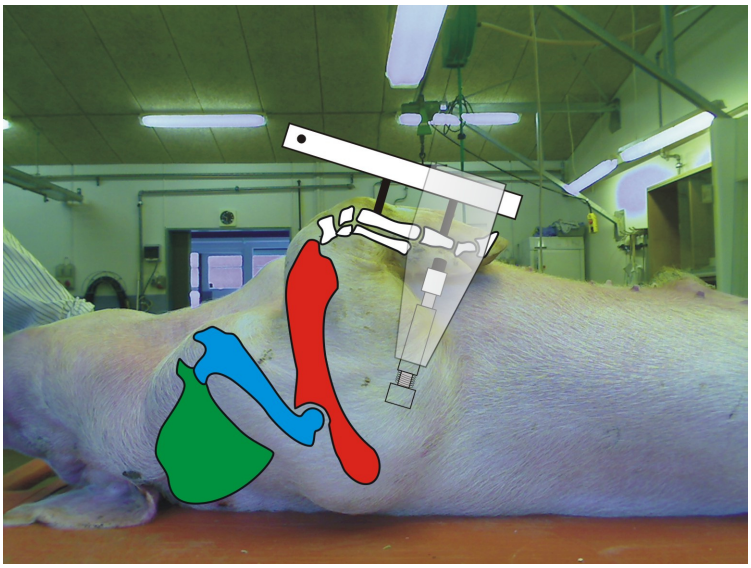

Figure 5-17 – Position of the solenoid/load-cell in the wrist fixation set-up.

As can be seen from the above picture, when the pig is lying in its natural position on its back, which happens to be the initial position of the set of movements planned, the solenoid can be seen to be too far into the side of the pig. When this was tried in the laboratory, the solenoid was clearly being obstructed. This issue definitely needed tackling.

5.4 Test Rig – Design 3

Considering the issues seen previously, in the first instance this design reduced the length of the crank shaft and added a support on the other side of the limb using a ball-bearing attached to a vertical support. Finally, the solenoid mechanism was modified.

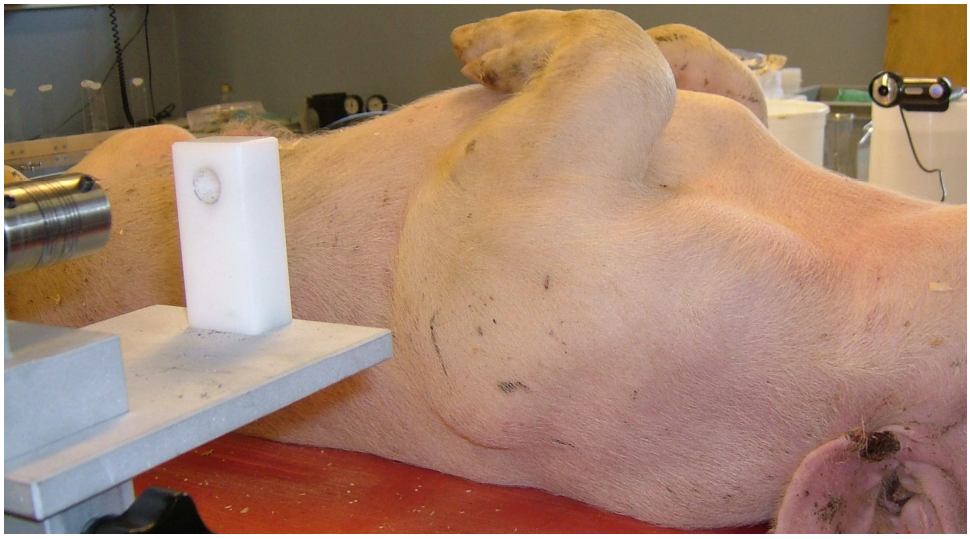

Figure 5-18 – Resting position of the pig.

The above picture shows the size of Danish Landrace obtained for this specific experiment, carried out at the Foulum Facility in the north of Denmark. The first step was to align the motor to the same level as that of the joint between the wrist and the lower arm.

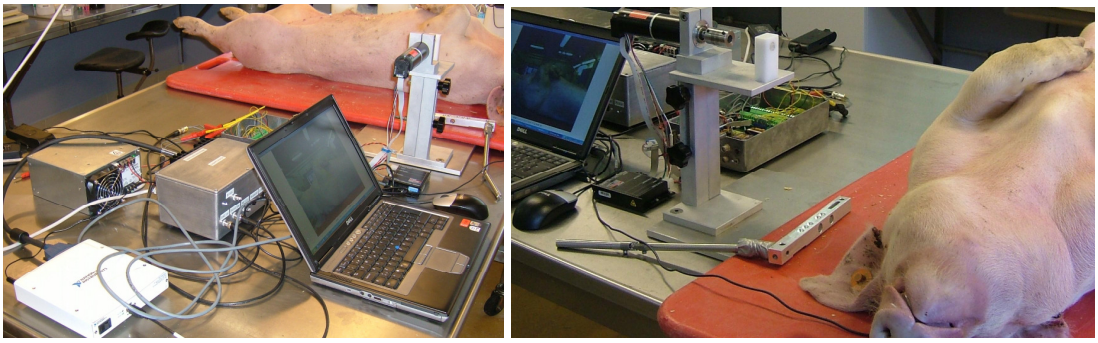

Figure 5-19 – Equipment set-up.

The equipment was set-up as shown in the above pictures, with the DAQ box, amplifier box, and PID controller located within close range as per the protocol. It was seen that when using the full crank shaft as mentioned previously, the natural freedom of motion of the limb added to that of the crank shaft, giving the limb an uncontrolled trajectory. In order to correct this, various ways were thought of to make the trajectory as controlled as possible, as well as allowing the limb to move in its own natural way. The next photo shows a messy set-up of one solution reached. This came down to shortening the crank shaft.

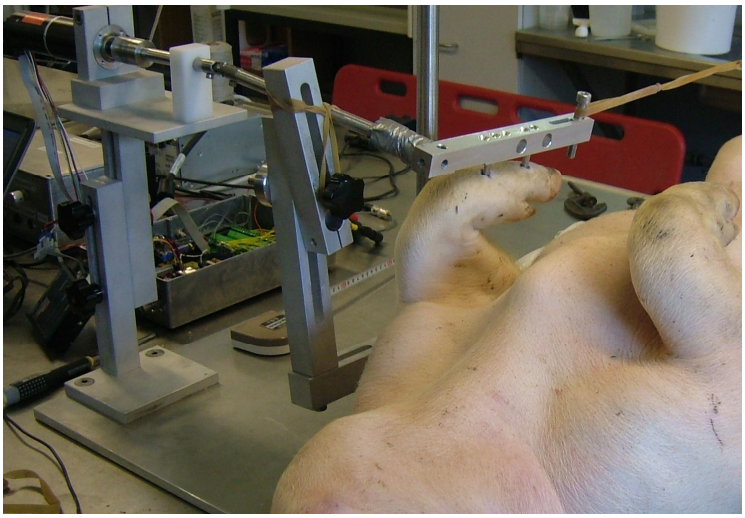

Figure 5-20 – An attempt to disable one of the joint of the crank shaft.

The resulting crank shaft set-up is as shown next. This followed further trials to investigate the limb motion.

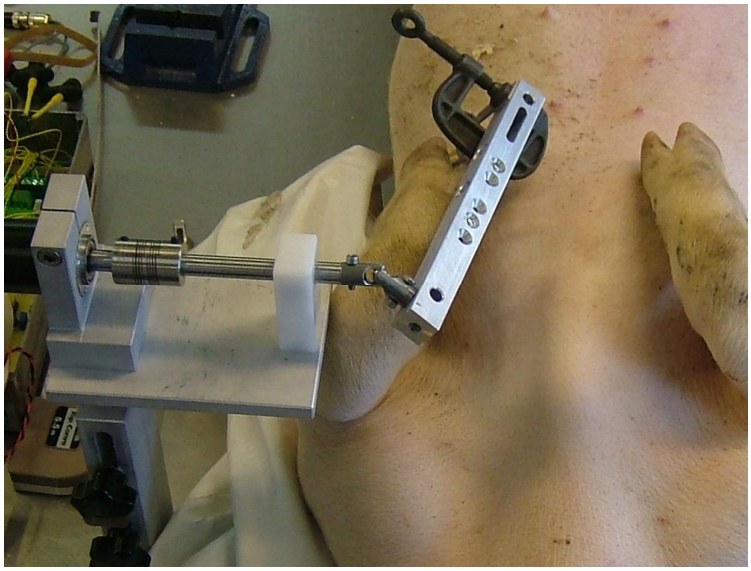

Figure 5-21 – Shortened crank shaft.

However, the set-up still did not show a perfect controlled movement. This still gave the limb total freedom of motion in all directions. It has been deducted that even if the most natural limb trajectory was required, it would have to be restricted to freedom in one plane only; that parallel to the pigs side. Therefore, the whole crank shaft idea has to be replaced with a universal system that allows the point of rotation of the motor shaft to be able to be adjusted according to the pig's limb anatomy.

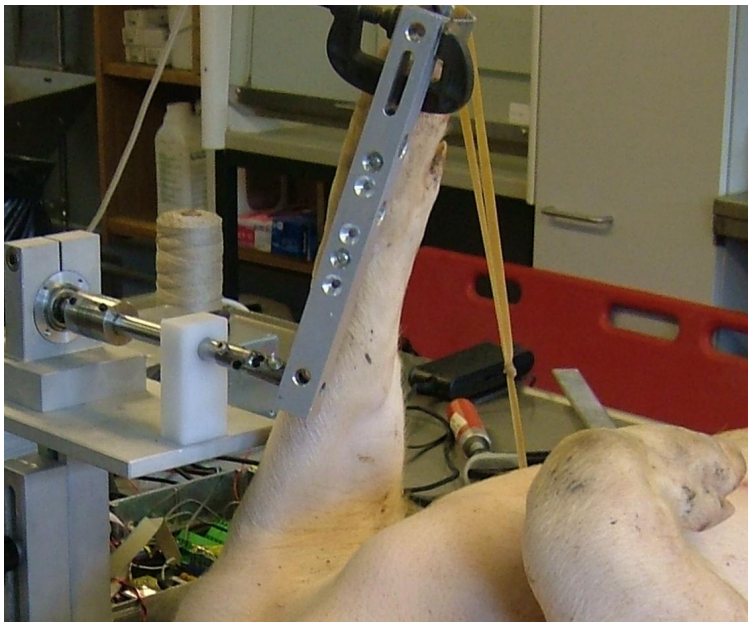

Figure 5-22 – Simplified crank shaft in action.

With regards to modifying the solenoid attachment, after several designs and prototypes, the following was achieved. Instead of having the solenoid mechanically coupled behind the load-cell, it was designed such that it would be out of the way and in front. Again, this was achieved using thin rigid aluminium plates. This means that, now, the only feature present between the pig's torso and the metal block used for the wrist fixation, is the solenoid only.

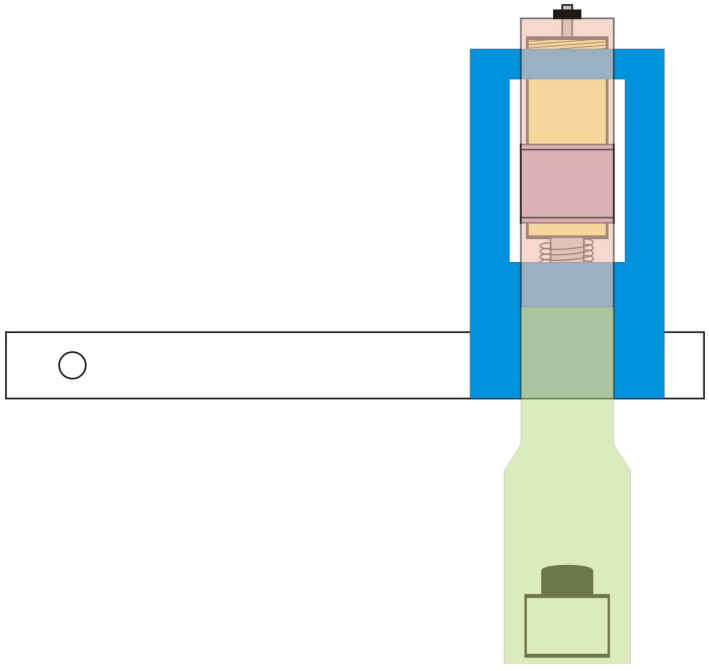

Figure 5-23 – Final design of the solenoid/load-cell set-up. -

The only precaution to be taken using this set-up is that, after placing this 'metal shoe' over the pig's wrist, we need to make sure that the solenoid and load-cell are always aligned in a straight line. Once this is tackled, the bolts responsible for this alignment can be tightened and the set-up is finally ready for the whole duration of the experiment. Initially, there was also a concern about the friction that would be involved. But this was not too serious of a problem as we are only interested in the force applied with respect to time, and not power consumption of the solenoid. Furthermore, some friction might be useful in providing some damping to the unwanted oscillations. The next photos show the set-up of the final design of the solenoid/load-cell.

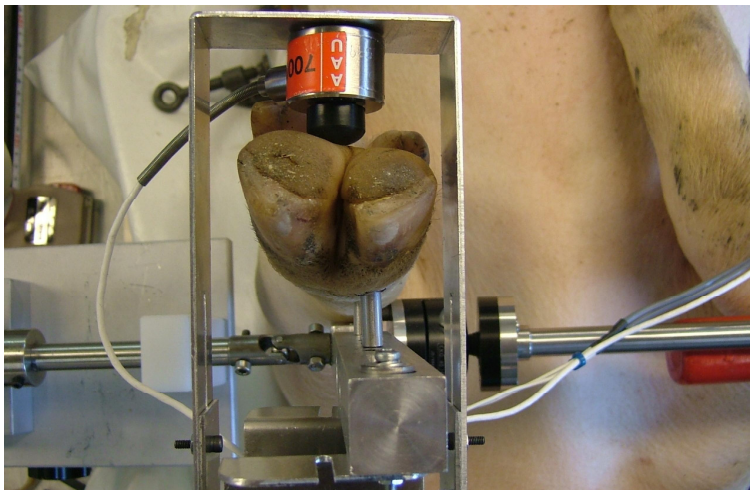

Figure 5-24 – Wrist fixation including the final design of the solenoid/load-cell. -

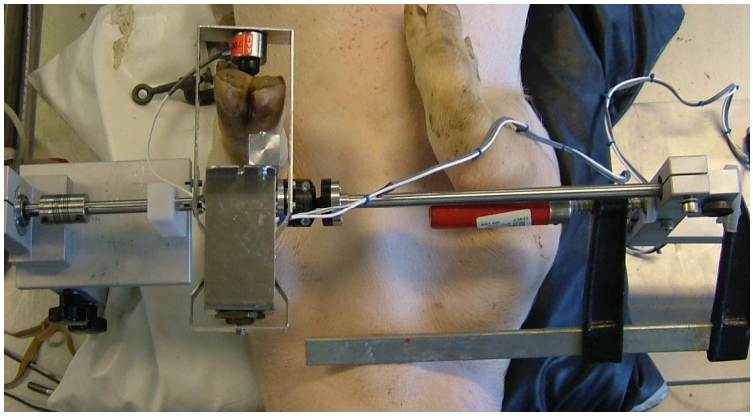

Figure 5-25 – Wrist fixation overview.

In the overview of the set-up in Fig. 5-25 above, the horizontal rod present on the right hand side of the solenoid was temporarily included to keep the limb motion in one plane. This added support on the other side of the metal block fixated to the wrist used a ball-bearing on a rod that was secured to a vertical support.

The following photos would better demonstrate the solenoid set-up:

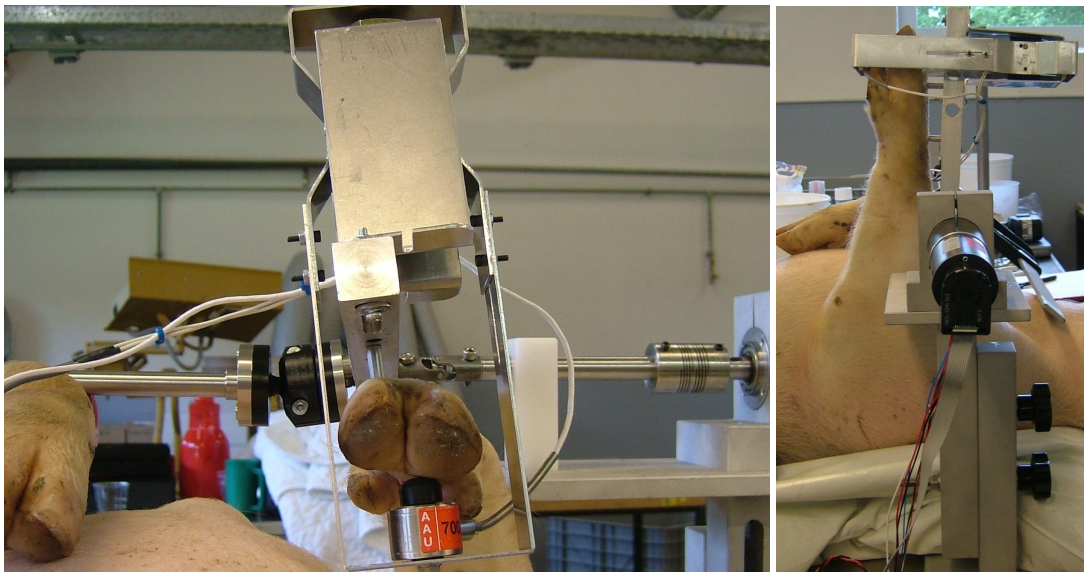

Figure 5-26 – *LHS*: Position of the load-cell on the toe-pad. *RHS*: Limb extended. -

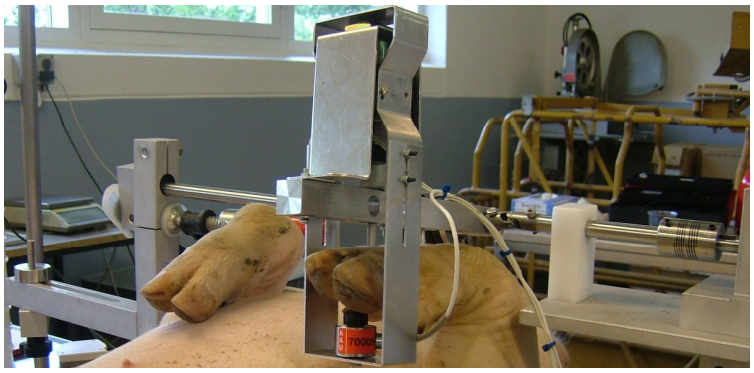

Figure 5-27 – Suitability of the new solenoid/load-cell set-up on a flexed limb.

One of the primary aims of modifying the test rig was to facilitate the implantation of the electrode and thus ease the experimentation process. This has successfully been achieved as plenty of room was made available for the surgeon to conveniently work on the pig's limb. This can be shown in the next picture. It is also interesting to point out at this instance, when a freshly euthanised pig was being worked on, that there is absolutely no bleeding at the bone-screw locations. The rig is just one step away from being fully functional. The final step of the modification is explained in the next section. All of the media files showing the evolution of Design 3 are located in Appendix F.

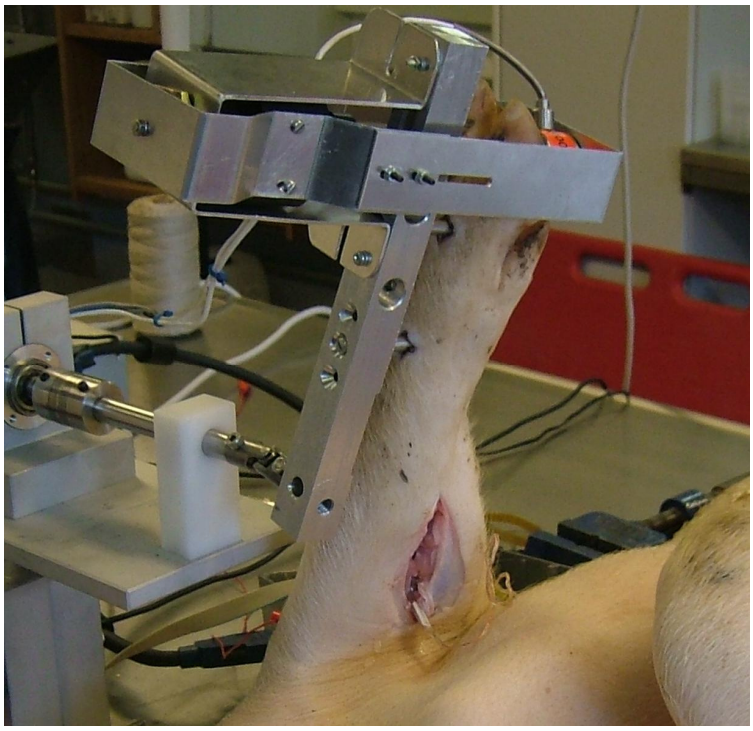

Figure 5-28 – Implant location.

5.5 Test Rig – Design 4 (Final design)

Going back to the graphical representation of the pig's tri-segmented forelimb, the following picture shows the location of the bones when the animal is on its feet. The green part represents the scapula, the upper arm in blue, lower arm in red and the hand in white. The final design of the test rig will be explained using these definitions.

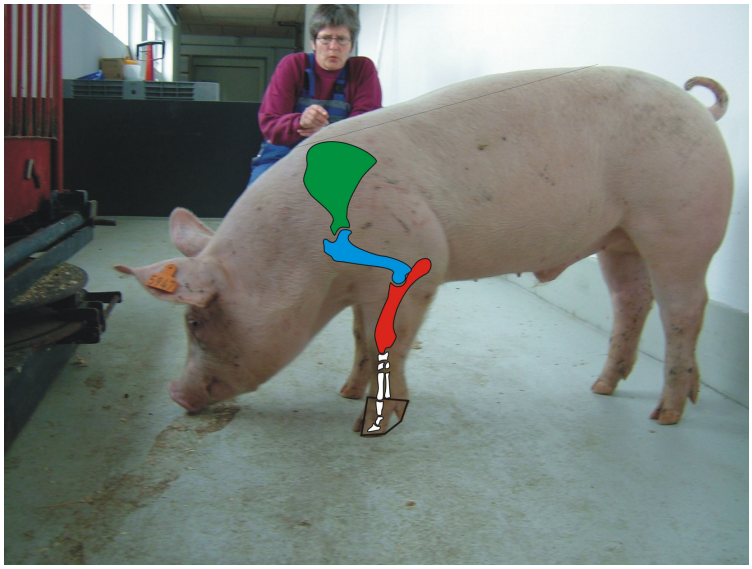

Figure 5-29 – Front View: Bone screw wrist fixation. -

In the next diagram, the most likely positions of the wrist joint when flexed and extended are shown. It is also shown that, when extended, this specific point could also be at a higher position, depending on the size of the pig obtained on the day of the experiment.

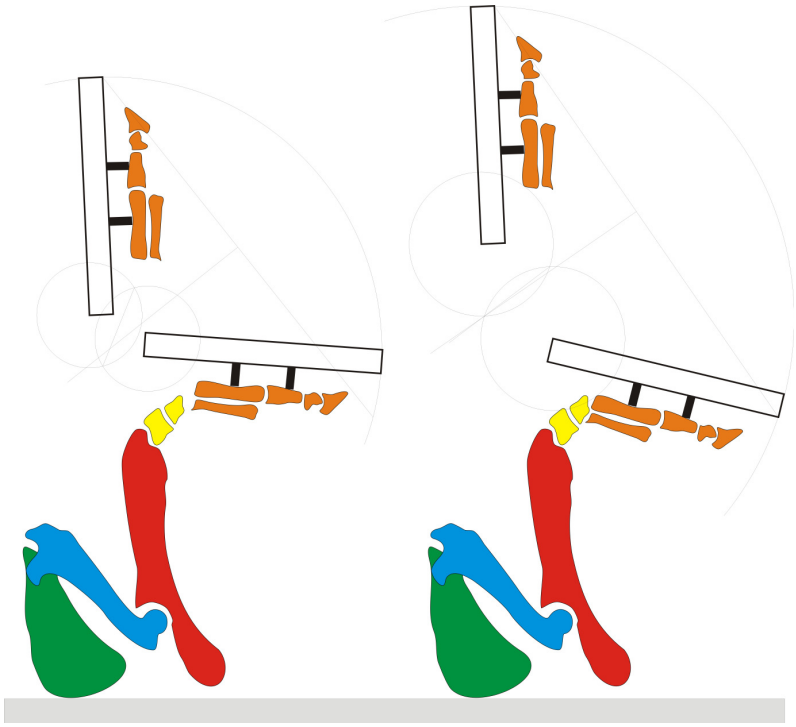

Figure 5-30 – Wrist positions when flexed and extended.

Based on this theory that the point of rotation could be anywhere within the surrounding area of the wrist joint in that plane, we have come up with an idea of having a metal plate with several pre-drilled locations. This way, based on the size of pig received on the day of the experiment, the user can first of all have a feel of the wrist movement by manually moving it around, and once the approximate location of the most ideal point of rotation is found, the plate is bolted in place, and the experiment can proceed as per the protocol.

The following pictures show the final test rig set-up in action. In this specific experiment, the wound does seem a bit bloody reason being the surgeon had to fiddle with the cuff from time to time as a few rings on the cuff were not picking any signals and also a lot of noise was being picked up by the amplifier. At the time, the surgeon thought it worse to flush the cuff and the exposed nerve with warm saline solution as one possible problem could have been a bad connection. Other than this, this test rig design did solve all the mechanical issues we had initially

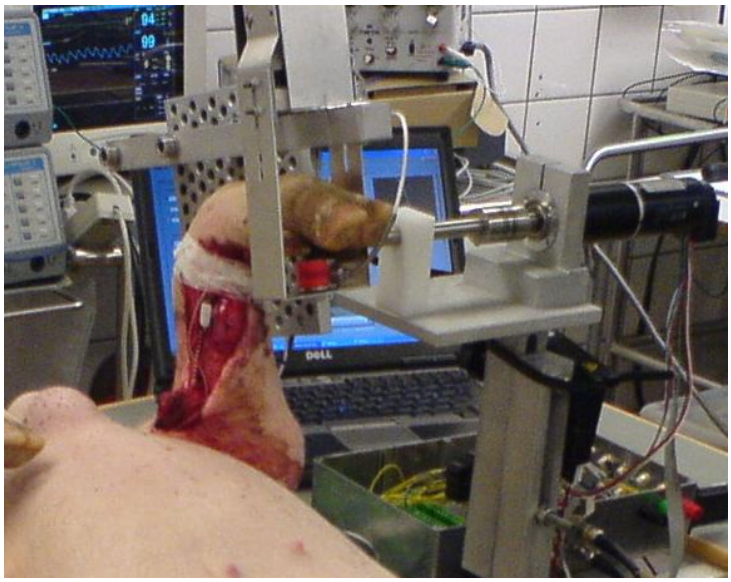

Figure 5-31 – Final design of the test rig in action. -

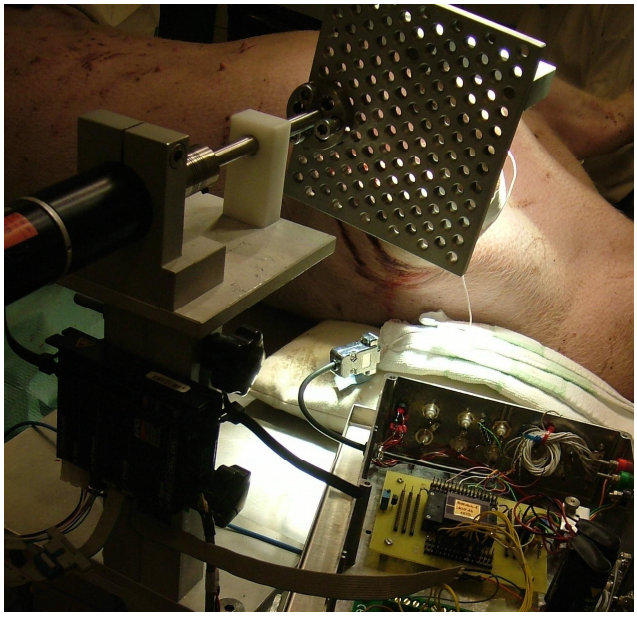

Figure 5-32 – Final design showing the connection of the motor shaft to the metal plate. -

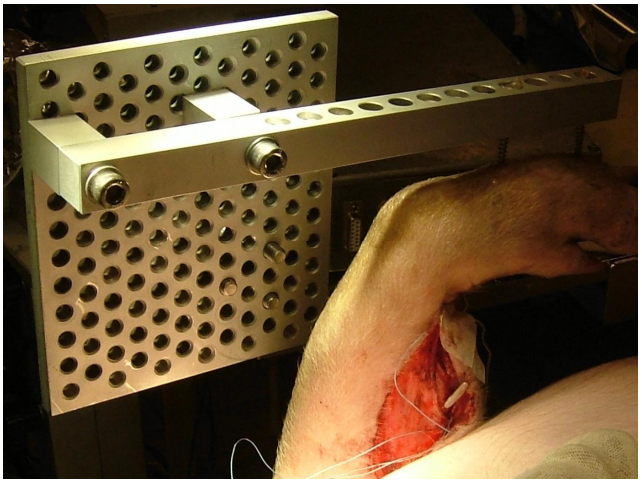

Figure 5-33 – Final design showing the connection of the wrist fixation to the metal plate. -

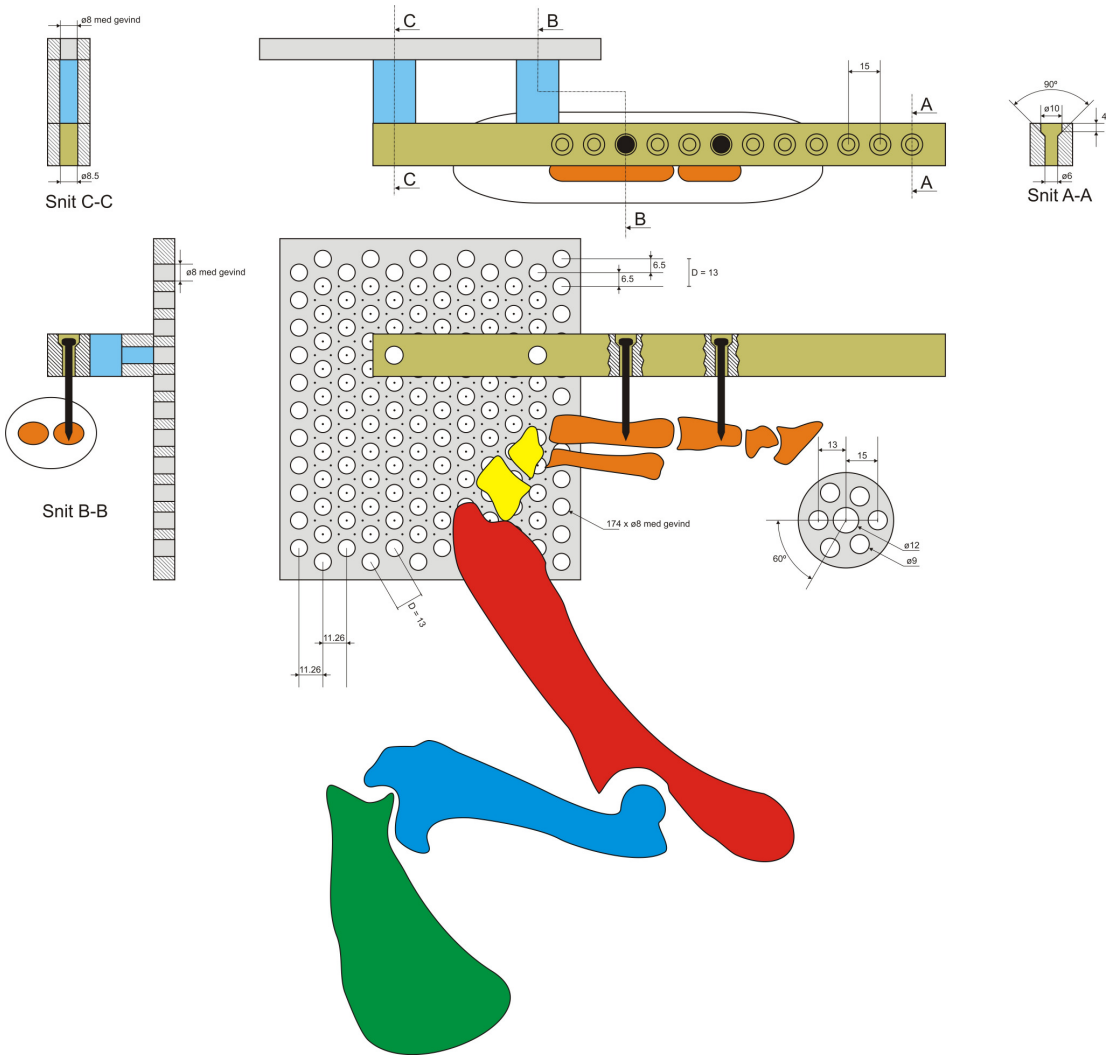

Figure 5-34 – Detailed drawing of the new components of the rotation system.

Furthermore, additional tests were carried out to ensure that the solenoid/load-cell set-up did work fine while simultaneously running the main Maxon motor. The following graphs show some results obtained during these specific experiments

The following figures consist of a set of two graphs each. The top shows the shape of the square profile of the solenoid motion in red line along with the resulting amplitude in white, measured by the load-cell. The lower graph shows the acceleration curve of the Maxon motor within the same timeframe.

To start off, the solenoid was activated without a pre-load. This can be seen on the first graph as both the red and the white plots starting off at zero. For both clockwise (Fig. 5-35) and ant-clockwise (Fig. 5-36) rotation of the Maxon motor, the solenoid and load-cell seem to be working in accordance to each other. In our experiments, a clockwise motion by the motor causes flexion of the limb, meaning the extensor muscle group is being stretched; On the other

hand, an anticlockwise motion causes extension of the limb, resulting in the flexor group being stretched.

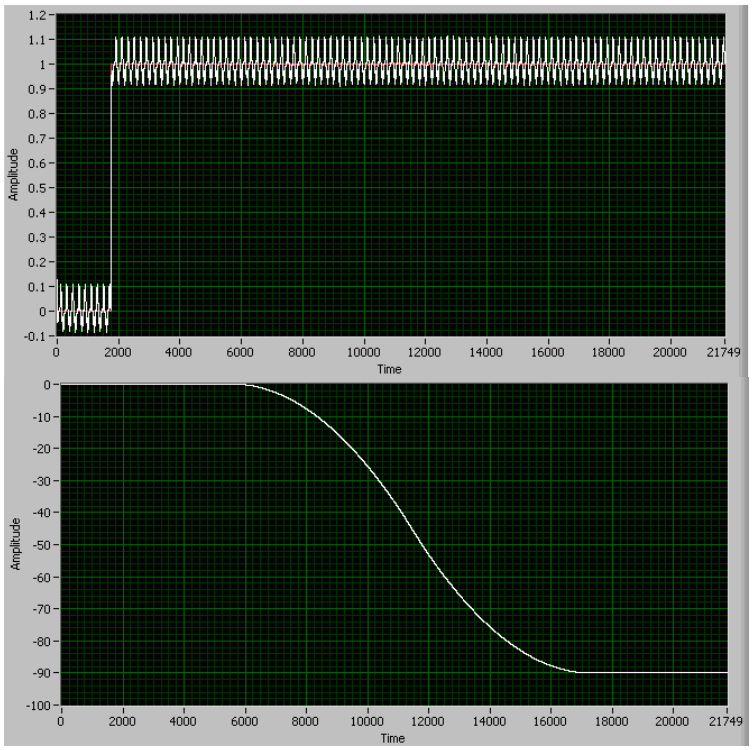

Figure 5-35 – Graph showing the effect of flexion of the limb on the solenoid. -

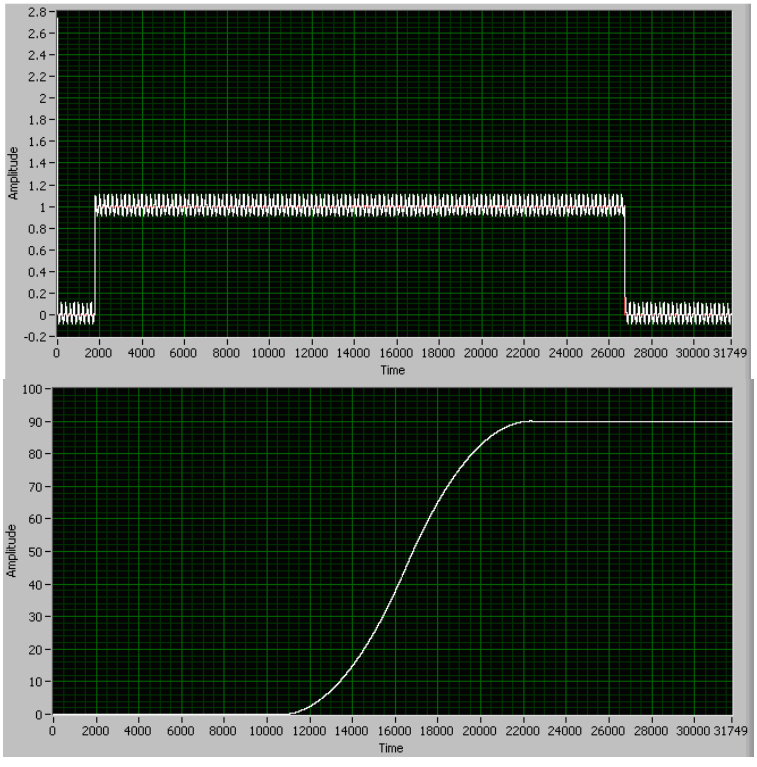

Figure 5-36 – Graph showing the effect of extension of the limb on the solenoid. -

The next step was to investigate the addition of a pre-load. The whole purpose of the pre-load is to prevent the loop from being broken. During one of the tests, the solenoid experienced a sudden jitter in the profile. This was found to occur in the event that the gap between the contactor and the skin was about 1 cm or more apart. While investigating the most suitable gaps, it was found that the gap between the contactor and the toe pad should be no bigger than 0.5 cm. This is because if the shaft of the solenoid is extended too much, this means that there is not enough material for the magnetic field to grasp on, and with reference to the section on the solenoid performance chart (Fig. 4-15), it is seen that the further the extension of the shaft, the weaker is the experienced force. This explains the sudden jitter halfway through the trend line.

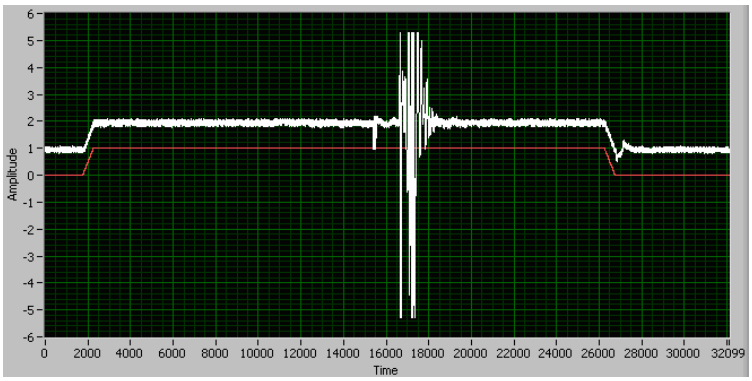

Figure 5-37 – Solenoid profile when leaving a gap bigger than 1cm between the toe pad and the load-cell contactor.

On the other hand, leaving a gap of just 5mm caused the pattern of the profile to be followed conveniently and relatively accurately for a home-made PID controller. The rise-time, fall-time and amplitude all corresponded to the desired ramp profile of the solenoid. Appendix G has all the data for this experiment.

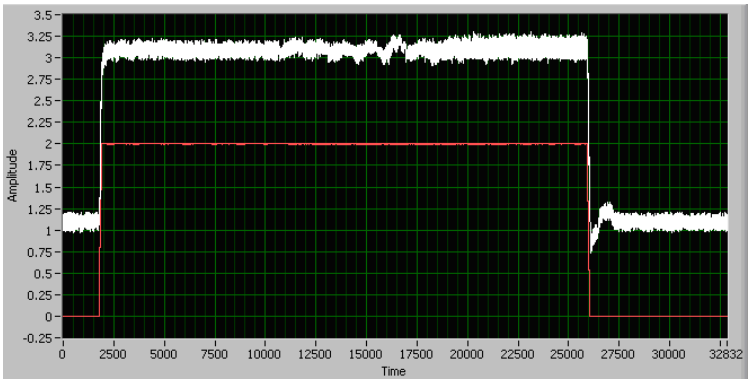

Figure 5-38 – Solenoid profile when leaving a gap of 0.5cm between the toe pad and the load-cell contactor. -

5.6 Amplifier Box

In order to solve the noise issue, a systematic approach was adopted by firstly investigating the equipment at hand: the amplifier box. The latter was originally built such that it required the cuff electrode to be attached to a connector (Connector 2 in Fig. 5-40) with 12-pins at the electrode end and 16-pins at the other end. This was in turn connected to another connector (Connector 1 in Fig. 5-40) that had 16-pins on one end and a 15-pins male D-Connector at the other. The amplifier box therefore had a female D-Connector to accommodate the cuff. The D-Connector was then directly wired to the ENG amplifier which was in turn fed to the screw terminals of a CB-68LPR National Instruments board with the mass termination of the board leading to the NI-USB 6251 DAQ module. Further details of the amplifier box are described in [3, 38, 45, 47, 77-79]. The pins on the ENG amplifier chip were allocated as in the following diagram. On the 'cuff side' of the chip, the pins were connected to the 11 channels (Ch) of the cuff and the DAQ side of the chip was wired to the Analogue Inputs (Ai) of the CB-68LPR board.

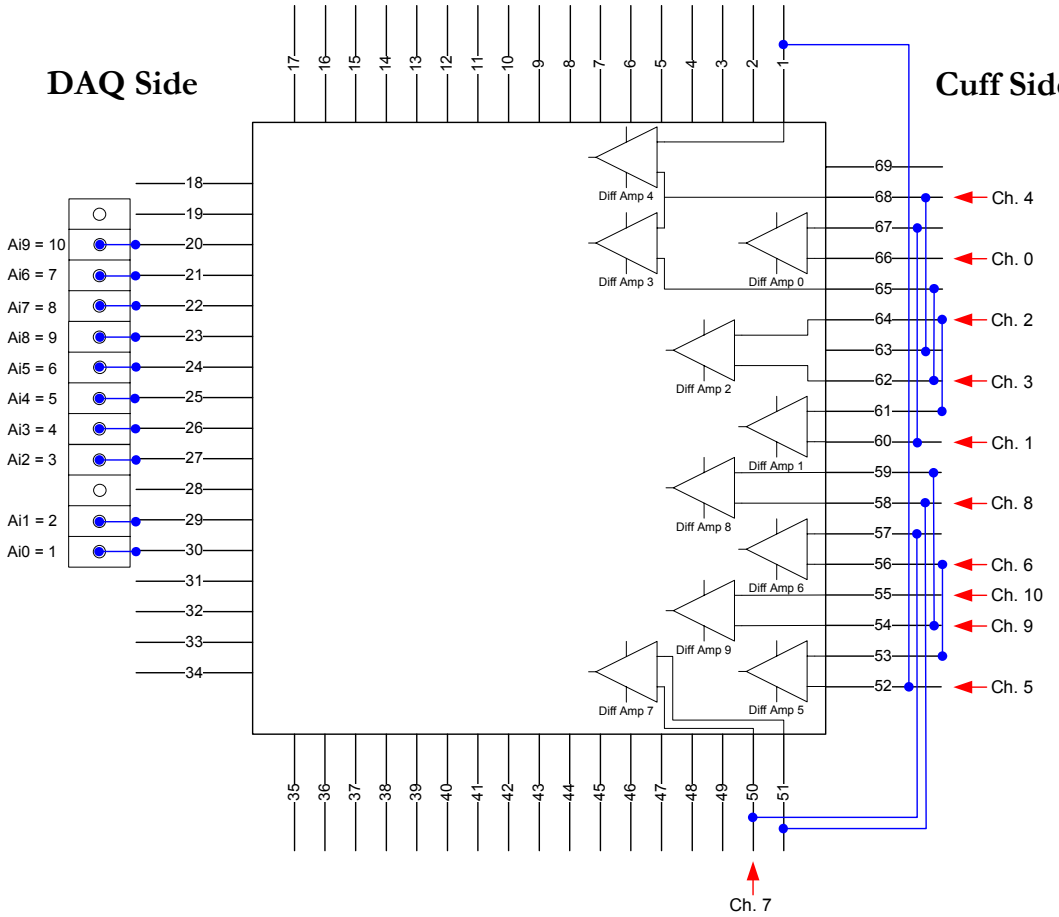

Figure 5-39 – Pins allocation on the ENG chip.

The set-up was such that the chip was connected to the cuff electrode by means of connectors, - with a female D-connector on the amplifier box. This could be problematic and possibly be the -

cause of the noise pick-up, and as a result the micro-volts being measured would just be lost in the way. Appendix J has the data supporting this argument.

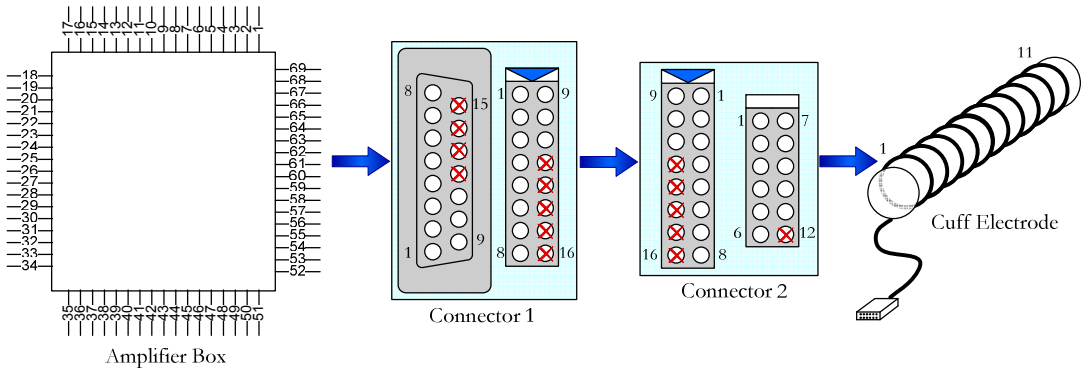

Figure 5-40 – Connector arrangement.

A possible solution was to eliminate the two connectors and connect the cuff electrode directly to the chip by means of a shielded cable. The connector to the cuff was custom-made to accommodate the size of electrodes available for the experiments. The following pictures show the new amplifier box after the necessary modifications.

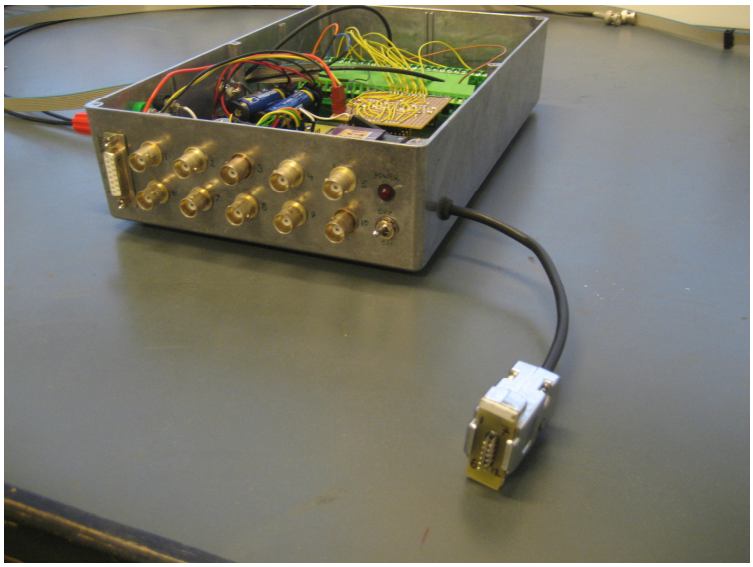

Figure 5-41 – New Amplifier box.

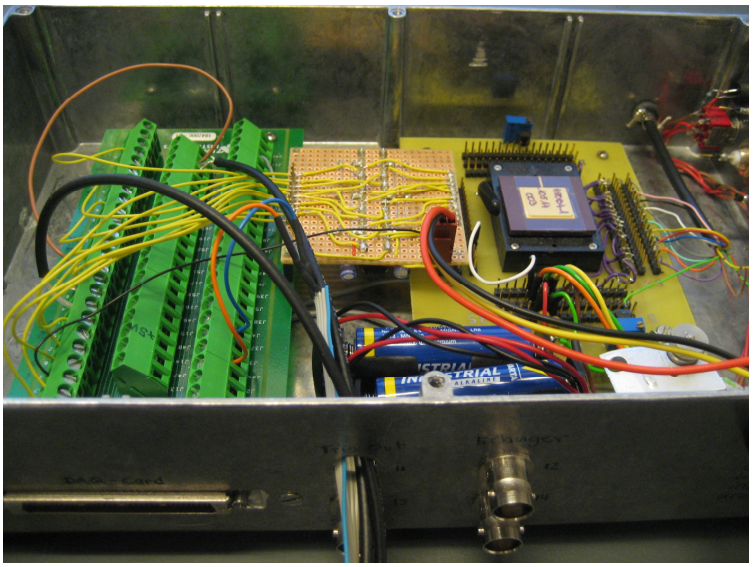

Figure 5-42 – Wiring access for the solenoid/load-cell. -

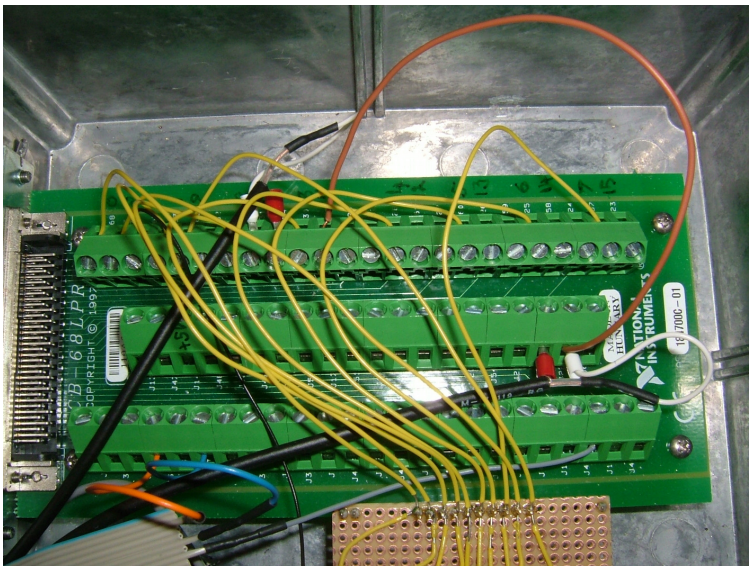

Figure 5-43 – Unity gain buffer connection. -

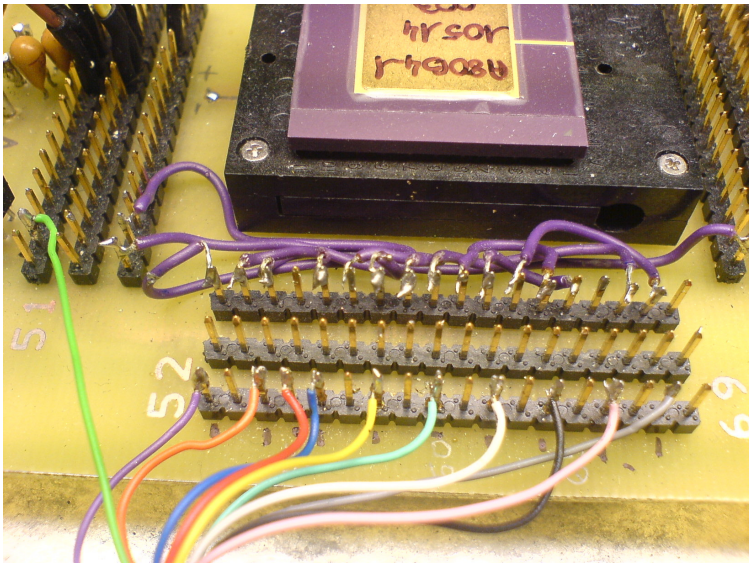

Figure 5-44 – Modified connections of the new cuff connector to the amplifier. -

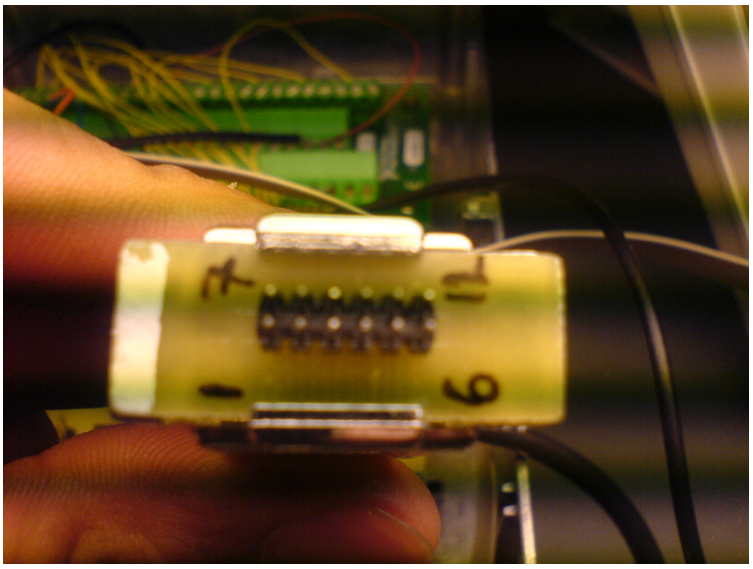

Figure 5-45 – Final cuff connector.

While carrying out some further tests (as in the set-up shown below), it was found that the output impedance of the ENG amplifier was around 10KΩ and this has a large effect on the cross-talk between channels. A unity gain buffer was therefore implemented between the amplifier chip and the USB data acquisition box.

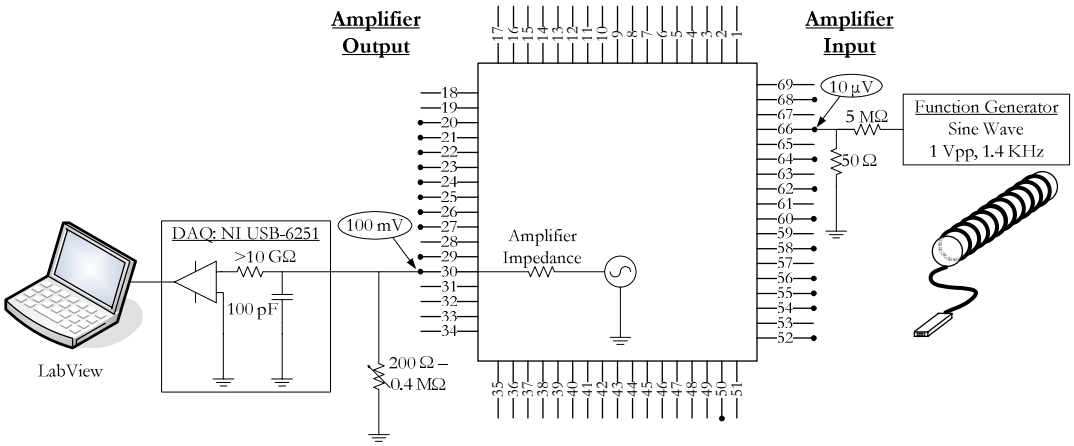

Figure 5-46 – Setup for test on output impedance of ENG amplifier.

5.7 Equipment shielding.

The next source of noise that could be polluting our recorded signals is that from the motor and the lengthy power cables driving much current from the power supply all the way to the motor. One way of dealing with this issue was to fit all wiring around the motor with Knitted Wire Mesh Gaskets. These show excellent shielding effectiveness against harmful electromagnetic/radio frequency interferences.

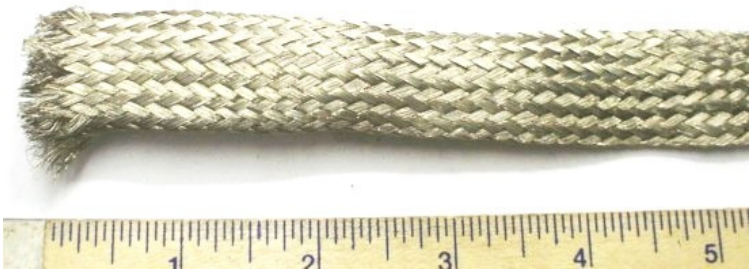

Figure 5-47 – Knitted wire mesh gasket.

A systematic approach was adopted whereby surrounding equipment was switched on and off so as to locate any interference source. When it came down to the Maxon motor, it was seen that having the motor off did have a huge impact on the recordings. Hence, to reduce the noise level due to the motor, it was directly shielded with aluminium-foil sheets, which was in turn grounded. Unfortunately this was still insufficient to clearly pick up Action Potentials from the recorded data. The next approach to this problem was to consider the cuff itself. Having a broken/loose connection in the electrode could possibly affect the rest of the signals. For this investigation, worms were used as they are simple organisms that would anatomically fit the cuff just as would a medial nerve and most importantly because it consists of nerves running along its whole length. See Appendix H.

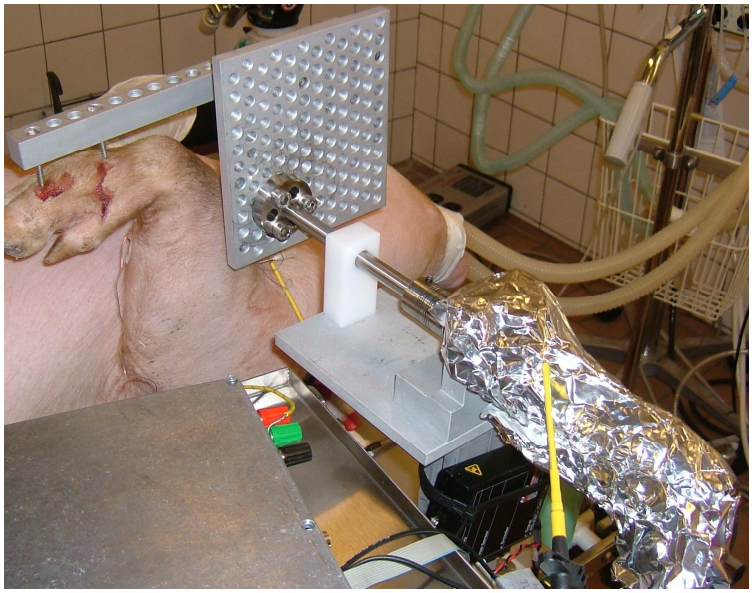

Figure 5-48 – Maxon motor wrapped with tin-foil. -

WORM EXPERIMENTS

6.1 Introduction

The work in this chapter had to be carried out in order to test the consistency of the cuff electrodes. It was feared that the rings of the electrodes might have been mishandled and possibly damaged in the process of placing them around the designated nerve. Earthworms were considered appropriate as a cheaper and more easily available medium for the tests rather than pig nerves. Earthworms been used for decades to investigate neuro-muscular systems ([80-85] for example). They have a segmented, compartmentalized, cylindrical body and range in length from several centimetres to nearly 3.3 m.

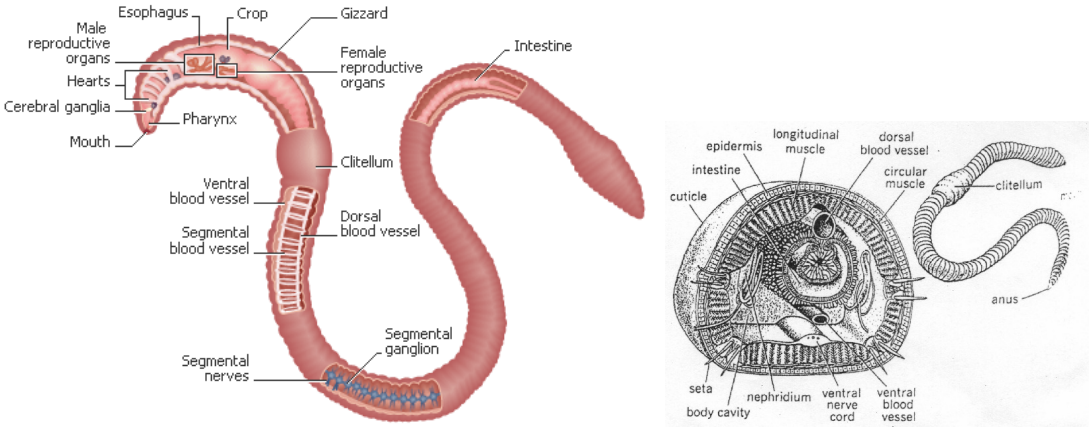

Figure 6-1 – Functional components of the worm.

The nervous system coordinates the movements of the worm and sends impulses received from sense organs to parts of the body. There is a very small nerve centre from which runs two nerves that form a connecting collar around the pharynx and join to become a long ventral nerve cord. There also are enlarged nerve centres, called ganglia, in each segment. Three pairs of nerves, in turn, branch from each ganglion. The latter are well coordinated with each other since they interact in order to control muscle contractions in each segment that are responsible for locomotion. Thanks to this responsive nervous system, earthworms are sensitive to touch, light, moisture, chemicals, temperature, and vibrations. The earthworm's brain consists of paired ganglia in the head end. When an impulse is detected by receptor cells in the skin, a pair of nerves in each of the earthworm's segments carries the signal to the brain and smaller ganglia in each segment, where the signals are analyzed. The central nervous system then transmits impulses on nerves that coordinate muscle action, causing the earthworm to move.

The earthworm nerve cord has three giant fibres, a median giant and two lateral giants. The median giant receives sensory input from the anterior portion of the worm while the lateral

giants receive sensory input from the posterior part. As a depolarization occurs at a point, the adjacent membrane is depolarized. This results in the voltage-gated ion channels in that region opening. Sodium enters the nerve cell, causing further depolarization. When the initial stimulus is above threshold for the membrane, an action potential occurs, taking the membrane to the sodium equilibrium potential. The driving force on potassium has been increased and it now exits the membrane and the sodium channels are inactivated, resulting in a brief under-shoot followed by a return to the resting potential. At the time of the action potential, the voltage in the axon will spread in a passive manner to the surrounding area. The voltage present at a point x on the axon is given by the equation

$$V_x = V_0 \times e^{-x/\lambda}$$

So a λ length of the axon will be above threshold, causing action potentials in this area of the axon. This action continues in a domino effect down the length of the axon. Axons with a larger diameter have a lower internal resistance which gives them a lower length constant (λ = square root of the quotient of membrane resistance with the sum of internal and external resistance). We therefore expect the conductance velocity to be faster for a larger diameter axon.

6.2 Worm Tests

The worm was anaesthetised using ethanol solution and then pinned to a dissecting block with the lighter side facing up. Additional media files for the worm experiments are located in Appendix K

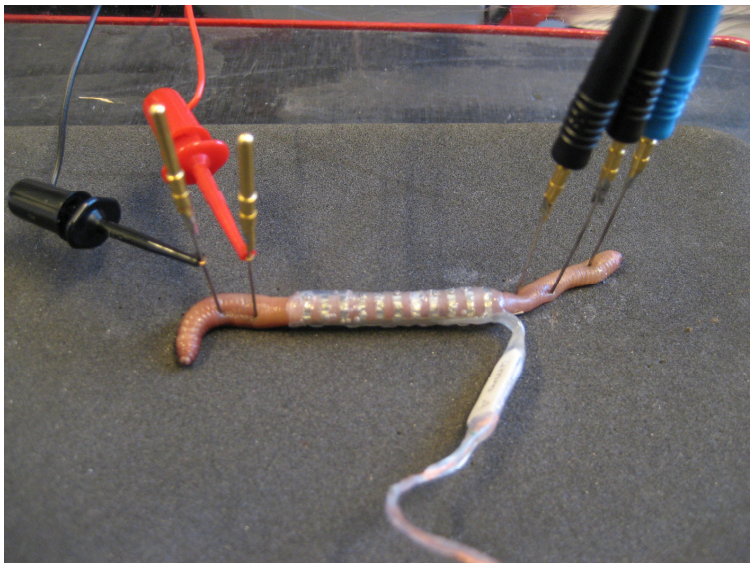

Figure 6-2 – Worm experiment set-up. -

At one end, a stimulator was used to generate current controlled, charge balanced, rectangular - shaped pulses on two latched channels. The stimulating pulse was adjustable in amplitude and - pulse width. A set of stimulation parameters was found that just excited a single population of -

large fibres, resulting in a simple-shaped biphasic CAP recording picked up by the recording cuff electrode. Another set of stimulation parameters was worked out that resulted in a neurogram which suggested the presence of at least a second fibre population, slower in propagation than the first one. We saw two separate action potentials. The first action potential represents the median giant axon and the second represents the lateral axons. Once again, this proves that multi-contact cuff recordings can be interpreted with ease. Using worms as nerve models, it has been demonstrated that this method is applicable to such setups and provides information in the shape of a profile of the conduction velocity of the active fibres as well as their direction of propagation.

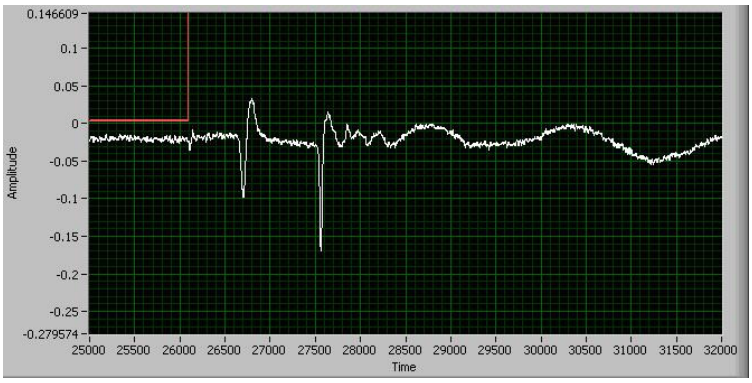

Figure 6-3 – Worm action potentials.

6.3 Cuff Electrode Tests

In our quest to narrow down the source of the noise problem, some tests were performed on the 4 cuff electrodes that were available for the experiments. In order to test their reliability, they were first used in the labs and then compared to their performance in the hospital environment. The cuffs were tagged with numbers 1-4 and an impedance meter (IM002-02 SMI2001) was used to measure impedance between every ring on each cuff. (This impedance meter generates a sine wave of 65 nA at 1024 Hz). The following graph shows the performance of each cuff.

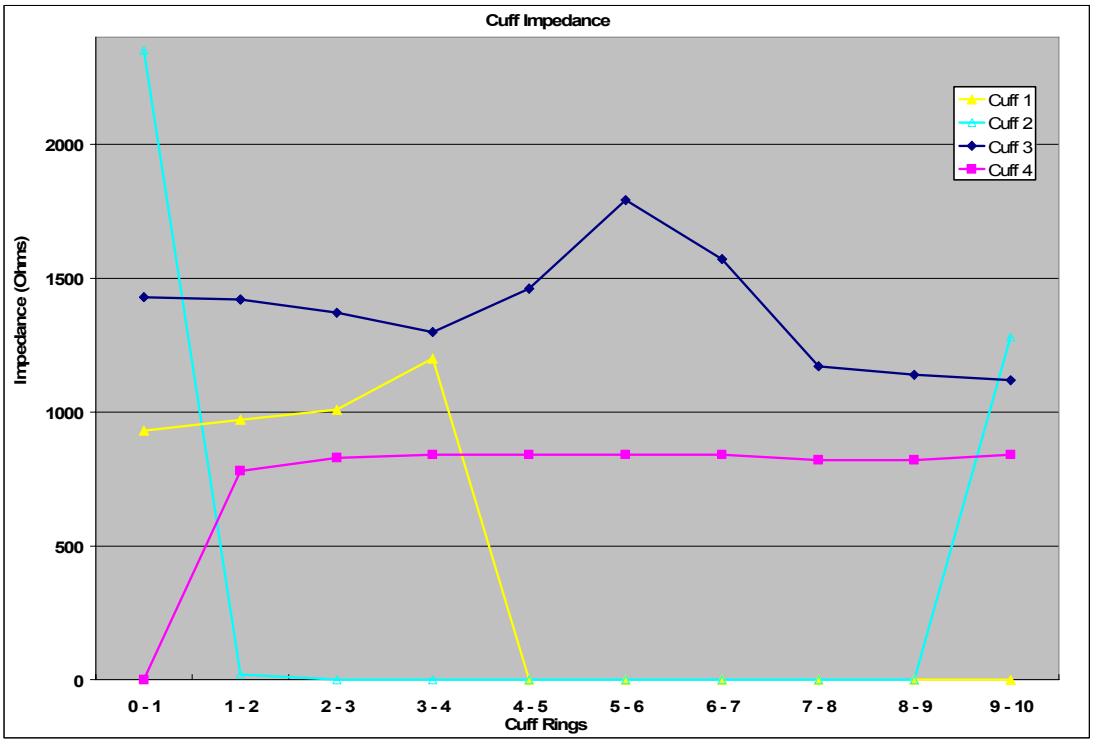

Figure 6-4 – Cuff Impedance measurement.

After being used on the past experiments, Cuffs 3 and 4 still seem to be usable, provided that the end electrode on Cuff 4 is neglected. Cuffs 1 & 2 were the smaller ones at 2mm internal diameter (ID) and cuffs 3 & 4 were the bigger ones with 4mm ID. Furthermore, Cuff 3 was tested as being the good one and was therefore used during the final experiments. However some impedance measurements were performed before and after implantation, and it was found that, after placing the cuff on the nerve, signals on rings 0, 1 and 2 were actually lost in the process. This was later confirmed during the recording session, as these 3 channels were picking up an awful lot of noise and getting saturated as a result.

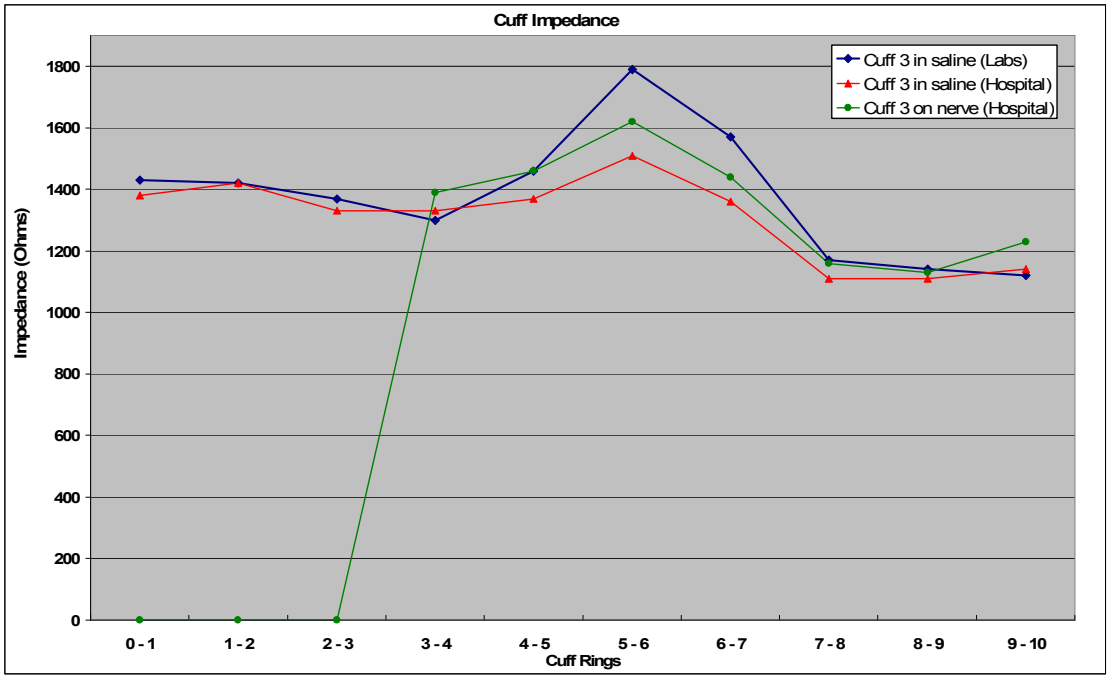

Figure 6-5 – Impedance on Cuff 3.

The lack of alternative cuffs with different internal diameters did cause a problem. In the final experiment, the median nerve was much smaller than the cuff, even though the pig was a fairly large one (the biggest so far). This could be tricky in the sense that the surface area of the nerve being in contact with the cuff electrodes is minimal.

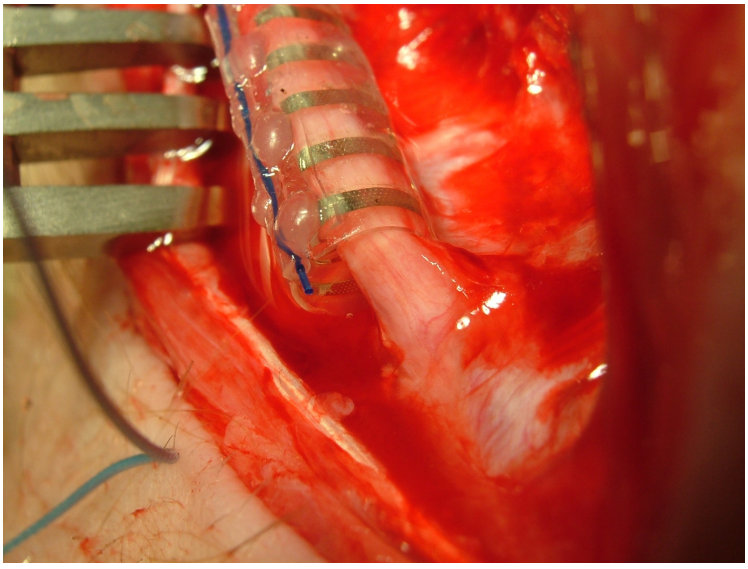

Figure 6-6 – Cuff 3 placed on the Median nerve.

The following picture shows a cuff lying freely in a bath of saline and it can be seen how this ribbon is twisted and consequently influenced by the position of the cuff on one side, and the blue connector on the other.

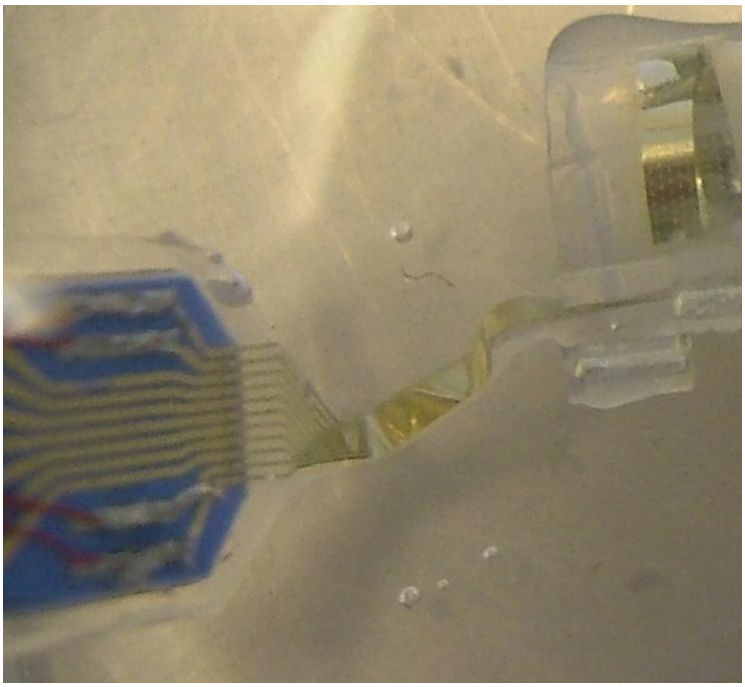

Figure 6-7 – Twisted ribbon.

Considering the cuff as a whole, the ribbon is the only part of the entire cuff that is shorter and thinner than the rest (9mm x 1mm). So the amount of material (friction and mass to be considered) on either side of this strip does have an effect on its behaviour. This strip is more prone to damage and should therefore be made much stronger in future designs.

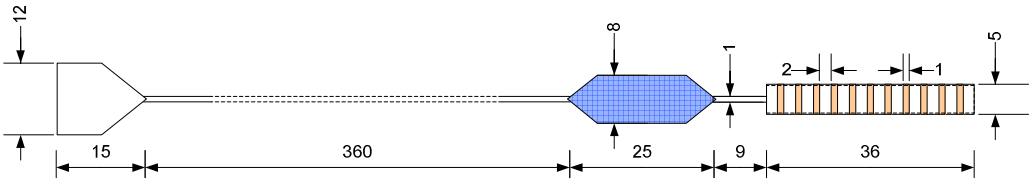

Figure 6-8 – Detailed drawing of a cuff electrode.

In order to screen the cuffs for any physical damage, it was analysed using a digital microscope. For example, Cuff 1 was considered, which according to the impedance analysis, suffered some damage, except for rings 0 to 3. So when examining this particular cuff, we tried to find any broken paths that would probably explain the remaining rings. Some unusual findings did crop up; one of the paths seemed to have been fixed with some solder as seen below:

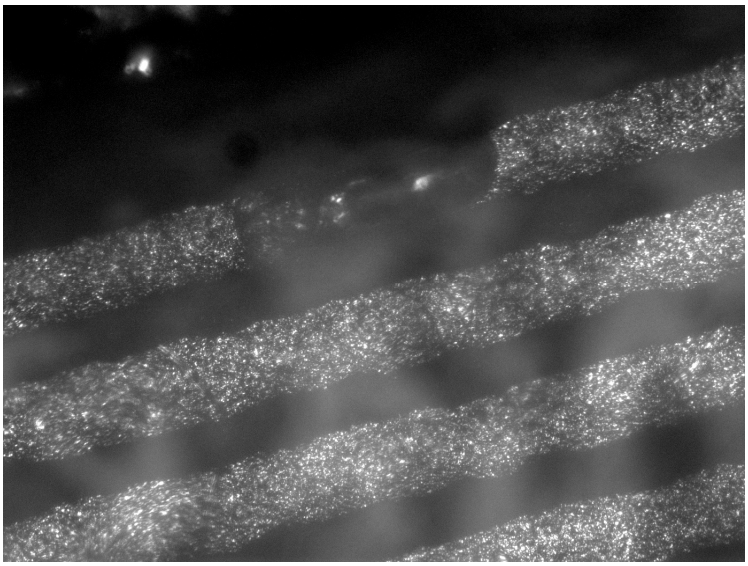

Figure 6-9 – Solder found along a strip in the cuff.

Further down on the same print, the material seen on one of the track seemed much less than that on others. This could well be a photo-illusion, but if not, it would definitely explain the irregularity of the cuff.

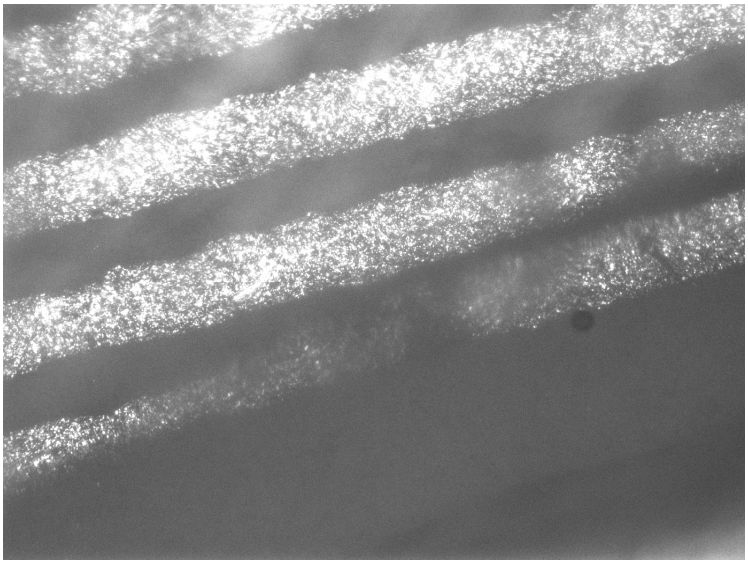

Figure 6-10 – Lack of material along a strip in the cuff.

When analysing ring 1 of the cuff, some cracks were also noticed. Surprisingly enough, ring 1 was one of the good ones in that cuff. So it might well be that it is only a matter of seconds after further manipulation that the ring might go bad. Along the surface of the ring itself, some cracks are also seen and this might well have been caused by continuous handling (opening and closing of the cuff to place it on and remove it from a nerve). But what is hard to explain at this point is the lack of material in the region which is so close to the part where the ring is connected to the track that going out of the cuff to the thin ribbon.

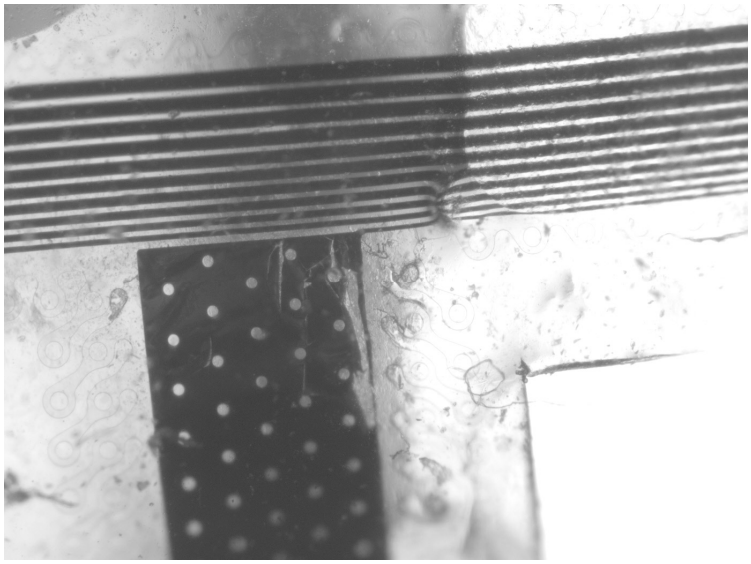

Figure 6-11 – Lack of conducting material on one ring.

The same picture zoomed on the crack clearly shows how the performance of one ring of the cuff is dependant on the quality of material linking the ring to the rest of the ribbon. See Appendix I for more photos.

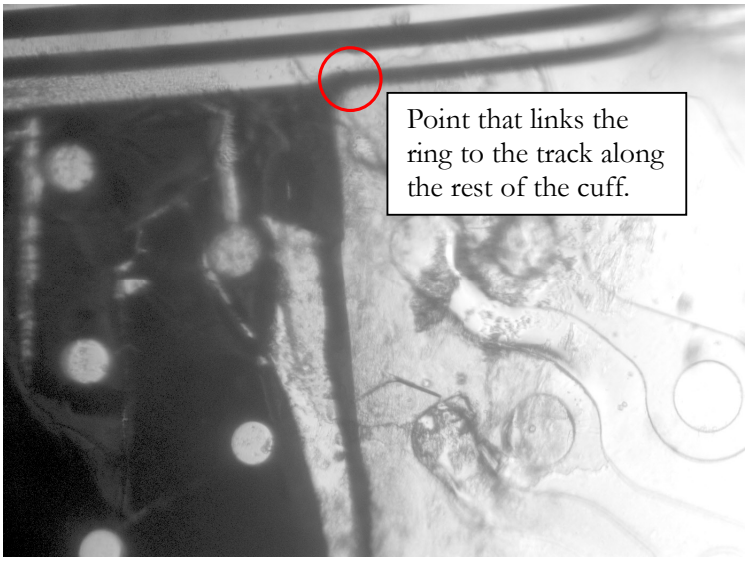

Figure 6-12 – Zoomed view showing lack of conducting material. -

Chapter 7

CONCLUSIONS & FUTURE WORKS

The main purpose of the this research was to test the model of the nerve/electrodes/processing using Compound Action Potentials (CAPs), propagating in velocity ranges in vitro, and to furthermore show that three distinct naturally occurring nerve signals (cutaneous, joint receptors and tendon stretch receptors) in one nerve can be separated in vivo.

This thesis did indeed present the successful application of conduction velocity-selective ENG recording system to electrically evoked potentials using the frog sciatic nerve in-vitro, as described in Chapter 3. However, when it came to testing the recording system on naturally-occurring neural signals from the pig's median nerve, time constraints along with equipment malfunction did not allow for successful recordings. It all started off with the unsuitability of the initial rig to accommodate the pig's limb as per the intended protocol. This in turn delayed the subsequent experiments and this time was instead dedicated in developing new designs for the test rig. However, after extensive re-designing of the equipment and experiment set-up, a lot has been learnt when it comes to mounting a pig's limb to a test rig and the mechanism behind this tri-segmented limb. Chapter 5 covered the evolution of the initial rig design to the final working product.

Unfortunately, the rig was just one of the problems encountered; the recorded data was being polluted with interfering noise and more time had to be dedicated to finding this source. Chapters 5 and 6 covered the attempts of solving this issue by investigating the other electrical components present in these experiments: the amplifier box, the motors and the cuffs. These investigations involved worm experiments whereby the multi electrode cuff was placed on worms to record signals generated by a stimulator at one end of the worm.

The final design of the apparatus will surely be a good continuation for further research in this area. Before such a system can successfully be used in conjunction with neuroprosthesis in chronic pig experiments, a large amount of work remains to be completed. The following points are issues that need to be addressed:

- Further experiments on the noise performance of the MEC need to be conducted. This should take into consideration all surrounding equipment of the surgical environment – motors, laptops, PID controllers, shielding solutions, etc.
- Additional understanding of the mechanism of the pig's limb and an improvement of the limb fixation technique.
- Improvement on the mechanical strength of the cuff electrodes.

Chapter 8

APPENDICES

The Appendices mainly consist of media files and different software versions along with the data collected during the various experiments that have been carried out. These are supplied on 2 separate DVDs labelled 'Disc 1' and 'Disc 2'.

Appendix A: London Frog Experiments - August 2005

Appendix B: Aalborg Pig Experiments - September 2005

Appendix C: PID Controller - March 2007

Appendix D: Pig Fitting

Appendix E: Bone Tests

Appendix F: Foulum Pig Experiments - July 2007

Appendix G: Solenoid-Loadcell Experiments - July 2007

Appendix H: Aalborg Pig Experiments - October 2007

Appendix I: Microscope Media - October 2007

Appendix J: Cuff Connector Experiments - November 2007

Appendix K: Worm Experiments - December 2007

Appendix L: Corel Version 12 Files

Appendix M: Random Software Used

REFERENCES

1. - Erlanger, J. and H.S. Gasser, *The comparative physiological characteristics of nerve fibres.* Electrical Signs of Nervous Activity, The Eldridge Reeves Johnson Foundation for Medical Physics, 1937: p. 34-78.
2. - Rushton, W.A.H., *A theory of the effects of fibre size in medullated nerve.* Journal of Physiology, 1951. **115**: p. 101-122.
3. - Taylor, J., N. Donaldson, and J. Winter, *Multiple-electrode nerve cuffs for low-velocity and velocity-selective neural recording.* Medical & Biological Engineering & Computing, 2004. **42**: p. 634-643.
4. - Giuliodori, M.J. and S.E. DiCarlo, *Myelinated vs. unmyelinated nerve conduction: A novel way of understanding the mechanisms* Advances in Physiology Education, 2004. **28**: p. 80-81.
5. - Goodman, B.E. and S.B. Waller, *Propagation of action potentials in myelinated vs. unmyelinated neurons.* Advances in Physiology Education, 2002. **26**: p. 223.
6. - Carpenter, R.H.S., *Neurophysiology*. 4 ed. 2003, United Kingdom: Edward Arnold.
7. - Hodgkin, A.L. and A.F. Huxley, *A quantitative description of membrane current and its application to conduction and excitation in nerve.* Journal of Physiology, 1952. **117**: p. 500-544.
8. - Hoffer, A.J., *Techniques to study spinal cord peripheral nerve and muscle activity in freely moving animals*. Neuromethods - Neurophysiological Techniques: Applications to Neural Systems, ed. A.A. Boulton, B.G. B., and C.H. Vanderwolf. Vol. 15. 1990, New York: The Humana Press Inc., Clifton, NJ. 65-145.
9. - Roberts, W.M. and D.K. Hartline, *Separation of multi-unit nerve impulse trains by a multi-channel linear filter algorithm.* Brain Research, 1975. **94**: p. 141-149.
10. - Andreassen, S., R.B. Stein, and M.N. Oğuztöreli, *Application of optimal multichannel filtering to simulated nerve signals.* Biological Cybernetics, 1979. **32**(1): p. 25-33.
11. - Heetderks, W.J. and W.J. Williams, *Partition of gross peripheral nerve activity into single unit responses by correlation techniques.* Science, 1975. **188**: p. 373-375.
12. - Haugland, M.K. and T. Sinkjær, *Cutaneous whole nerve recordings used for correction of footdrop in hemiplegic man.* IEEE Transactions on Rehabilitation Engineering, 1995. **3**(4): p. 307 - 317.
13. - Haugland, M.K., A.J. Hoffer, and T. Sinkjær, *Skin contact force information in sensory nerve signals recorded by implanted cuff electrodes.* IEEE Transactions on Rehabilitation Engineering, 1994. **2**(1): p. 18 - 28.
14. - Hoffer, A.J. and M. Haugland, *Signals form tactile sensors in glabrous skin: Recording, processing, and applications for the restoration of motor functions in paralysed humans*. Neural prostheses: Replacing motor function after disease or disability., ed. Stein/Peckham/Popovic. 1992: Oxford University Press. 99-125.
15. - Stein, R., et al., *Principles underlying new methods for chronic neural recording.* Canadian Journal of Neurological Sciences, 1975. **2**: p. 235-244.
16. - Haugland, M.K. and A.J. Hoffer, *Slip information provided by nerve signals: Application in closed-loop control of Functional Electrical Stimulation.* IEEE Transactions on Rehabilitation Engineering, 1994. **2**(1): p. 29 - 36.
17. - Haugland, M.K., et al., *Control of FES thumb force using slip information obtained from the cutaneous electroneurogram in quadriplegic man.* IEEE Transactions on Rehabilitation Engineering, 1999. **7**(2): p. 215 - 227.
18. - Stein, R., et al., *Impedence properties of metal electrodes for chronic recording from mammalian nerves.* IEEE Transactions On Biomedical Engineering, 1978. **25**(6): p. 532-536.
19. - Rodriguez, F.J., et al., *Polyimide cuff electrodes for peripheral nerve stimulation.* Journal of Neuroscience Methods, 2000. **98**: p. 105-118.
20. - Sahin, M. and D.M. Durand, *Improved nerve cuff electrode recordings with subthreshold anodic currents.* IEEE Transactions On Biomedical Engineering, 1998. **45**(8): p. 1044-1050.

21. - Haugland, M., *A flexible method for fabrication of nerve cuff electrodes*, in *18th Annual International Conference of the IEEE Engineering in Medicine and Biology Society*. 1996: Amsterdam. p. 359-360.
22. - Sahin, M., et al., *Spiral nerve cuff electrode for recordings of respiratory output*. Journal of Applied Physiology, 1997. **83**: p. 317-322.
23. - Hoffer, A.J., *Techniques to study spinal-cord, peripheral nerve, and muscle activity in freely moving animals*. Neuromethods, 1990. **15**: p. 65-115.
24. - Stein, R., et al., *Stable long-term recordings from cat peripheral nerves*. Brain Research, 1977. **128**: p. 21-38.
25. - Thomsen, M., *Characterisation and optimisation of whole nerve recording cuff electrodes*, in *SMI*. 1998, Aalborg University.: Aalborg, Denmark.
26. - Winter, J., et al. *Improved spatial filtering of ENG signals using a multielectrode nerve cuff*. in *5th International Functional Electrical Stimulation Society (IFESS)*. 2000. Aalborg, Denmark.
27. - Rahal, M., J. Taylor, and N. Donaldson, *The effect of nerve cuff geometry on interference reduction: A study by computer modeling*. IEEE Transactions on Biomedical Engineering, 2000. **47**(1): p. 136 - 138.
28. - Rahal, M., et al., *An improved configuration for the reduction of EMG in electrode cuff recordings: A theoretical approach*. IEEE Transactions on Biomedical Engineering, 2000. **47**(9): p. 1281 - 1284.
29. - Andreasen, L.N.S. and J.J. Struijk, *Signal strength versus cuff length in nerve cuff electrode recordings*. IEEE Transactions On Biomedical Engineering, 2002. **49**(9): p. 1045-1050.
30. - Peckham, P. *Coordinated two mode grasp in the quadriplegic initiated by functional neuromuscular stimulation*. in *IFAC Control aspects of prosthetics and orthotics*. 1982. Ohio, USA.
31. - Peckham, P. and M. Keith, *Motor prostheses for restoration of upper extremity function*. Neural Prostheses: Replacing motor function after disease or disability. 1992, New York: Oxford University Press. 162-190.
32. - Pflaum, C., R.R. Riso, and G. Wiesspeiner. *Performance of alternative amplifier configurations for tripolar nerve cuff recorded ENG*. in *18th Annual International Conference of the IEEE Engineering in medicine and Biology Society*. 1996. Amsterdam.
33. - Schuettler, M., et al. *Multichannel neural cuff electrodes with integrated multiplexer circuit*. in *1st Annual International IEEE-EMBS Special Topic Conference on Microtechnologies in Medicine & Biology*. 2000. Lyon, France.
34. - Stein, R.B. and K.G. Pearson, *Predicted amplitude and form of action potentials recorded from unmyelinated nerve fibres*. Journal of Theoretical Biology, 1971. **32**: p. 539-558.
35. - Marks, W.B. and D.E. Loeb, *Action currents, internodal potentials, and extracellular records of myelinated mammalian nerve fibers derived from node potentials*. Biophysical Journal, 1976. **16**: p. 655-668.
36. - Struijk, J.J., *The extracellular potential of a myelinated nerve fiber in an unbounded medium and in nerve cuff models*. Biophysical Journal, 1997. **72**: p. 2457-2469.
37. - Steyaert, M., W. Sansen, and C. Zhongyuan, *A micropower low-noise monolithic instrumentation amplifier for medical purposes*. IEEE Journal Of Solid-State Circuits, 1987. **SC-22**(6).
38. - Rieger, R., et al., *Design of a low-noise preamplifier for nerve cuff electrode recording*. IEEE Journal Of Solid-State Circuits, 2003. **38**(8): p. 1373 - 1379.
39. - Rahal, M., et al., *Application of closed-loop control in the reduction of interference in nerve cuff recordings*. IEEE, 1999: p. 1039 - 1042.
40. - Jezernik, S., W. Grill, and T. Sinkjær. *Neurographic recordings, electrical stimulation and new neural signal processing methods for closed-loop neuroprosthetic control of bladder hyper-reflexia* in *4th Proceedings of the IFESS Conference*. 1999. Sendai, Japan.
41. - Schoonhoven, R. and D.F. Stegeman, *Models and analysis of compound action nerve potentials*. Critical Reviews in Biomedical Engineering, 1991. **19**(1): p. 47-111.

42. - Donaldson, N., J. Taylor, and J. Winter. *Velocity-selective recording using multi-electrode nerve cuffs*. in *7th Proceedings of the IFESS Conference*. 2002. Ljubljana.
43. - Farina, D., E. Fortunato, and M. Merletti, *Non-invasive estimation of motorunit conduction velocity distribution using linear electrode arrays*. IEEE Transactions On Biomedical Engineering, 2000. **47**(3).
44. - Merletti, R., et al., *Modeling of surface myoelectric signals - Part II: model-based signal interpretation*. IEEE Transactions on Biomedical Engineering, 1999. **46**(7): p. 821- 829.
45. - Rieger, R., *Implantable analogue circuits for improved methods of nerve signal recording*, in *Department of Electronic and Electrical Engineering*. 2004, University College London: London.
46. - Rieger, R., et al., *Experimental determination of compound action potential direction and propagation velocity from multi-electrode nerve cuffs*. Medical Engineering & Physics, 2004. **26**: p. 531-534.
47. - Rieger, R., et al., *Very low-noise ENG amplifier system using CMOS technology*. IEEE Transactions On Neural Systems And Rehabilitation Engineering, 2006. **14**(4): p. 427-437.
48. - Stieglitz, T., et al., *Micromachined polyimide-based devices for flexible neural interfaces*. Biomedical Microdevices, 2000. **2**(4): p. 283-294.
49. - Rijkhoff, N.J.M., et al., *Acute animal studies on the use of an anodal block to reduce urethral resistance in sacral root stimulation*. IEEE Transactions on Rehabilitation Engineering, 1994. **2**(2): p. 92-99.
50. - Woo, M.Y. and B. Campbell, *Asynchronous firing and block of peripheral nerve conduction by 20 KC alternating current*. Bulletin of the Los Angeles Neurological Society, 1964. **29**(2): p. 87-94.
51. - Rijkhoff , N.J.M., J. Holsheimer, and E.L. Koldewijn, *Selective stimulation of sacral nerve roots for bladder control: A study by computer modelling*. IEEE Transactions On Biomedical Engineering, 1994. **41**(5): p. 413-424.
52. - Popesko, P., *Atlas der topographischen anatomie der haustiere*. 1993. **3**: p. 107, 109.
53. - Basilio, J.C. and S.R. Matos, *Design of PI and PID controllers with transient performance specification*. IEEE Transactions on education, 2002. **45**(4): p. 364-370.
54. - Dey, C., R.K. Mudi, and T.T. Lee, *A PID controller with dynamic set-point weighting*. IEEE, 2006.
55. - Drljević, E., B. Peruničić, and Ž. Jurić. *A new closed-loop identification method of a hammerstein-type system with a pure time delay*. in *2007 Mediterranean conference on control and automation*. 2007. Athens, Greece: IEEE.
56. - Garcia, D., et al. *PID controller design with constraints on sensitivity functions using loop slope adjustment*. in *Proceedings of the 2006 American Control Conference*. 2006. Minneapolis, Minnesota, USA: IEEE.
57. - Hang, C.C., *The choice of controller zeros*. IEEE Control Systems Magazine, 1989: p. 72-75.
58. - Hang, C.C., K.J. Astrom, and W.K. Ho, *Refinements of the Ziegler-Nichols tuning formula*. IEE PROCEEDINGS-D, 1991. **138**(2): p. 111-118.
59. - Meyrath, T.P., *Multipurpose analog PID controller*. 2005, University of Texas at Austin: Texas.
60. - Oubrahim, R. and F. Leonard. *PID auto-tuning by a composed structure*. in *Proceedings of the 1998 IEEE International Conference on Control Applications*. 1998. Trieste, Italy: IEEE.
61. - Oubrahim, R. and F. Leonard. *PID tuning by a composed structure*. in *UKACC International Conference on Control '98*. 1998. UK.
62. - Jurić, Ž. and B. Peruničić. *A simple extension of Ziegler-Nichols' method based on damped oscillations*. in *Proceedings of the 16th IEEE International Conference on Electronics, Communications and Computers (CONIELECOMP 2006)*. 2006: IEEE.
63. - Ziegler, J.G. and N.B. Nichols, *Optimal settings for automatic controllers*. Trans. ASME, 1942. **64**: p. 759-768.

64. - Aida, S., T. Tobita, and K. Shimoji, *Effects of continuous epidural block on motor nerve conduction velocity in patients with lower spine disorders.* Journal of Anesthesia, 1994. **8**: p. 32-35.
65. - Al-Nasser, B., *Toxic effects of epidural analgesia with ropivacaine 0.2% in a diabetic patient.* Journal of Clinical Anesthesia, 2004. **16**: p. 220-223.
66. - Altunkaya, H., et al., *Comparison of local anaesthetic effects of tramadol with prilocaine for minor surgical procedures.* British Journal of Anaesthesia, 2003. **90**(3): p. 320-322.
67. - Weese-Mayer, D.E., et al., *Effects of almitrine on hypoglossal and phrenic electroneurograms.* Journal of Applied Physiology, 1985. **59**(1): p. 105-112.
68. - Mateu, L., et al., *The action of local anesthetics on myelin structure and nerve conduction in toad sciatic nerve.* Biophysical Journal, 1997. **70**: p. 2581-2587.
69. - Mert, T., et al., *Blocking action of tramadol on nerve conduction.* The Internet Journal of Pharmacology, 2001. **1**(2).
70. - Okamoto, T., Y. Atsuta, and S. Shimazaki, *Sensory afferent properties of immobilised or inflamed rat knees during continuous passive movement.* The Journal of Bone and Joint Surgery, 1999. **81-B**(1): p. 171-177.
71. - Seo, J.-H. and S.J. Oh, *Near-nerve needle sensory conduction study of the medial calcaneal nerve: New method and report of four cases of medial calcaneal neuropathy.* Muscle & Nerve, 2002. **26**: p. 654-658.
72. - Smith, A., *Valg av preparater til sedasjon, anestesi og analgesi, og avlivnings-metoder.*
73. - Stange, G. and K.-E. Kaissling, *The site of action of general anaesthetics in insect olfactory receptor neurons.* Chemical Senses, 1995: p. 423-432.
74. - Visan, A., et al., *Cutaneous nerve blocks of the lower extremity.* Techniques in Regional Anesthesia and Pain Management, 2003. **7**(1): p. 26-31.
75. - Close, B., et al., *Recommendations for euthanasia of experimental animals: Part 1.* Laboratory Animals, 1996. **30**: p. 293-316.
76. - Fischer, M.S. and R. Blickhan, *The tri-segmented limbs of therian mammals: kinematics, dynamics, and self-stabilization - A review.* Journal of Experimental Zoology, 2006. **305A**: p. 935-952.
77. - Schuettler, M., et al. *Velocity-selective recording from frog nerve using a multi-contact cuff electrode.* in *Proceedings of the 28th IEEE EMBS Annual International Conference.* 2006. New York City, USA.
78. - Taylor, J., et al., *Some recent developments in the design of biopotential amplifiers for ENG recording systems.* 2006, University of Bath.
79. - Taylor, J., et al., *10-channel low noise CMOS amplifier system of velocity selective ENG recording.* 2006, University of Bath.
80. - Drewes, C.D. and R.A. Pax, *Neuromuscular physiology of the longitudinal muscle of the earthworm, lumbricus terrestris.* The Journal of Experimental Biology, 1974. **60**: p. 445-452.
81. - Drewes, C. *Tested studies for laboratory teaching: Non-invasive recording of giant nerve fiber action potentials from freely moving oligochaetes.* in *Proceedings of the 20th Workshop/Conference of the Association for Biology Laboratory Education (ABLE).* 1999.
82. - Drewes, C., *Functional organization of the nervous system in Lumbriculus variegatus.* 2002, Iowa State University.
83. - Pickens, P.E., *Conduction along the ventral nerve cord of a hemichordate worm.* The Journal of Experimental Biology, 1970. **53**: p. 515-528.
84. - Martin, N. and M. Anctil, *Luminescence control in the tube-worm chaetopterus variopedatus: Role of nerve cord and photogenic gland. .* The Biological Bulletin, 1984. **166**: p. 583-593.
85. - Olivo, R.F., *Lab 4: Action Potentials in Earthworm Giant Axons*, S.C. Biological Sciences 300/301, Editor. 2008.